Exclusive processes in perturbative quantum chromodynamics

G. Peter Lepage

Laboratory of Nuclear Studies, Cornell University, Ithaca, New York 14853

Stanley J. Brodsky

Stanford Linear Accelerator Center, Stanford University, Stanford, California 94305

(Received 27 May 1980)

We present a systematic analysis in perturbative quantum chromodynamics (QCD) of large-momentum-transfer exclusive processes. Predictions are given for the scaling behavior, angular dependence, helicity structure, and normalization of elastic and inelastic form factors and large-angle exclusive scattering amplitudes for hadrons and photons. We prove that these reactions are dominated by quark and gluon subprocesses at short distances, and thus that the dimensional-counting rules for the power-law falloff of these amplitudes with momentum transfer are rigorous predictions of QCD, modulo calculable logarithmic corrections from the behavior of the hadronic wave functions at short distances. These anomalous-dimension corrections are determined by evolution equations for process-independent meson and baryon "distribution amplitudes" $\phi(x_i, Q)$ which control the valence-quark distributions in high-momentum-transfer exclusive reactions. The analysis can be carried out systematically in powers of $\alpha_s(Q^2)$, the QCD running coupling constant. Although the calculations are most conveniently carried out using light-cone perturbation theory and the light-cone gauge, we also present a gauge-independent analysis and relate the distribution amplitude to a gauge-invariant Bethe-Salpeter amplitude.

I. INTRODUCTION

In this paper we present a systematic analysis in quantum chromodynamics (QCD) of exclusive processes involving transfer of large momenta.[1] The results lead to a comprehensive new range of rigorous predictions of perturbative QCD which test both the scaling and spin properties of quark and gluon interactions at large momentum as well as the detailed structure of hadronic wave functions at short distances. Predictions are possible for a huge number of experimentally accessible phenomena including the elastic and inelastic electromagnetic and weak form factors of hadrons,[2] and, more generally, large-angle exclusive scattering reactions where the interacting particles can be either hadrons or photons. We confirm that the dimensional-counting rules[3] for the power-law falloff of these amplitudes at large momentum transfer are rigorous predictions of QCD, up to calculable powers of the running coupling constant $\alpha_s(Q^2)$ or $(\ln Q^2/\Lambda^2)^{-1}$. Angular dependence, helicity structure, relative and sometimes even the absolute normalization can be computed for all such processes.

A simple picture emerges from our analysis of these processes. For example, consider the proton's magnetic form factor $G_M(Q^2)$ at large $-q^2 = Q^2$. This is most easily understood in the infinite-momentum frame where the proton is initially moving along the z axis and then is struck by a highly virtual photon carrying large transverse momentum $q_\perp^2 = -q^2$. The form factor is the amplitude for the composite hadron to absorb large transverge momentum while remaining intact. In effect, an "intact" baryon can be pictured as three valence quarks, each carrying some fraction x_i of the baryon's momentum ($\sum_{i=1}^{3} x_i = 1$) and all moving roughly parallel with the hadron. As we shall see, the more complicated nonvalence Fock states in the proton (i.e., $qqq q\bar{q}$, $qqqg$, ...) are unimportant as $Q^2 \to \infty$. The form factor is then the product of three probability amplitudes: (a) the amplitude ϕ for finding the three-quark valence state in the incoming proton; (b) the amplitude T_H for this quark state to scatter with the photon producing three quarks in the final state whose momenta are roughly collinear; and (c) the amplitude ϕ^* for this final quark state to reform into a hadron. Thus the magnetic form factor can be written [see Fig. 1(a)]

$$G_M(Q^2) = \int_0^1 [dx] \int_0^1 [dy] \phi^*(y_i, \tilde{Q}_y) T_H(x_i, y_i, Q) \times \phi(x_i, \tilde{Q}_x)[1 + O(m^2/Q^2)],$$

$$(1.1)$$

where $[dx] \equiv dx_1 dx_2 dx_3 \delta(1 - \sum_i x_i)$ and $\tilde{Q}_x \equiv \min_i(x_i Q)$.

To leading order in $\alpha_s(Q^2)$, the "hard-scattering amplitude" T_H is the sum of all Born diagrams for $\gamma^* + 3q \to 3q$ in perturbative QCD.[4] The transverse-momentum fluctuations of the quarks in the initial and final protons are negligible relative to $q_\perp$, as are all particle masses. These can be ignored in T_H so that in effect each hadron is replaced by collinear on-shell valence partons. Since the final quarks are collinear, momentum of $O(q_\perp) \to \infty$ must be transferred from quark line
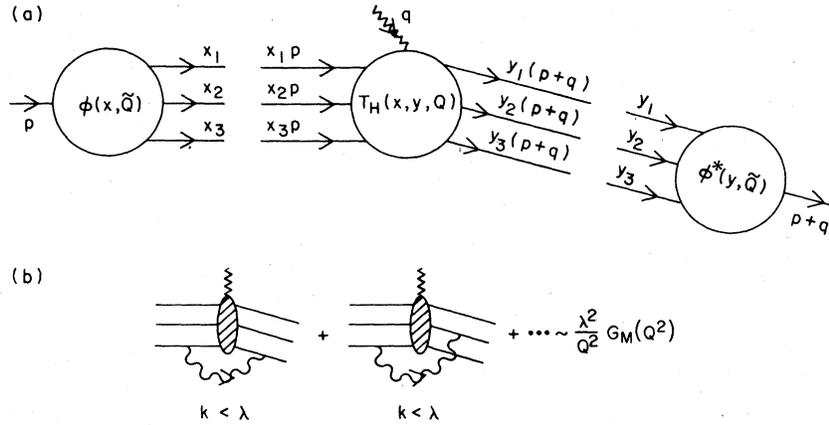
FIG. 1. (a) The general structure of the proton's magnetic form factor at large Q^2. (b) Soft (infrared) interactions between color-singlet hadrons cancel.

to quark line (via gluons) in T_H. This justifies our use of perturbation theory in computing T_H, since all internal propagators in the Born diagrams must then be off shell by $O(Q^2)$. Furthermore, the most important dynamical feature of the form factor—its power-law falloff—can then be traced to the behavior of T_H, which falls for increasing Q^2 with a factor $[\alpha_s(Q^2)/Q^2]$ for each constituent, after the first, scattered from the incident to the final direction: i.e.,

$$T_H(x_i, y_i, Q) = \left(\frac{\alpha_s(Q^2)}{Q^2}\right)^2 T(x_i, y_i)[1 + O(\alpha_s(Q^2))],$$

(1.2)

where $\alpha_s(Q^2) = (4\pi/\beta)(\ln Q^2/\Lambda^2)^{-1}$ is the running coupling constant.

It is now clear that nonvalence Fock states in the proton cannot contribute since all such states contain four or more constituents, each of which must be turned to the final direction. Thus T_H for these states falls as $[\alpha_s(Q^2)/Q^2]^3$ or faster and is negligible relative to (1.2) as $Q^2 \to \infty$. [This observation, while strictly true in light-cone gauge $(\eta \cdot A = A^+ = 0)$, has a different interpretation in covariant gauges—see Appendix C.] Thus non-valence ("sea") quarks and gluons in the proton do not contribute.

The "quark distribution amplitude" $\phi(x_i, Q)$ is the amplitude for converting the proton into three valence quarks. The quarks each carry some fraction

$$x_i = \frac{k_i^+}{p^+} = \frac{k_i^0 + k_i^3}{p^0 + p^3}$$

of the proton's longitudinal momentum and are all collinear up to scale Q. In light-cone gauge, ϕ is simply related to the hadronic wave function:

$$\phi(x_i, Q) \propto \int^Q \prod_{i=1}^{3} d^2 k_{\perp i} \delta^2\left(\sum_i k_{\perp i}\right) \psi(x_i, k_{\perp i}).$$

(1.3)

(To be precise, ψ is the Fourier transform of the positive-energy projection of the usual Bethe-Salpeter wave function evaluated at relative light-cone "times" $z^+ = z^0 + z^3 = 0$.) This amplitude is obviously process independent. It contains the essential physics of that part of the hadronic wave function which affects exclusive processes with large momentum transfer. The distribution amplitude is only weakly dependent on Q^2, and this dependence is completely specified by an evolution equation of the form (in leading order)

$$Q^2 \frac{\partial}{\partial Q^2} \phi(x_i, Q) = \frac{\alpha_s(Q^2)}{4\pi} \int_0^1 [dy] V(x_i, y_i) \phi(y_i, Q),$$

(1.4)

where V can be computed from a single-gluon-exchange kernel. The general solution of this equation is

$$\phi(x_i, Q) = x_1 x_2 x_3 \sum_{n=0}^{\infty} a_n \left(\ln \frac{Q^2}{\Lambda^2}\right)^{-\gamma_n} \tilde{\phi}_n(x_i).$$

(1.5)

Combining this expansion with Eqs. (1.1) and (1.2), we obtain the general form of G_M:

$$G_M(Q^2) = \left(\frac{\alpha_s(Q^2)}{Q^2}\right)^2 \sum_{n,m} b_{nm} \left(\ln \frac{Q^2}{\Lambda^2}\right)^{-\gamma_n - \gamma_m}.$$

(1.6)

The factorized form of Eq. (1.1) implies a simple space-time picture. The exchange of large transverse momentum in the hard-scattering amplitude T_H occurs only when the relative separation of the constituents approaches the light cone—i.e., $-(z^{(i)} - z^{(j)})^2 \sim (z_\perp^{(i)} - z_\perp^{(j)})^2 \to O(1/Q^2)$. The distribution amplitude ϕ is the probability amplitude for

finding the valence quarks sufficiently near the light cone; by the uncertainty principle, this corresponds to a momentum-space wave function smeared over all $k_\perp^2 \lesssim 1/z_\perp^2 \sim Q^2$, as in Eq. (1.3). Each (polynomial) eigensolution $\tilde{\phi}_n(x_i)$ [Eq. (1.5)] of the evolution equation is directly related to a term in the operator-product expansion of the wave function[5] evaluated near the light cone. The eigenvalues γ_n are the corresponding anomalous dimensions.

Beyond leading order, both the hard-scattering amplitude and the potential in the evolution equation have expansions in $\alpha_s(Q^2)$:

$$T_H(x_i, y_i, Q) = \left(\frac{\alpha_s(Q^2)}{Q^2}\right)^2$$

$$\times [T_0(x_i, y_i) + \alpha_s(Q^2)T_1(x_i, y_i) + \cdots],$$

$$V(x_i, y_i, \alpha_s(Q^2)) = V_0(x_i, y_i) + \alpha_s(Q^2)V_1(x_i, y_i) + \cdots.$$

These corrections can be systematically evaluated and the basic equations [Eqs. (1.1) and (1.4)] made exact to any order in $\alpha_s(Q^2)$.

An essential part of the derivation of these results is an analysis of the end-point behavior of the x_i and y_i integrations in Eq. (1.1), and especially of the region $x_i \to 1$ or $y_i \to 1$. As long as $(1 - x_i) \gg m/Q$, we find that the distribution amplitude vanishes as $\phi(x_i, \tilde{Q}) \sim (1 - x_i)^{\epsilon(\tilde{Q})}$ with $\epsilon(\tilde{Q}) > 1$ as $x_i \to 1$. This follows from a perturbative analysis of the $x_i \sim 1$ region coupled with the realization that $\epsilon(\tilde{Q}) \to 2$ as $\tilde{Q} \to \infty$, which is a necessary consequence of the evolution equation (1.4). Consequently, ϕ and ϕ^* vanish sufficiently quickly that the x_i, y_i integrations are well behaved, at least for $(1 - x_i) \gg m/Q$. [In particular, the evolution of the amplitude eliminates any potential logarithmic singularities in the region $1 \gg (1 - x_i) \gg m/Q$. In Ref. 6, it is argued that such singularities do occur resulting in an additional correction to T_H of order $\alpha_s^2(Q) \ln(Q/m)T_H$; however, this calculation neglects the effects due to the evolution of ϕ occurring when higher-order corrections are properly included.]

The region $1 - x_i \lesssim m/Q$ must be analyzed separately. Contributions from this region were first discussed by Drell and Yan, and by West.[7] They related the Q^2 dependence of these contributions to the $x \sim 1$ behavior of the deep-inelastic structure function νW_2. Taking $\nu W_2 \sim (1 - x)^3$ as $x \to 1$, in accord (roughly) both with experiment and with naive theoretical expectations, the Drell-Yan-West connection implies a term in the form factor which falls as $1/Q^4$—i.e., just as in Eq. (1.6). However, a detailed examination reveals that this term is suppressed by at least two full powers of $\alpha_s(Q^2)$ relative to (1.6). Furthermore, in perturbation theory, gluonic corrections to the quark-photon

vertex result in a Sudakov form factor which suppresses the end-point contributions by additional powers of m/Q. Thus the infinitesimal region $1 - x_i \lesssim m/Q$ makes only a negligible contribution to the form factor. It is also clear then that the Drell-Yan-West connection between deep-inelastic scattering and hadronic form factors is invalid in QCD. Notice finally that the proof of light-cone dominance [i.e., dominance of finite-x_i, y_i region in (1.1)] in the asymptotic form factors does not even require consideration of the Sudakov corrections—end-point contributions are suppressed by $\alpha_s^2(Q^2)$ for baryons and, it turns out, by $O(m/Q)$ for mesons.

The remainder of the paper is organized as follows.

In Sec. II we treat the simplest example of an exclusive process in QCD, the $\pi^0 \to \gamma$ transition form factor $F_{\pi\gamma}(Q^2)$. This quantity is measurable both in e^+e^- annihilation ($e^+e^- \to \pi^0\gamma$) and in two-photon reactions ($e\gamma \to e\pi^0$). The basic analysis tool is light-cone perturbation theory[8] which is developed and summarized in Appendix A. The calculation of the $\gamma^*\pi \to \gamma$ transition involves all the basic steps required in computing any of the hadronic form factors. A detailed derivation of the meson's evolution equation [to leading order in $\alpha_s(Q^2)$] is also given in Sec. II. General procedures for its solution are given in Appendix D. We also show that $F_{\pi\gamma}$ is exactly normalized at $Q^2 \to \infty$ by the pion decay constant[9]:

$$\lim_{Q^2 \to \infty} Q^2 F_{\pi\gamma}(Q^2) = 2f_\pi.$$

The absence of true infrared singularities in exclusive amplitudes is due to the fact that hadron states are color singlets. In particular, soft interactions ($k \lesssim \lambda$) between initial and/or final quarks in T_H all cancel since the quarks enter and leave in (collinear) color-singlet states [see Fig. 1(b)]. This also allows us to define a Fock-state expansion of the hadronic wave function in terms of states with a finite number of quark and gluon quanta. An important feature of the light-cone gauge (as employed in Sec. II) is that the leading terms in any exclusive amplitude are due to the minimal or valence Fock states in each hadron. Nonvalence states are suppressed by powers of m^2/Q^2, as discussed above. The use of light-cone perturbation theory together with the light-cone gauge thus leads to a number of significant computational simplifications. The generalization to other gauges and to covariant perturbation theory is given in Appendix C. There we also relate the quark distribution amplitude to the operator

$$\bar{\psi} \exp\left[-ie_s \int dz \cdot A\right] \psi$$

(with all fields appropriately smeared in the transverse direction), correcting certain defects in the analysis given in Ref. 10.

Section III outlines a general procedure for computing corrections of order $\alpha_s(Q^2)$ and higher in the form factors. This includes the analysis of higher-order terms in T_H (see also Appendix B) and in the potential V for the evolution equation. The analysis of $\phi(x_i, Q)$ using the operator-product expansion (OPE), as given in Ref. 5, is also reviewed here. In general, the formalism presented in this paper provides a gauge-invariant calculational method for composite-system matrix elements.

To simplify the analysis Secs. II and III deal primarily with $F_{\pi\gamma}$ [although the analysis of $\phi(x_i, Q)$ is obviously process independent]. As $Q^2 \to \infty$, this form factor is determined by the matrix element $\langle 0 | T J_\mu(z) J_\nu(0) | \pi \rangle$ with $z^2 \sim -1/Q^2 \to 0$. The fact that $z^2 \to 0$ for this process is not obvious *a priori*, but rather is a consequence of the results given in Sec. II. However, given this fact, one can determine the Q^2 behavior of $F_{\pi\gamma}$ directly by using the standard OPE of $J_\mu(z) J_\nu(0)$ near the light cone. This analysis gives results identical to ours. Unfortunately such an approach is useless for studying most other exclusive amplitudes. For example, in the case of the proton form factor $F(Q^2) \sim \langle p | J_\mu(z) | p \rangle$, it is hard to see which is the "short distance" to be analyzed using the OPE. Only by dissecting the amplitude, as in Eq. (1.1), do we see that it is the structure of the hadronic wave function near the light cone, together with that of a hard subprocess (i.e., T_H), which determines the form factor's behavior at large Q^2. The "short distance" is buried inside the process. So whereas the OPE analysis of $J_\mu J_\nu$ is useful only for $F_{\pi\gamma}$, the techniques developed in Secs. II and III for reducing such an amplitude to a form analogous to (1.1) are universally applicable. In addition, they provide a compelling picture of the microscopic processes which govern this area of large-$p_\perp$ physics.

Detailed applications of our analysis to hadronic form factors (mesons and baryons) are given in Sec. IV. The techniques required to solve the more complicated baryon evolution equation are given in Appendix D. In addition to normalizing mesonic form factors, important predictions testing the spin of the gluon can be made for both mesons and baryons, including specific QCD spin selection rules. The absolute sign of meson form factors and the absence of zeros are also nontrivial consequences of a vector gluon theory. We also discuss at length the end-point contributions to form factors.

In Sec. V we describe the general features pre-

dicted for large-angle exclusive reactions involving hadrons and/or photons. An important feature of the QCD analysis is the huge number of Born diagrams contributing to T_H in purely hadronic reactions. This may help explain the anomalously large cross sections for πp and pp elastic scattering at 90°. It also explains why the Landshoff pinch singularity[11] plays no role in wide-angle scattering, at least at current energies. Such contributions are overwhelmed by the large number of hard-scattering subprocesses. Furthermore, we show in Sec. VB that the pinch singularity is suppressed by Sudakov form factors which fall faster than any power of t as $-t \to \infty$ (at least in perturbation theory).[12] The potential role of Landshoff processes in very-high-energy small-angle processes ($|t| \ll s$) is critically examined. A brief discussion of the data available for large-angle scattering is also given.

Finally, in Sec. VI we summarize our basic results and discuss future prospects. This paper is an elaboration of the results presented in Ref. 1. Similar results for the pion form factor were obtained independently by Efremov and Radyushkin.[10,13,14]

In this paper we show that large-momentum-transfer exclusive amplitudes are dominated by quark and gluon subprocesses at short distances. As in any calculation in perturbative QCD we implicitly assume that the most singular contributions of the theory near the light cone are given by perturbation theory, i.e., that any nonperturbative contribution is relatively more regular at short distances. We also ignore here distinctions between timelike and spacelike form factors since they are identical to leading order in $\alpha_s(Q^2)$.
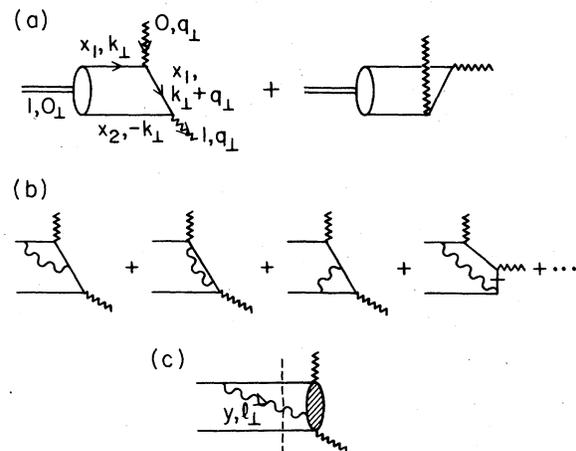

FIG. 2. Diagrams contributing to $F_{\pi\gamma}$: (a) lowest-order terms, (b) one-loop corrections, and (c) generic structure of one-loop corrections.

II. SUMMING LEADING LOGARITHMS IN QCD

A. The π-γ transition form factor

The $\gamma^* \pi^0 \to \gamma$ vertex in the amplitude for $e\pi \to e\gamma$ defines the π-γ transition form factor $F_{\pi\gamma}$:

$$\Gamma_\mu = -ie^2 F_{\pi\gamma}(Q^2)\epsilon_{\mu\nu\rho\sigma} p_\pi^\nu \epsilon^\rho q^\sigma, \qquad (2.1)$$

where p_π and q are the momenta of the incident pion and virtual photon, respectively, and ϵ is the polarization vector of the final (on-shell) photon. In the standard "infinite-momentum" frame where

$$p_\pi \equiv (p^+, p^-, p_\perp) = (1, m_\pi^2, 0_\perp),$$

$$q = (0, q_\perp^2 - m_\pi^2, q_\perp) \Rightarrow q^2 = -q_\perp^2 \equiv -Q^2$$

(p^+ is arbitrary; for simplicity we choose $p^+ = 1$), $F_{\pi\gamma}$ is given by[15]

$$F_{\pi\gamma}(Q^2) = \frac{\Gamma^+}{-ie^2(\epsilon_\perp \times q_\perp)},$$

where $\epsilon = (0, 0, \epsilon_\perp)$, $\epsilon_\perp \cdot q_\perp = 0$ is chosen.

The lowest-order contribution to $F_{\pi\gamma}$ is [Fig. 2(a); see also Appendix A] ($n_c = 3$)

$$F_{\pi\gamma}(Q^2) = \frac{\sqrt{n_c}(e_u^2 - e_d^2)}{i(\epsilon_\perp \times q_\perp)} \int_0^1 [dx] \int_0^\infty \frac{d^2 k_\perp}{16\pi^3} \psi(x_i, k_\perp) \left[\frac{\bar{v}_\downarrow(x_2, -k_\perp)}{\sqrt{x_2}} \not\!\epsilon \frac{u_\uparrow(x_1, k_\perp + q_\perp)}{\sqrt{x_1}} \frac{\bar{u}_\uparrow(x_1, k_\perp + q_\perp)}{\sqrt{x_1}} \gamma^+ \frac{u_\uparrow(x_1, k_\perp)}{\sqrt{x_1}} \right.$$

$$\left. \times \frac{1}{q_\perp^2 - [(k_\perp + q_\perp)^2 + m^2]/x_1 - [k_\perp^2 + m^2]/x_2} + (1 \to 2) \right], \qquad (2.2)$$

where $[dx] = dx_1 dx_2 \delta(1 - x_1 - x_2)$ and $e_{u,d}$ are the quark charges in units of e. Here we are considering only the $L_z = S_z = 0$ component of the general $q\bar{q}$ wave function, i.e.,[16]

$$\Psi_\pi \to \frac{\delta_b^a}{\sqrt{n_c}} \frac{1}{\sqrt{2}} \left(\frac{u_\uparrow \bar{u}_\downarrow - u_\downarrow \bar{u}_\uparrow}{\sqrt{2}} - \frac{d_\uparrow \bar{d}_\downarrow - d_\downarrow \bar{d}_\uparrow}{\sqrt{2}} \right) \frac{\psi(x_i, k_\perp)}{(x_1 x_2)^{1/2}}, \qquad (2.3)$$

where a, b are color indices, $n_c = 3$ is the number of colors, and $u, \bar{u}, \ldots$ represent on-shell spinor wave functions for the quarks and antiquarks. Charge conjugation invariance requires ψ to be symmetric under the exchange $1 \to 2$. Neglecting quark masses relative to Q^2, Eq. (2.2) becomes (see Appendix A)

$$F_{\pi\gamma}(Q^2) = 2\sqrt{n_c}(e_u^2 - e_d^2) \int_0^1 [dx] \int_0^\infty \frac{d^2 k_\perp}{16\pi^3} \psi(x_i, k_\perp) \left[\frac{(q_\perp x_2 + k_\perp) \times \epsilon_\perp}{(q_\perp \times \epsilon_\perp)(q_\perp x_2 + k_\perp)^2} + (x_1 \to x_2) \right]. \qquad (2.4)$$

Intuitively, the wave function must be peaked at low $k_\perp$, since a composite particle has little amplitude for existing while its constituents are flying apart with large $k_\perp$. The leading behavior for $F_{\pi\gamma}$ as $q_\perp \to \infty$ is then obtained from (2.4) by neglecting $k_\perp$ relative to $q_\perp$, and integrating over all $k_\perp \lesssim \bar{Q}$ $= \min_i(x_i)Q$, at which point the energy denominator in (2.4) damps out the integrand:

$$F_{\pi\gamma}(Q^2) \to \frac{2\sqrt{n_c}(e_u^2 - e_d^2)}{Q^2} \int_0^1 \frac{[dx]}{x_1 x_2} \int^{\bar{Q}^2} \frac{dk_\perp^2}{16\pi^2} \psi(x_i, k_\perp). \qquad (2.5)$$

This approximation would be valid up to corrections of order $(m/Q)^\epsilon \to 0$ if $\psi \sim (1/k_\perp)^{2+\epsilon}$ with $\epsilon > 0$ as $k_\perp \to \infty$. Furthermore, $F_{\pi\gamma}$ would then fall as $1/Q^2$ since the $k_\perp$ integration in (2.5) would be insensitive to its upper limit. In fact, ψ vanishes as $1/k_\perp^2$ up to a factors of $\ln k_\perp^2$ in QCD (see Sec. II B), so that the approximation (2.5) is valid up to corrections of $O(1/\ln Q^2)$.[17] The integral $\int^{\bar{Q}^2} dk_\perp^2 \psi$ then varies logarithmically with $\bar{Q}^2$. In the next section we calculate this Q^2 dependence in QCD.

Notice that quark helicity is conserved at each vertex in (2.2) in the limit of vanishing quark

mass, since the photon is a vector particle (Tables II and III). Thus only states having zero spin projection along the incident direction contribute; components of the pion wave function with $S_z \neq 0$ are suppressed in $F_{\pi\gamma}$ by m/Q. Indeed, for pions, $S_z \neq 0$ implies orbital angular momentum $L_z \neq 0$ in ψ and such a contribution vanishes after the integration over $d^2 k_\perp$ in (2.5). Thus (2.3) is the only relevant component of the general wave function, up to corrections of order m/Q in $F_{\pi\gamma}$.

The one-loop radiative corrections to (2.4) include all two-particle irreducible corrections to the $\gamma^* + q\bar{q} \to \gamma$ amplitude [Fig. 2(b)]. To analyze the contribution from each of these diagrams, we divide the integration over gluon momenta $l_\perp$ into two regions: (a) the collinear region $l_\perp^2 < \bar{Q}^2$; and (b) the ultraviolet (UV) region $l_\perp^2 > \bar{Q}^2$. In the collinear region, each diagram, aside from the self-energy correction, has the general structure of Fig. 2(c):

$$F_{\pi\gamma} \sim \frac{e_s^2}{Q^2} \int^{\bar{Q}^2} \frac{dl_\perp^2}{l_\perp^2} \bar{u}(-l_\perp)\gamma_\mu u(0) d^{\mu\nu} \left[\frac{\bar{u}(q_\perp)\gamma_\nu u(q_\perp + l_\perp)}{q_\perp^2 + l_\perp^2 + \cdots} \right]$$

$$\times \int^{\bar{Q}^2} dk_\perp^2 \psi(k_\perp), \qquad (2.6)$$

where the dependence on the longitudinal momenta x_i, y is implicit, and where $d^{\mu\nu} = -g^{\mu\nu} + (\eta^\mu l^\nu + \eta^\nu l^\mu)/y$ is the transverse polarization sum for the gluon in light-cone gauge ($\eta \cdot A = A^+ = 0$) with $l = (y, l_\perp^2/y, l_\perp)$. The factor $\bar{u}(-l_\perp)\gamma_\mu d^{\mu\nu}u(0)$ vanishes linearly with $l_\perp$ in this gauge. Consequently, these terms are of the form

$$F_{\pi\gamma} \sim \frac{e_s^2}{Q^2} \int^{\bar{Q}^2} \frac{dl_\perp^2}{l_\perp^2} \frac{l_\perp \cdot q_\perp + l_\perp^2}{q_\perp^2 + l_\perp^2 + \cdots} \int^{\bar{Q}^2} dk_\perp^2 \psi(k_\perp)$$

$$\sim \frac{e_s^2}{Q^2} \int^{\bar{Q}^2} dk_\perp^2 \psi(k_\perp) \times \text{const}.$$

The use of perturbative QCD is valid here since only $l_\perp^2$ of order Q^2 contribute. The $l_\perp$ integration does not diverge as $l_\perp \to 0$. Vacuum polarization, self-energy, and vertex insertions into these diagrams combine to replace $e_s^2/4\pi$ by the running coupling constant

$$\alpha_s(Q^2) \cong \frac{4\pi}{\beta \ln Q^2/\Lambda^2} , \qquad (2.7)$$

where $\beta = 11 - \frac{2}{3}n_f$, n_f is the number of flavors, and Λ^2 is the QCD scale parameter. Thus these corrections from the collinear region are suppressed by $\alpha_s(Q^2)$ relative to (2.5) and can be ignored for large Q^2. Mass terms in the numerator of (2.6) are also negligible, being suppressed by m/Q in $F_{\pi\gamma}$.

The ultraviolet region ($l_\perp^2 > \bar{Q}^2$) of these integrals is, by definition, dominated by the short-distance behavior of the theory, and thus is amenable to analysis via the renormalization group. Loop momenta in UV finite diagrams are of order Q^2. As above, such contributions are suppressed by a factor $\alpha_s(Q^2)$ and can be dropped in leading order. Vertex and self-energy corrections have UV divergences of the generic form

$$\left[-\gamma \int_{\bar{Q}^2} \frac{dl_\perp^2}{l_\perp^2} \frac{\alpha_s(l_\perp^2)}{4\pi} + O(\alpha_s(Q^2)) \right] F_{\pi\gamma}^{(0)}(Q^2), \quad (2.8)$$

where $F_{\pi\gamma}^{(0)}$ is the form factor in the lowest order [Eq. (2.5)]. From (2.7), the leading term becomes $(\gamma/\beta) \ln\ln(\bar{Q}^2/\Lambda^2)F_{\pi\gamma}^{(0)}$ after renormalization. The renormalization group requires that such terms exponentiate as higher-order corrections are added, yielding

$$\left(\ln\frac{\bar{Q}^2}{\Lambda^2} \right)^{\gamma/\beta} F_{\pi\gamma}^{(0)} + O(\alpha_s F_{\pi\gamma}^{(0)}). \qquad (2.9)$$
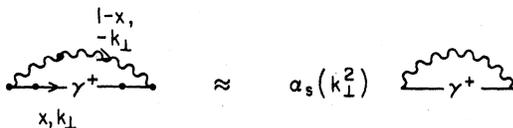

FIG. 3. One-loop vertex correction.

To illustrate, consider the UV-divergent part of the photon-quark vertex correction in light-cone gauge (Fig. 3):

$$\Lambda^+ = \gamma^+ \int_0^1 \frac{dx}{1-x} \int_{\bar{Q}^2} dk_\perp^2 \frac{C_F \alpha_s(k_\perp^2)}{4\pi} \frac{1}{[k_\perp^2/x + k_\perp^2/(1-x)]^2}$$

$$\times \bar{u}(1,0)\gamma_\mu \frac{u(x,k_\perp)}{\sqrt{x}} d^{\mu\nu} \frac{\bar{u}(x,k_\perp)}{\sqrt{x}}$$

$$\times \gamma_\nu u(1,0),$$

where $C_F = (n_c^2 - 1)/2n_c = \frac{4}{3}$. Here again the leading effect of vertex and propagator corrections is included in $\alpha_s(k_\perp^2)$ (Fig. 3). After some simple algebra, Λ^+ becomes

$$\Lambda^+ = \gamma^+ \int_{\bar{Q}^2} \frac{dk_\perp^2}{k_\perp^2} \frac{\alpha_s(k_\perp^2)}{4\pi} C_F \int_0^1 dx \left[2(1-x) + \frac{4x}{1-x} \right],$$

and the anomalous dimension associated with the QED vertex is $-\gamma_F$ where [cf. Eq. (2.8)]

$$\gamma_F = C_F \left(1 + 4 \int_0^1 dx \frac{x}{1-x} \right). \qquad (2.10)$$

The Ward identity in QED implies that the anomalous dimension for self-energy diagrams is then γ_F. The vertex and propagator corrections in Fig. 2(b) together introduce a factor $(\ln \bar{Q}^2/\Lambda^2)^{\gamma_F/\beta}$ into (2.5).

Therefore, to leading order in $\alpha_s(Q^2)$, the π-γ transition form factor in QCD can then be written as [recall $\bar{Q} \equiv \min(x_i)Q$]

$$F_{\pi\gamma}(Q^2) = \int_0^1 dx_1 dx_2 \delta(1 - x_1 - x_2) T_H(x_i, Q)\phi(x_i, \bar{Q}),$$

$$\qquad (2.11)$$

where T_H is the hard-scattering amplitude for $\gamma^* + q\bar{q} \to \gamma$ with on-shell collinear quarks:

$$T_H(x_i, Q) = \frac{2\sqrt{n_c}(e_u^2 - e_d^2)}{x_1 x_2 Q^2}. \qquad (2.12)$$

The quark *distribution amplitude* $\phi(x_i, Q)$ is the amplitude for finding constituents with longitudinal momenta x_i in the pion which are collinear up to the scale Q^2:

$$\phi(x_i, Q) \equiv \left(\ln \frac{Q^2}{\Lambda^2} \right)^{-\gamma_F/\beta} \int^{Q^2} \frac{dk_\perp^2}{16\pi^2} \psi(x_i, k_\perp). \quad (2.13)$$

In the next section, we demonstrate how the infrared divergence at $x = 1$ in γ_F [Eq. (2.10)] exactly cancels a similar divergence in ψ, and thus $\phi(x_i, Q)$ is well defined.

Two-loop and higher corrections to the two-particle irreducible $\gamma^* + q\bar{q} \to \gamma$ amplitude are suppressed by additional powers of $\alpha_s(Q^2)$, in much the same way one-loop corrections are suppressed. This is illustrated in Appendix B. The key in-

gredient of this analysis is that the amplitude for the emission of a collinear, virtual gluon by a massless quark vanishes—i.e., $\bar{u}(x-y, l_\perp)\gamma_\mu d^{\mu\nu}$ $\times u(x, 0) \to l_\perp \to 0$ when $l_\perp \to 0$, as in Eq. (2.6). This property follows in physical gauges, such as light-cone gauge, from two observations: (a) the vector coupling of the gluon conserves the helicity of massless quarks, and (b) the polarization tensor $d^{\mu\nu}$ for the virtual gluon admits only transversely polarized gluons (helicity $=\pm 1$) as the gluons go on shell (i.e., as $l_\perp \to 0$). Thus it is impossible to conserve angular momentum along the direction of motion when the quark emits a collinear gluon, and the amplitude must vanish. In covariant gauges, $d^{\mu\nu}$ contains longitudinal polarizations, and the amplitude $\bar{u}(l_\perp)\gamma_\mu d^{\mu\nu} u(0)$ no longer vanishes as $l_\perp \to 0$. Then the collinear region in Eq. (2.6) is no longer negligible, giving a contribution

$$\frac{1}{Q^2} \int_{m^2}^{Q^2} \frac{dl_\perp^2}{l_\perp^2} \frac{q_\perp^2}{q_\perp^2} \alpha_s(l_\perp^2) \int^{Q^2} dk_\perp^2 \psi(k_\perp)$$

$$\sim \left(\ln\ln\frac{Q^2}{\Lambda^2}\right) F_{\pi'}^{(0)}(Q^2).$$

Indeed irreducible diagrams with any number of loops contribute to leading order in these gauges (see Appendix C).

B. Quark distribution amplitudes and evolution equations for mesons

The $q\bar{q}$ wave function in Eq. (2.3) is the Fourier transform (FT) of the positive-energy projection of the Bethe-Salpeter wave function evaluated at equal "time" $z^+ = z^3 + z^0 = 0$:

$$\psi \sim \text{FT}\langle 0 | T\psi(0)\bar{\psi}(z) | \pi\rangle\big|_{z^+ = 0}.$$

The behavior of the distribution amplitude $\phi(x_i, Q)$ [Eq. (2.13)] at fixed x_i as $Q^2 \to \infty$ is therefore determined by the behavior of $T\psi(0)\bar{\psi}(z)$ for $z^2 = -z_\perp^2 \sim -1/Q^2 \to 0$. This light-cone region can be
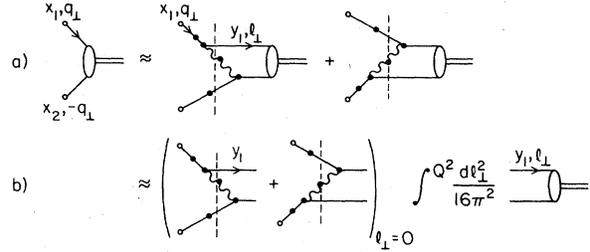

FIG. 4. (a) The bound-state wave equation for $\psi(x_i, q_\perp)$ to leading order in $\alpha_s(Q^2)$. (b) The relation between $\psi(x_i, q_\perp)$ and the distribution amplitude.

studied using Wilson's operator-product expansion and the renormalization group. This analysis is described in Ref. 5, and again, very briefly, in Sec. III. Here we derive a simple evolution equation directly from perturbation theory, which describes the variation of ϕ with Q^2 [to leading order in $\alpha_s(Q^2)$]. In practical applications, evolution equations are usually the most efficient tool for including the perturbative effects of QCD in $\phi(x_i, Q)$.

An evolution equation is obtained by differentiating both sides of Eq. (2.13) with respect to Q^2:

$$Q^2 \frac{\partial}{\partial Q^2} \phi(x_i, Q) = \left(\ln\frac{Q^2}{\Lambda^2}\right)^{-\gamma_F/\beta} \frac{\psi(x_i, q_\perp)Q^2}{16\pi^2}$$

$$- \frac{\gamma_F}{\beta} \frac{\phi(x_i, Q)}{\ln Q^2/\Lambda^2}. \tag{2.14}$$

The wave function $\psi(x_i, q_\perp)$ satisfies the wave equation $\psi = SK\psi$, where S is the renormalized two particle propagator and K is the sum of all two-particle irreducible $q\bar{q} \to q\bar{q}$ kernels (see Appendix A). The leading-order kernel is the one-gluon interaction for which the wave equation becomes (see Fig. 4)

$$\psi(x_i, q_\perp) = \frac{-4\pi C_F}{m_\pi^2 - (q_\perp^2 + m^2)/x_1 x_2} \int_0^1 [dy] \int \frac{d^2 l_\perp}{16\pi^3} \alpha_s(q_\perp^2) \frac{\bar{u}(x_1, q_\perp)}{\sqrt{x_1}} \gamma_\mu \frac{u(y_1, l_\perp)}{\sqrt{y_1}} d^{\mu\nu} \frac{\bar{v}(y_2, -l_\perp)}{\sqrt{y_2}} \gamma_\nu \frac{v(x_2, -q_\perp)}{\sqrt{x_2}}$$

$$\times \left[\frac{\theta(y_1 - x_1)}{y_1 - x_1} \frac{1}{m_\pi^2 - (q_\perp^2 + m^2)/x_1 - (l_\perp^2 + m^2)/y_2 - (q_\perp - l_\perp)^2/(y_1 - x_1)}\right.$$

$$\left. + (1 \leftrightarrow 2)\right] \psi(y_i, l_\perp). \tag{2.15}$$

The leading effects due to vertex and propagator corrections are again included in the running coupling constant (cf. Fig. 3). As before, the dominant behavior for $q_\perp \to \infty$ is obtained from Eq. (2.15) by neglecting $m, l_\perp$ relative to $q_\perp$ and integrating over $l_\perp \lesssim q_\perp$ [Fig. 4(b)]. This follows since $\psi(y_i, l_\perp)$ is peaked at low $l_\perp$. In fact, it is then clear from Eq. (2.15) that $\psi(x_i, q_\perp) \to 1/q_\perp^2$ up to logarithms of $q_\perp^2$ as $q_\perp \to \infty$, which implies that the corrections to this approximation are of order $1/\ln Q^2 \sim \alpha_s(Q^2)$. Thus, to leading order Eq. (2.15) becomes

$$\frac{\psi(x_i, q_\perp)Q^2}{16\pi^2} = 2C_F \frac{\alpha_s(Q^2)}{4\pi} \int_0^1 [dy]\left[x_1 y_2 \theta(y_1 - x_1)\left(\delta_{h_1 \bar{h}_2} + \frac{1}{y_1 - x_1}\right) + (1 \leftrightarrow 2)\right] \int^{Q^2} \frac{dl_\perp^2}{16\pi^2} \frac{\psi(y_i, l_\perp)}{y_1 y_2}, \tag{2.16}$$

where $\delta_{h_1 \bar{h}_2} = 1(0)$ when the constituents' helicities are antiparallel (parallel). Our use of perturbative QCD is again justified since only momenta of order $q_\perp$ flow through the kernel. Combining this equation with Eqs. (2.14), (2.13), and (2.10), we obtain an evolution equation for $\phi(x_i, Q)$ $\equiv x_1 x_2 \tilde{\phi}(x_i, Q)$:

$$x_1 x_2 Q^2 \frac{\partial}{\partial Q^2} \tilde{\phi}(x_i, Q)$$

$$= C_F \frac{\alpha_s(Q^2)}{4\pi} \left\{ \int_0^1 [dy] V(x_i, y_i) \tilde{\phi}(y_i, Q) \right.$$

$$\left. - x_1 x_2 \tilde{\phi}(x_i, Q) \right\}, \quad (2.17a)$$

where

$$V(x_i, y_i) = 2 \left[x_1 y_2 \theta(y_1 - x_1) \left(\delta_{h_1 \bar{h}_2} + \frac{\Delta}{y_1 - x_1} \right) \right.$$

$$\left. + (1 \leftrightarrow 2) \right]$$

$$= V(y_i, x_i), \quad (2.17b)$$

and $\Delta \tilde{\phi}(y_i, Q) \equiv \tilde{\phi}(y_i, Q) - \tilde{\phi}(x_i, Q)$. Notice that the infrared divergence in Eq. (2.16) at $x_i = y_i$ is completely canceled by that in γ_F [we have rescaled x in Eq. (2.10) by x_2 for the first and x_1 for the second term in (2.17b)]. This is only true because the color factor for the ladder kernel is identical to that associated with the propagator corrections. This in turn is a consequence of the color-singlet nature of the meson.

High-order kernels entering in the wave equation include all two-particle irreducible amplitudes for $q\bar{q} \to q\bar{q}$ (Fig. 5). However, these corrections to $V(x_i, y_i)$ are all suppressed by powers of $\alpha_s(Q^2)$, because they are irreducible. This follows from the same arguments used in the previous section in analyzing corrections to T_H.

By defining

$$\xi = \frac{\beta}{4\pi} \int^{Q^2} \frac{dk_\perp^2}{k_\perp^2} \alpha_s(k_\perp^2) \sim \ln \ln \frac{Q^2}{\Lambda^2}, \quad (2.18a)$$

we can recast the evolution equation in a more useful form

$$x_1 x_2 \left[\frac{\partial}{\partial \xi} \tilde{\phi}(x_i, Q) + \frac{C_F}{\beta} \tilde{\phi}(x_i, Q) \right]$$

$$= \frac{C_F}{\beta} \int_0^1 [dy] V(x_i, y_i) \tilde{\phi}(y_i, Q). \quad (2.18b)$$

Given $\phi(x, Q_0)$, this equation can be integrated (numerically or otherwise) to obtain $\phi(x_i, Q)$ for any $Q^2 > Q_0^2$. Alternatively, the general procedure described in Appendix D can be applied to determine the most general solution of (2.18):
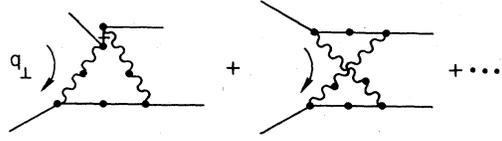
$$\phi(x_i, Q) = x_1 x_2 \sum_{n=0}^{\infty} a_n C_n^{3/2}(x_1 - x_2) \left(\ln \frac{Q^2}{\Lambda^2} \right)^{-\gamma_n}, \quad (2.19)$$

where

$$\gamma_n = \frac{C_F}{\beta} \left(1 + 4 \sum_2^{n+1} \frac{1}{k} - \frac{2\delta_{h_1 \bar{h}_2}}{(n+1)(n+2)} \right) \geqslant 0.$$

For pions, $\delta_{h_1 \bar{h}_2} = 1$ and only even n contribute since $\phi(x_1, x_2, Q) = \phi(x_2, x_1, Q)$ is required (by C invariance). The coefficients a_n can be determined from $\phi(x_i, Q_0)$ by using the orthogonality relations for the Gegenbauer polynominals, $C_n^{3/2}$:

$$a_n \left(\ln \frac{Q_0^2}{\Lambda^2} \right)^{-\gamma_n} = \frac{2(2n+3)}{(2+n)(1+n)}$$

$$\times \int_{-1}^1 d(x_1 - x_2) C_n^{3/2}(x_1 - x_2) \phi(x_i, Q_0). \quad (2.20)$$

The convergence of series (2.19) is assured by the elementary properties of orthogonal polynomial if (and only if) ϕ satisfies the boundary condition[18]

$$\phi(x_i, Q) \leqslant K x_i^\epsilon \text{ as } x_i \to 0 \quad (2.21)$$

for some $\epsilon > 0$. In fact, this condition is automatically satisfied by wave functions representing truly composite states—i.e., by solutions of the homogeneous bound-state equation [Eq. (A5)] which are regular at high energies. In theories with an elementary field representing (or mixing strongly with) the meson, the bound-state equation has a source term corresponding to the bare coupling $\bar{\psi}\phi\gamma_5\psi$, and consequently the wave function tends to a constant ($\neq 0$) as $x_i \to 0$.[19]

Notice that as $Q^2 \to \infty$, the quark distribution amplitude becomes particularly simple since only the $n = 0$ term survives ($\gamma_0 < \gamma_n$ for all $n > 0$):

$$\phi(x_i, Q) \to \begin{cases} a_0 x_1 x_2, & h_1 + h_2 = 0 \\ a_0 x_1 x_2 \left(\ln \frac{Q^2}{\Lambda^2} \right)^{-C_F/\beta}, & h_1 + h_2 = \pm 1 \end{cases} \cdot \quad (2.22)$$

The coefficient a_0 is just the renormalized quark-antiquark wave function evaluated at the origin in

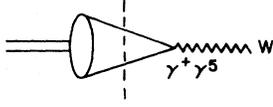FIG. 5. Higher-order corrections to the potential V of the evolution equation (2.17).

FIG. 6. Matrix element of the charged axial-vector current controlling the decay $\pi \to e\bar{\nu}$.

coordinate space. Combining Eqs. (2.20) and (2.13) for helicity-zero states, we obtain

$$\frac{a_0}{6} = \lim_{Q^2 \to \infty} \left(\ln \frac{Q^2}{\Lambda^2} \right)^{\gamma_F/\beta} \int_0^1 [dx] \int^Q \frac{d^2 k_\perp}{16\pi^3} \psi(x_i, k_\perp)$$

$$= Z_2 \int_0^1 [dx] \int \frac{d^2 k_\perp}{16\pi^3} \psi(x_i, k_\perp),$$

where Z_2 renormalizes the quark field operators in wave function $\psi(x_i, k_\perp)$ (recall that γ_F [Eq. (2.10)] is the anomalous dimension associated with the quark self-energy). The same renormalization enters for the charged weak current, $J_W^\mu = \bar{u}\gamma^\mu(1 - \gamma_5)d$, whose matrix element between a pion and the vacuum is[20] (for $\mu = +$; see Fig. 6)

$$\langle 0 | J_W^+ | \pi \rangle = Z_2 \int_0^1 [dx] \int \frac{d^2 k_\perp}{16\pi^3} \psi(x_i, k_\perp) \frac{\sqrt{n_c}}{\sqrt{2}}$$

$$\times \left[\frac{\bar{v}_\uparrow}{\sqrt{x_2}} \gamma^+ (1 - \gamma_5) \frac{u_\downarrow}{\sqrt{x_1}} - (\uparrow \to \downarrow) \right]$$

$$= \sqrt{2}\sqrt{n_c} \frac{a_0}{3}. \tag{2.23}$$

If we define $\langle 0 | J_W^\mu | \pi^+ \rangle = \sqrt{2} f_\pi p^\mu$, where $f_\pi \simeq 93$ MeV is measured in the decay $\pi \to \mu\nu$, we obtain a sum rule for $\phi(x_i, Q)$:

$$a_0 = 6 \int_0^1 [dx]\phi_\pi(x_i, Q) = \frac{3}{\sqrt{n_c}} f_\pi. \tag{2.24a}$$

Equations (2.22) and (2.24a) completely determine the asymptotic behavior of the pion's quark distribution amplitude (given isospin invariance, these are identical for π^+, π^0). Furthermore, sum rule (2.24a) is valid for all Q^2, up to corrections of order $\alpha_s(Q^2)$. Thus it imposes an important constraint upon the normalization of ϕ_π at arbitrary Q^2 when the amplitude is smooth and free of nodes in x_i, as might be expected for a ground-state wave function.

Similar analyses follow for K mesons $(f_\pi \to f_K$

$\simeq 112$ MeV) and for longitudinally polarized ρ mesons. In the latter case, a_0 is normalized using the decay $\rho \to e^+ e^-$. Defining $\langle 0 | J_{em}^\mu | \rho \rangle = \sqrt{2} m_\rho f_\rho \epsilon^\mu$ implies

$$a_0 = \frac{3}{\sqrt{n_c}} \sqrt{2} f_\rho, \tag{2.24b}$$

where $f_\rho \simeq 107$ MeV.

Finally, we can combine Eqs. (2.11), (2.12), (2.19), and (2.24) to obtain the QCD prediction for the π-γ transition form factor[21]:

$$F_{\pi\gamma}(Q^2) = \frac{2\sqrt{n_c}\,(e_u^2 - e_d^2)}{Q^2}$$

$$\times \sum_{n=0,2,4,\ldots} a_n \left(\ln \frac{Q^2}{\Lambda^2} \right)^{-\gamma_n} \left[1 + O\left(\alpha_s(Q^2), \frac{m^2}{Q^2} \right) \right]$$

$$\to 2(f_\pi/Q^2) \quad \text{as } Q^2 \to \infty. \tag{2.25}$$

Notice that because of boundary condition (2.21), the singularity in T_H [Eq. (2.12)] at $x_2 = 0$ does not result in additional factors of $\ln Q^2$. For this reason also we have replaced $\tilde{Q}$ by Q in (2.11) to leading order in $\alpha_s(Q^2)$. (The replacement $\tilde{Q} \to \langle x_i \rangle Q = Q/2$ is perhaps more appropriate; but again the difference is nonleading.)

Similar results apply for the η-γ form factor. Assuming SU(3) symmetry, we find [to all orders in $\alpha_s(Q^2)$]

$$\frac{F_{\eta\gamma}}{F_{\pi\gamma}} = \frac{1}{\sqrt{3}} \frac{e_u^2 + e_d^2 - 2e_s^2}{e_u^2 - e_d^2} = \frac{1}{\sqrt{3}}. \tag{2.26}$$

III. BEYOND LEADING LOGARITHMS

A. General formalism in light-cone gauge

The preceding analysis (Sec. II) for $F_{\pi\gamma}$ can be generalized to include terms of any order in $\alpha_s(Q^2)$. One source of such terms is the set of two-particle irreducible corrections to the hard-scattering amplitude T_H. As illustrated earlier, these involve only hard-loop momenta $(l_\perp \sim Q)$ and as such can be organized in a power series in $\alpha_s(Q^2)$ (see Appendix B).

Another set of terms corrects the approximation made in passing from Eqs. (2.4) to (2.5)—i.e., from $T\psi$ to $T_H\phi$. The difference between these equations is

$$(\epsilon_\perp \times q_\perp)\delta F_{\pi\gamma} \propto \int_0^1 [dx] \int \frac{d^2 k_\perp}{16\pi^3} \psi(x_i, k_\perp) \left[\frac{(q_\perp x_2 + k_\perp) \times \epsilon_\perp}{(q_\perp x_2 + k_\perp)^2} - \frac{q_\perp \times \epsilon_\perp}{x_2 q_\perp^2} \theta(\tilde{Q}^2 - k_\perp^2) + (1 \to 2) \right]. \tag{3.1}$$

Clearly only $k_\perp \sim x_i q_\perp$ or larger contribute. Since $k_\perp$ is large, we can use Eq. (2.16) to replace $\psi(x_i, k_\perp)$ by $SK_{1g}\phi$ (to leading order):

$$\delta F_{\pi\gamma} \propto \int_0^1 [dx] \int \frac{d^2 k_\perp}{16\pi^3} \{\cdots\} \frac{1}{-k_\perp^2/x_1 - k_\perp^2/x_2} \int_0^1 [dy] K_{1g}(x_i, k_\perp; y_i, 0_\perp)\phi(y_i, \tilde{Q})$$

$$\equiv \int_0^1 [dy]\delta T_H(y_i, Q)\phi(y_i, \tilde{Q})[1 + O(\alpha_s(Q^2))], \tag{3.2}$$
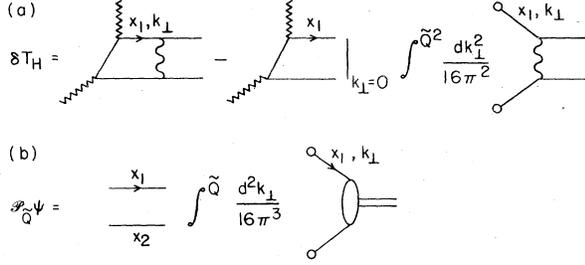
FIG. 7. (a) The $O(\alpha_s)$ correction to T_H due to the subtracted one-loop ladder diagram. (b) The collinear projection operator acting on the wave function $\psi(x_i, k_\perp)$.

where K_{1g} is the one-gluon-exchange kernel and $\tilde{Q} = \min_i(y_i Q)$. δT_H is then just the one-loop ladder correction to T_H, but with the low-$k_\perp$ region subtracted [Fig. 7(a)]. Once all vertices and propagators are renormalized, it is suppressed by $\alpha_s(Q^2)$ relative to T_H.

This analysis can be extended to arbitrary order in $\alpha_s(Q^2)$ and a similar analysis can be applied to the distribution amplitude ϕ. The procedure is to use perturbation theory wherever loop momenta are restricted to be large—restricted by an explicit subtraction for two-particle reducible loops or by the inherent properties of irreducible diagrams (in light-cone gauge) for the rest. Our ignorance about the theory at soft momenta ($k_\perp \ll \tilde{Q}$) is absorbed into the quark distribution amplitude ϕ, whose variation with increasing Q^2 is nevertheless well determined.

To facilitate this separation of hard from soft momenta, it is convenient to introduce a collinear projection operator which isolates the nonperturbative collinear region in two-particle reducible loops[22]:

$$\mathcal{P}_Q(k_\perp, l_\perp) \equiv 16\pi^2 \delta(k_\perp^2)\theta(Q^2 - l_\perp^2). \tag{3.3}$$

Notice that $\mathcal{P}_Q$ limits the flow of transverse momentum ($l_\perp^2 < Q^2$) through functions to the right and replaces them by a δ function. Applying $\mathcal{P}_Q$ to the wave function, for example, gives [Fig. 7(b)]

$$\mathcal{P}_Q\psi \equiv \int \frac{d^2l_\perp}{16\pi^3} \mathcal{P}_Q(k_\perp, l_\perp)\psi(x_i, l_\perp)$$

$$= 16\pi^2 \delta(k_\perp^2) \int^Q \frac{d^2l_\perp}{16\pi^3} \psi(x_i, l_\perp), \tag{3.4}$$

which up to a factor defines the distribution amplitude $\phi(x_i, Q)$. Replacing ψ by $\mathcal{P}_Q\psi$ is precisely the approximation made in going from Eqs. (2.4) to (2.5)—i.e., where quarks in the hadronic wave function are replaced by a collinear (on-shell) $q\bar{q}$ pair whose longitudinal momenta are weighted by the distribution amplitude: $T\psi \to T\mathcal{P}_Q\psi = T_H\phi$. We can express the exact wave function in terms of its soft component $\mathcal{P}_Q\psi$ through use of the bound-state

equation (A5):

$$\psi = \mathcal{P}_Q\psi + (1 - \mathcal{P}_Q)\psi = \mathcal{P}_Q\psi + (1 - \mathcal{P}_Q)SK\psi$$

$$= \mathcal{P}_Q\psi + G^{(Q)}K\mathcal{P}_Q\psi, \tag{3.5a}$$

where

$$G^{(Q)} = (1 - \mathcal{P}_Q)S \sum_{n=0}^{\infty} [K(1 - \mathcal{P}_Q)S]^n, \tag{3.5b}$$

and where S is the renormalized $q\bar{q}$ propagator. K is the sum of all two-particle irreducible kernels.

Notice, in Eq. (3.4), that $\mathcal{P}_Q\psi$ contains only momenta $l_\perp^2 < Q^2$. The region ($l_\perp^2 \gtrsim Q^2$) is included perturbatively in $G^{(Q)}$. Any two-particle reducible loop containing $(1 - \mathcal{P}_Q)$ is protected from collinear singularities—e.g.,

$$T(1 - \mathcal{P}_Q)\psi = \int \frac{d^2k_\perp}{16\pi^3} \frac{d^2l_\perp}{16\pi^3} T(k_\perp, q_\perp)$$

$$\times [16\pi^3\delta^2(k_\perp - l_\perp)$$

$$- 16\pi^2\delta(k_\perp^2)\theta(Q^2 - l_\perp^2)]\psi(l_\perp)$$

$$= \int \frac{d^2l_\perp}{16\pi^3}[T(l_\perp, q_\perp) - T(0, q_\perp)\theta(Q^2 - l_\perp^2)]\psi(l_\perp).$$

The exact π-γ form factor can now be written [from Eq. (3.5)]

$$F_{\pi\gamma}(Q^2) = \int [dx] \frac{d^2k_\perp}{16\pi^3} T(x_i, k_\perp, q_\perp)\psi(x_i, k_\perp)$$

$$= \int_0^1 [dx] T_H(x_i, Q)\phi(x_i, \tilde{Q}), \tag{3.6a}$$

where the general hard-scattering amplitude is defined as

$$T_H \equiv d_F(\tilde{Q})(T + TG^{(Q)}K)$$

$$= d_F(\tilde{Q})[T + T(1 - \mathcal{P}_{\tilde{Q}})SK$$

$$+ T(1 - \mathcal{P}_Q)SK(1 - \mathcal{P}_{\tilde{Q}})SK + \cdots] \tag{3.6b}$$

with the external quark legs having zero $k_\perp$ (and thus on shell when ignoring quark masses). The quark distribution amplitude is

$$\phi(x_i, Q) \equiv d_F^{-1}(Q) \int^{\tilde{Q}} \frac{d^2k_\perp}{16\pi^3} \psi(x_i, k_\perp). \tag{3.6c}$$

The factor $d_F(Q)$ is related to the renormalization of the quark field operator $[S_F(p) \to d_F(p)/\not{p}$ as $p^2 \to -\infty]$. In leading order it is $(\ln Q^2/\Lambda^2)^{\gamma_F/\beta}$.

The first term in T_H [Eq. (3.6b)] is, to leading order, just that given in Eq. (2.12). The correction δT_H [Eq. (3.2)] appears in (3.6b) as the dominant part of the second term: $T(1 - \mathcal{P}_{\tilde{Q}})SK \simeq T^{(0)}(1 - \mathcal{P}_{\tilde{Q}})SK_{1g}$. Notice that T_H includes all two-particle reducible and irreducible amplitudes for $\gamma^* + q\bar{q} \to \gamma$ with on-shell quarks. It is however "col-

linear irreducible" in the sense that the low momentum region of each two-particle reducible loop is removed by the subtractions involving $\mathcal{P}_Q$. Thus there are no collinear singularities as $k_\perp \to 0$ in the loop integrations of T_H. After renormalization, T_H is UV finite. It is free of infrared singularities as well, since the external particles are in color-singlet states. Consequently, all loop momenta $k_\perp^2$ in T_H are scaled by Q^2 (i.e., other scales such as infrared cutoffs can be set to zero since there are no divergences in T_H), and the hard-scattering amplitude has a power-series expansion in $\alpha_s(Q^2)$: $Q^2 T_H = f_0(x_i) + \alpha_s(Q^2)f_1(x_i) + \alpha_s^2(Q^2)f_2(x_i) + \cdots$ corresponding to $0, 1, 2, \ldots$ loop diagrams in the UV-finite skeleton expansion. In principle, end-point singularities in the x_i integrations [e.g., as $x_i \to 0$ in (2.11)] can generate additional factors of $\ln Q^2$. However, as we have seen, the wave function vanishes sufficiently quickly in this region to prohibit such terms (see also the discussion in Sec. IV).

Notice finally that T_H is always manifestly gauge invariant to leading order, since it is a renormalized Born amplitude with its external (constituent) lines all on shell. Thus it can be computed in any convenient gauge using either light-cone perturbation theory or covariant perturbation theory. It is possible to make T_H gauge invariant to all orders in α_s by slightly redefining the factors $d_F(Q)$ appearing in Eqs. (3.6), but this is of little practical value.

An exact evolution equation for $\phi(x_i, Q)$ is derived by differentiating (3.6c) with respect to Q^2:

$$Q^2 \frac{\partial}{\partial Q^2} \phi(x_i, Q) = \left[Q^2 \frac{d}{dQ^2} \ln d_F^{-1}(Q) \right] \phi(x_i, Q) + \frac{d_F^{-1}(Q)}{16\pi^2} \psi(x_i, q_\perp) Q^2 .$$

The Callan-Symanzik equation for $d_F(Q)$ can be written

$$Q^2 \frac{d}{dQ^2} \ln d_F^{-1}(Q) = -\bar{\gamma}(\alpha_s(Q^2)), \qquad (3.7)$$

where $\bar{\gamma} = (\alpha_s(Q^2)/4\pi)\gamma_F + \cdots$.[23] Generalizing our earlier analysis, we can rewrite $\psi(x_i, q_\perp)$ in terms of ϕ by combining the bound-state equation (A5) with Eqs. (3.5):

$$\frac{d_F^{-1}(Q)}{16\pi^2} Q^2 \psi(x_i, q_\perp) = \frac{d_F^{-1}(Q)}{16\pi^2} Q^2 (SK\psi)$$

$$= \frac{d_F^{-1}(Q)}{16\pi^2} Q^2 (SK + SKG^{(Q)}K)\mathcal{P}_Q \psi$$

$$\equiv \frac{\alpha_s(Q^2)}{4\pi} \int_0^1 [dy] V(x_i, y_i, \alpha_s(Q^2))$$
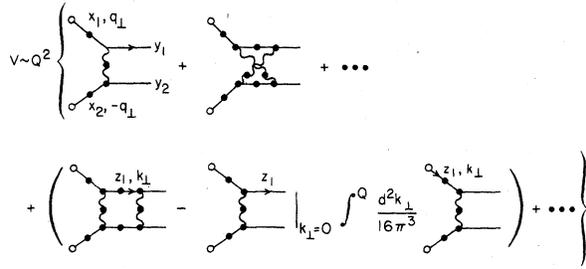
$$\times \phi(y_i, Q) .$$

FIG. 8. Terms contributing to the potential in the evolution equation; each diagram has several time orderings, all of which contribute.

Thus the general evolution equation is

$$Q^2 \frac{\partial}{\partial Q^2} \phi(x_i, Q)$$

$$= \frac{\alpha_s(Q^2)}{4\pi} \left[\int_0^1 [dy] V(x_i, y_i, \alpha_s(Q^2))\phi(y_i, Q) - \bar{\gamma}(\alpha_s(Q^2))\phi(x_i, Q) \right], \qquad (3.8)$$

where $V = V^{(1)}(x_i, y_i) + \alpha_s(Q^2)V^{(2)}(x_i, y_i) + \cdots$ has contributions from all two-particle irreducible kernels as well as subtracted reducible kernels (as in T_H; see Fig. 8)—i.e., V is collinear irreducible.

Notice that ϕ has contributions only from terms in the wave function having orbital angular momentum $L_z = 0$. All other terms vanish after the angular integration in (3.6c). The leading contributions from $L_z \neq 0$ terms are obtained by expanding the $q\bar{q} + \gamma^* \to \gamma$ amplitude in powers of $k_\perp \cdot q_\perp/q_\perp^2$, which has $L_z = \pm 1$ with respect to the $k_\perp$ integration. These are then suppressed by $1/Q$ or more and can be ignored.

As mentioned earlier, $\phi(x_i, Q)$ can also be studied via the renormalization group and the operator-product expansion of $T\psi(0)\bar{\psi}(z)$ with $z^+ = 0$, $z^2 = -z_\perp^2$
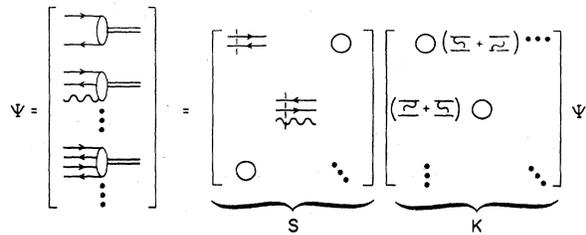

FIG. 9. Coupled bound-state wave equation for multiparton Fock states.

$\sim 1/Q^2 \to 0$ (Ref. 5):

$$T\psi(0)\overline{\psi}(z) = \sum_{\substack{m \geq n \\ i}} C_n^i (z^2 - i\epsilon) z^{\mu_1} \cdots z^{\mu_m} \Gamma^{(i)} \sum_{k=0}^{n} d_{mnk} \partial_{\mu_{k+1}} \cdots \partial_{\mu_m} [\overline{\psi}(0)\Gamma^{(i)}\overline{D}_{\mu_1} \cdots \overline{D}_{\mu_n}\psi(0)] + \cdots, \qquad (3.9)$$

where $\Gamma^{(i)} = \{1, \gamma_5, \gamma_\mu, \gamma_\mu\gamma_5, \sigma_{\mu\nu}\}$. In general, this expansion includes operators having explicit factors of the gluon field. However, these do not contribute to the wave function $\langle 0| T\psi(0)\overline{\psi}(z)|\pi\rangle_{z^+ \to 0}$ since $\langle 0|\overline{\psi}(0) \cdots A_\nu \cdots \psi(0)|\pi\rangle \propto \eta_\nu$ in light-cone gauge $\eta \cdot A = A^+ = 0$ (the only other vector available is p_π, but $p_\pi^+ \neq 0$), and $\eta \cdot z = z^+ = 0$. Fourier transforming (3.9), we obtain

$$\phi(x_i, Q) = \sum_{n=0}^{\infty} a_n \phi_n(x_i, \alpha_s(Q^2)) \overline{C}_n(Q^2), \qquad (3.10)$$

where, as we found above, $\phi_n = x_1 x_2 C_n^{3/2}(x_1 - x_2) + O(\alpha_s(Q^2))$ and $\overline{C}_n(Q^2) = (\ln Q^2/\Lambda^2)^{-\gamma_n}[1 + O(\alpha_s(Q^2))]$. For pions, the anomalous dimension of $\overline{C}_n(Q^2)$ is that associated with the operator $\overline{\psi}(0)\gamma_\mu\gamma_5\overline{D}_{\mu_1} \cdots \overline{D}_{\mu_n}\psi(0)$. For longitudinally and transversely polarized ρ mesons, $\gamma_\mu\gamma_5$ is replaced by γ_μ and $\sigma_{\mu\nu}$, respectively. The evolution equation (3.8) is formally equivalent to the Callan-Symanzik equations for each term in (3.10).

B. General gauges—Fock-state decomposition

We required only the $q\overline{q}$ wave function in Sec. II. This is not the case in general gauges, where it becomes convenient to represent a hadron by an infinite column vector Ψ of wave functions—one for each of the Fock states $q\overline{q}, q\overline{q}g, \ldots$ in the meson, for example. In general, Ψ satisfies a bound-state equation $\Psi = SK\Psi$, which is an infinite set of coupled equations where the matrix K is the completely irreducible kernel and S_{nn} is the n-particle propagator (Fig. 9). In complete analogy to the $q\overline{q}$ analysis just completed, we can define a projection operator which isolates the nonperturbative region in the n-particle intermediate state:

$$\mathcal{O}_Q^n = \prod_{j=1}^{n-1} 16\pi^2 \delta(k_{\perp j}^2) \theta\left(Q - \sum_j |l_{\perp j}|\right). \qquad (3.11)$$

We can then systematically reduce $F_{\pi\gamma}$ to the form $F_{\pi\gamma} = T_H^{(q\overline{q})}\phi_{q\overline{q}} + T_H^{(q\overline{q}g)}\phi_{q\overline{q}g} + \cdots$ where the hadronic distribution amplitudes, defined in analogy to (3.6c), satisfy evolution equations.

The first term in this series is precisely that described in the previous section. In light-cone gauge, the remaining terms are suppressed by powers of $1/Q$. For example, the leading hard-scattering amplitude for the $qq\overline{q}\overline{q}$ state includes diagrams such as in Fig. 10(a) which fall as $1/Q^4$ because of the additional propagators. Similarly, the $q\overline{q}g$ contribution to $F_{\pi\gamma}$ includes [Fig. 10(b)]

$$F_{\pi\gamma}^{(q\overline{q}g)} \sim \int [dx] \frac{\overline{u}(1 - x_3, q_\perp)\gamma_\mu u(x_1, q_\perp)}{((1 - x_1)^2 Q^2)(x_3 Q^2)} \phi_{q\overline{q}g}^\mu(x_i, x_i Q), \qquad (3.12a)$$

where the leading-order distribution amplitude is

$$\phi^\mu(x_i, Q) = \left(\ln \frac{Q^2}{\Lambda^2}\right)^{-\gamma_F/\beta} \int^Q \prod_{i=1}^{2} d^2 k_{\perp i} d^{\mu\nu} \psi_\nu(x_i, k_{\perp i}), \qquad (3.12b)$$

and $d^{\mu\nu}$ is the gluon's polarization sum. The only vertices entering in (3.12a) are $\overline{u}\gamma^+u$ and $\overline{u}\gamma_\perp u$ since $d^{+\nu} = 0$ in light-cone gauge. There is then at most a factor $q_\perp$ in the numerator (and even this results in a factor $k_\perp \cdot q_\perp$ which integrates to zero). Thus $F_{\pi\gamma}^{(q\overline{q}g)}$ falls faster by $1/Q^2$ than $F_{\pi\gamma}^{(q\overline{q})}$ as computed earlier. Clearly adding further gluons to the Fock state leads to additional factors of $1/Q$ or $1/Q^2$ for each gluon.

Notice, however, that $d^{+\nu}$ does not vanish in general covariant gauges, and longitudinally polarized gluons (i.e., A^+) can couple to T_H via the vertex $\overline{u}\gamma^- u \sim q^- = q_\perp^2$ ($\gg q^+, q_\perp$). For this polarization, the numerator in (3.12a) cancels one power of Q^2 in the denominator so that $F_{\pi\gamma}^{(q\overline{q}g)} \sim 1/Q^2$ and is no longer suppressed. Indeed, Fock states having any number of longitudinally polarized gluons contribute to leading order in $F_{\pi\gamma}$ in such gauges. Just this problem is avoided by selecting a gauge in which virtual gluons have only physical polarizations—i.e., $\eta \cdot A = A^+ = 0$ gauge. We illustrate in Appendix C how this problem is overcome for covariant gauges through use of collinear Ward identities.

IV. ELECTROMAGNETIC FORM FACTORS OF HADRONS

A. Mesons

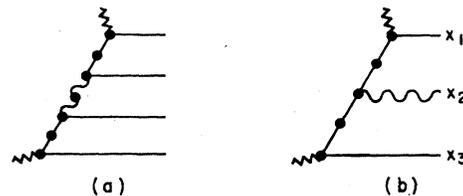Following the prescription set out in Sec. III, we can reduce the pion's electromagnetic form

FIG. 10. Hard-scattering amplitudes for nonvalence Fock states.

factor to the form

$$F_\pi(Q^2) = \int_0^1 [dx][dy] \int \frac{d^2k_\perp d^2l_\perp}{(16\pi^3)^2} \psi^*(y_i, l_\perp)$$

$$\times T(x_i, y_i, k_\perp, l_\perp, q_\perp)\psi(x_i, k_\perp)$$

$$= \int_0^1 [dx][dy]\phi^*(y_i, \tilde{Q}_y)T_H(x_i, y_i, Q)\phi(x_i, \tilde{Q}_x),$$

(4.1)

where T contains all two-particle irreducible amplitudes for $\gamma^* + q\bar{q} \to q\bar{q}$; and where the hard-scattering amplitude is $[\tilde{Q}_y = \min(y_i Q), \quad \tilde{Q}_x = \min(x_i Q)]$

$$T_H = d_F(\tilde{Q}_y)[T + T(1 - \mathcal{P}_{\tilde{Q}_x})SK + KS(1 - \mathcal{P}^\dagger_{\tilde{Q}_y})T$$

$$+ KS(1 - \mathcal{P}^\dagger_{\tilde{Q}_y})T(1 - \mathcal{P}_{\tilde{Q}_x})SK + \cdots]d_F(\tilde{Q}_x).$$

(4.2)

Here the collinear projection operators $\mathcal{P}^\dagger_{\tilde{Q}}$ and $\mathcal{P}_{\tilde{Q}}$ act to the left and right, respectively, and, in analogy to (3.6), the initial and final mesons are replaced by collinear $q\bar{q}$ pairs. The disconnected diagrams in T make no contribution to the first term in (4.2) because $\mathcal{P}^\dagger_{\tilde{Q}} T \mathcal{P}_{\tilde{Q}} \to 0$ when the quark lines are not connected. [For example, in Fig. 11(a), the incoming and outgoing $q\bar{q}$ pairs can only be collinear (i.e., $k_\perp = k_\perp + x_2 q_\perp = 0$) when $x_2 = 0$, at which point $\phi(x_i, \tilde{Q}_x)$ vanishes.] Thus the lowest-order contribution comes from one-gluon exchange in the second and third terms of (3.4) [Fig. 11(b)]:

$$T_H(x_i, y_i, Q) = \frac{16\pi C_F \alpha_s(Q^2)}{Q^2}\left[\frac{e_1}{x_2 y_2} + \frac{e_2}{x_1 y_1}\right]$$

$$\times [1 + O(\alpha_s(Q^2), m/Q)],$$

(4.3)

where e_1 and e_2 are the charges carried by particles 1 and 2 (in units of e). As for $F_{\pi\gamma}$, the boundary condition (2.21) on ϕ implies that there is no singularity in (4.1) at y_i or $x_i \sim 0$. Consequently, in leading order, we can replace $\tilde{Q}_x$ and $\tilde{Q}_y$ by Q in (4.1) to obtain the QCD prediction for the pion form factor [from Eq. (2.19) with $\delta_{h_1 \bar{h}_2} = 1$] (Refs.

1, 10, and 13)

$$F_\pi(Q^2) = \frac{4\pi C_F \alpha_s(Q^2)}{Q^2}\left|\sum_{n=0,2,4,\dots} a_n\left(\ln\frac{Q^2}{\Lambda^2}\right)^{-\gamma_n}\right|^2$$

$$\times [1 + O(\alpha_s(Q^2), m/Q)].$$

(4.4)

The $n = 0$ term dominates as Q^2 becomes very large and we obtain [Eq. (2.24)] (Refs. 14, 1, and 10)

$$F_\pi(Q^2) \to 16\pi\alpha_s(Q^2)(f_\pi^2/Q^2).$$

(4.5)

Figure 12 illustrates predictions for $Q^2 F_\pi$ given three different initial wave functions at $Q_0^2 = 2$ GeV^2:

   (a) $\phi(x_i, Q_0) \propto x_1 x_2$,

   (b) $\phi(x_i, Q_0) \propto \delta(x_i - \frac{1}{2})$,

   (c) $\phi(x_i, Q_0) \propto (x_1 x_2)^{1/4}$,

with representative values of the QCD scale parameter Λ^2. In each case the normalization is uniquely determined by sum rule (2.24a); all curves ultimately converge to the asymptotic limit (4.5) [i.e., Fig. 12(a)]. For Fig. 12, we have multiplied (4.4) by $(1 + m_\rho^2/Q^2)^{-1}$ to allow a smooth connection with the low-Q^2 behavior suggested by
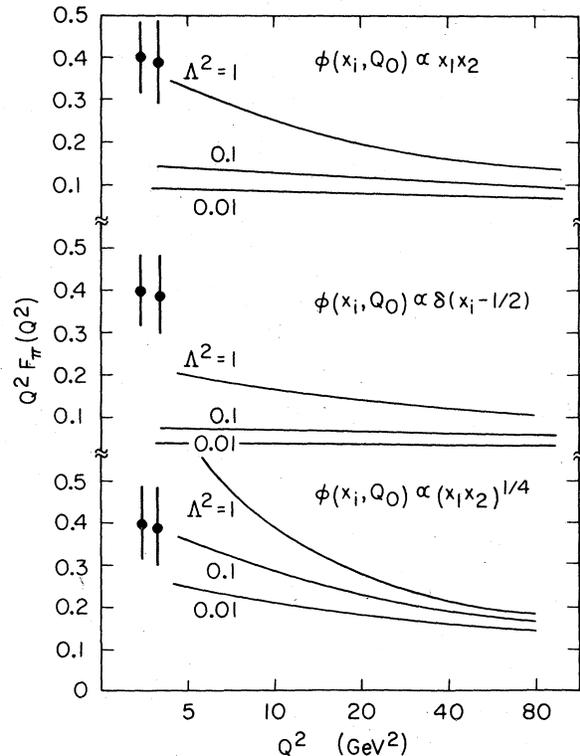
FIG. 12. QCD predictions for the pion form factor assuming various distribution amplitudes $\phi(x_i, Q_0)$ at $Q_0^2 = 2$ GeV^2 and various values of the QCD scale parameter Λ^2. The data are from the analysis of electroproduction $e^- p \to e^- + \pi^+ + n$; C. Bebek *et al.*, Ref. 24.
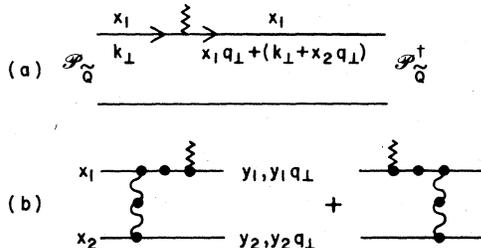
FIG. 11. Leading terms contributing to T_H for the pion form factor. Disconnected diagrams (a) vanish when sandwiched between collinear projection operators.

vector dominance models.

The behavior exhibited in Fig. 12 can be radically modified if $\phi(x_i, Q_0)$ has nodes or other complex structure in x_i. However, such behavior is unlikely for ground-state mesons such as the pion. For these, one intuitively expects a smooth, positive-definite distribution amplitude, peaked about $x_1, x_2 \sim \frac{1}{2}$. Given these constraints, the normalization of $F_\pi(Q^2)$ is largely determined by the breadth of the distribution—broad distributions [Fig. 12(c)] result in a large form factor, narrow distributions [Fig. 12(b)] in a small one. The magnitude of the form factor also depends to some extent upon the scale parameter Λ^2 through the factor $\alpha_s(Q^2)$ in (4.4).

Notice that we can completely remove dependence upon the distribution amplitude by comparing $F_{\pi\gamma}$ to F_π [Eqs. (2.25) and (4.4)]. In fact, a measurement of each provides a direct determination of $\alpha_s(Q^2)$:

$$\alpha_s(Q^2) = \frac{n_c(e_u^2 - e_d^2)^2}{\pi C_F} \frac{F_\pi(Q^2)}{Q^2 |F_{\pi\gamma}(Q^2)|^2} + O(\alpha_s^2(Q^2))$$

$$= \frac{1}{4\pi} \frac{F_\pi(Q^2)}{Q^2 |F_{\pi\gamma}(Q^2)|^2} + O(\alpha_s^2(Q^2)). \quad (4.6)$$

The electromagnetic form factors of K^+ mesons and longitudinally polarized ρ^+ mesons follow from the same analysis but with f_π replaced in the sum

rule by f_K and $\sqrt{2}f_\rho$, respectively [Eqs. (2.24)]. If the quark distribution amplitudes for these different mesons are similar in shape, the ratios of π to K to ρ_L form factors should be approximately $f_\pi^2 : f_K^2 : 2f_\rho^2 \sim 1 : 1.5 : 2.5$ for Q^2 large (becoming exact as $Q^2 \to \infty$).

An important constraint on the nature of the distribution amplitude for K mesons can be obtained from the K_L-K_S transition form factor which is measurable at large timelike Q^2 in the reaction $e^+e^- \to K_L K_S$. The K^0 wave function analogous to (2.3) is

$$\Psi_{K^0} = \frac{\delta_{ba}}{\sqrt{n_c}} \frac{1}{\sqrt{2}} \{d_\downarrow \bar{s}_\uparrow - d_\uparrow \bar{s}_\downarrow\} \frac{\Psi_{K^0}(x_i, k_\perp)}{(x_s x_d)^{1/2}},$$

where, because of the large m_s/m_d ratio, Ψ_{K^0} need not be symmetric in $x_s \leftrightarrow x_d$. Since T_H conserves flavor, we have

$$\langle K_L | J^\mu(0) | K_S \rangle \equiv \left\langle \frac{K^0 - \bar{K}^0}{\sqrt{2}} \middle| J^\mu(0) \middle| \frac{K^0 + \bar{K}^0}{\sqrt{2}} \right\rangle$$

$$= \langle K^0 | J^\mu(0) | K^0 \rangle.$$

The transition form factor $F_{K_S - K_L}(Q^2)$ at large Q^2 can then be written in the form of Eq. (4.1) with

$$T_H(x_i, y_i, Q) = \frac{16\pi \alpha_s(Q^2) C_F}{Q^2} \left[\frac{e_{\bar{s}}}{x_d y_d} + \frac{e_d}{x_{\bar{s}} x_{\bar{s}}} \right],$$

and thus [using the expansion (2.19)]

$$F_{K_S - K_L}(Q^2) = \left(\frac{1}{3}\right) \frac{16\pi \alpha_s(Q^2) C_F}{Q^2} \left[\left| \int [dx] \frac{\phi(x_i, \bar{Q})}{x_d} \right|^2 - \left| \int [dx] \frac{\phi(x_i, \bar{Q})}{x_{\bar{s}}} \right|^2 \right]$$

$$= \left(\frac{1}{3}\right) \frac{8\pi \alpha_s(Q^2) C_F}{Q^2} \left[\sum_{n(\text{even})} \sum_{m(\text{odd})} a_n^* a_m \left(\ln \frac{Q^2}{\Lambda^2} \right)^{-\gamma_n - \gamma_m} + \text{H.c.} \right] [1 + O(\alpha_s(Q^2), m/Q)].$$

Thus the form factor requires the odd (asymmetric under $x = x_d - x_{\bar{s}} \to -x$) Gegenbauer components of the K^0 distribution amplitude. Asymptotically, the transition form factor vanishes with an extra anomalous dimension

$$\frac{F_{K_S - K_L}(Q^2)}{F_{K^+}(Q^2)} \underset{Q^2 \to \infty}{=} (\tfrac{4}{3}) \text{Re} \left(\frac{a_1}{a_0} \right) \left(\ln \frac{Q^2}{\Lambda^2} \right)^{\gamma_1},$$

where $\gamma_1 = \frac{8}{3}(C_F/\beta)$ ($\cong 0.4$ for $n_f = 3$). If this ratio of form factors is indeed appreciable (i.e., of order 1), then the odd, asymmetric components play a major role in the structure of the kaon wave function. This would also imply a strong violation of the relation $F_{\rho^+}(Q^2)/F_{K^+}(Q^2) \cong f_\pi^2/f_K^2$ at subasymptotic Q^2. All of these results can, of course, be extended to mesons containing heavy quarks.[25]

As for $F_{\pi\gamma}$, quark helicity is conserved at each vertex in T_H, which is then diagonal in (hadronic) helicity up to corrections of order m/Q. Consequently, there are two selection rules restricting

the helicities of initial (h_i) and final (h_f) hadrons[26]:

(a) $\Delta h = h_f - h_i = 0$ (for timelike photon: $h_1 = -h_2$),

(b) $|h| = |h_{i,f}| \leq \frac{1}{2}$. $\quad (4.7)$

The second rule is easily derived from the first in the Breit frame. There the net change in the hadron's angular momentum along the direction of motion is $\Delta J_z = -h_f - h_i = -2h$, because the helicity is unchanged while the momentum is reversed. As the photon has spin 1, only $|h| \leq \frac{1}{2}$ is permitted, up to corrections of $O(m/Q)$.

Applying these selection rules to e^+e^- collisions beyond the resonance region, for example, we find that the final states $\pi\rho$, $\rho_L\rho_\perp$, $\rho_\perp\rho_\perp$ are suppressed by $\sim m^2/Q^2$ (in the cross section) relative to $\pi\pi$, KK, and $\rho_L\rho_L$ final states.

The selection rules are direct consequences of the vector nature of the gluon. In contrast, $e^+e^- \to \rho_\perp\rho_\perp$ is not suppressed in a theory with scalar gluons. Furthermore, while each of the "allowed"

form factors is positive at large Q^2 in QCD, they are negative in scalar gluon theories, and then must vanish at some finite Q^2 [since $F(0)=1$]. Scalar theories are probably already ruled out by existing data.

B. Baryons

Again from Sec. III, the baryon's electromagnetic form factor has the form

$$\phi(x_i, Q) = \left(\ln\frac{Q^2}{\Lambda^2}\right)^{-3\gamma_F/2\beta} \int^Q \prod_{i=1}^{3}\left(\frac{d^2 k_\perp^{(i)}}{16\pi^3}\right)16\pi^3\delta^2\left(\sum_i k_\perp^{(i)}\right)\psi(x_i, k_\perp^{(i)}),$$

(4.9)

where, as before, the factor $(\ln Q^2/\Lambda^2)^{-3\gamma_F/2\beta}$ is due to UV radiative corrections in T_H. We can derive an evolution equation for ϕ in direct analogy with the analysis of mesons. Indeed, since in leading order only pairwise interactions occur between quarks [Fig. 13(b)], the evolution equation follows immediately from Eq. (2.17):

$$x_1 x_2 x_3\left[\frac{\partial}{\partial\xi}\tilde{\phi}(x_i, Q) + \frac{3}{2}\frac{C_F}{\beta}\tilde{\phi}(x_i, Q)\right]$$

$$= \frac{C_B}{\beta}\int_0^1 [dy]V(x_i, y_i)\tilde{\phi}(y_i, Q).$$ (4.10a)

Here $\phi = x_1 x_2 x_3\tilde{\phi}$, $\xi = \ln\ln(Q^2/\Lambda^2)$, and

$$V(x_i, y_i) = 2x_1 x_2 x_3\sum_{i\neq j}\theta(y_i - x_i)\delta(x_k - y_k)$$

$$\times\frac{y_i}{x_j}\left(\frac{\delta_{h_i h_j}}{x_i + x_j} + \frac{\Delta}{y_i - x_i}\right)$$

$$= V(y_i, x_i)$$ (4.10b)

is the sum over interactions between quark pairs $\{i, j\}$ due to exchange of a single gluon [$C_B \equiv (n_c + 1)/2n_c = \frac{2}{3}$]. The infrared singularity at $x_i = y_i$ is canceled [recall $\Delta\tilde{\phi}(y_i, Q) \equiv \tilde{\phi}(y_i, Q) - \tilde{\phi}(x_i, Q)$] because the baryon is a color singlet. The evolution has a general solution of the form (see Appendix D)

$$\phi(x_i, Q) = x_1 x_2 x_3\sum_{n=0}^{\infty} a_n\phi_n(x_i)\left(\ln\frac{Q^2}{\Lambda^2}\right)^{-\gamma_n}$$

$$\rightarrow C x_1 x_2 x_3 \times\begin{cases}\left(\ln\dfrac{Q^2}{\Lambda^2}\right)^{-2/3\beta}, & |h| = \frac{1}{2}, \\[2mm] \left(\ln\dfrac{Q^2}{\Lambda^2}\right)^{-2/\beta}, & |h| = \frac{3}{2},\end{cases}$$

(4.11)

where the leading $\tilde{\phi}_n$, γ_n are given in Table I, and h is the total quark helicity (= hadron's helicity since $L_z = 0$). However, in practice it is generally more efficient to integrate (4.10) numerically rather than expanding ϕ as in (4.11).

The most general electromagnetic vertex for a

$$F_B(Q^2) = \int_0^1 [dx][dy]\phi^*(x_i, \tilde{Q}_x)T_H(x_i, y_i, Q)\phi(y_i, \tilde{Q}_y),$$

(4.8)

where in leading order T_H is the minimally connected amplitude for $\gamma^* + 3q \rightarrow 3q$ [Fig. 13(a)], and $[dx] \equiv dx_1 dx_2 dx_3\delta(1 - \sum_i x_i)$. The distribution amplitude is the three-quark wave function integrated over transverse momenta $k_\perp^{(i)2} \lesssim Q^2$:

nucleon is

$$\Gamma^\mu = e\bar{u}(p')\left[\gamma^\mu G_M(Q^2) - \frac{(p+p')^\mu}{2M}F_2(Q^2)\right]u(p),$$

(4.12)

where G_M and F_2 correspond to helicity-conserving and helicity-flip parts of Γ^μ, respectively (for large p, p'). The magnetic form factor G_M is given by Eq. (4.8) with hard-scattering amplitude[1,27]

$$T_H = 64\pi^2\left(\frac{C_B\alpha_s(Q^2)}{Q^2}\right)^2\left[\sum_{j=1}^{3}e_j T_j(x_i, y_i) + (x_i \leftrightarrow y_i)\right],$$

(4.13a)

where (particle 2 has opposite helicity)

$$T_1 = T_3(1 \leftrightarrow 3) = -\frac{1}{x_3(1-x_1)^2}\frac{1}{y_3(1-y_1)^2}$$

$$-\frac{1}{x_2(1-x_1)^2}\frac{1}{y_2(1-y_1)^2}$$

$$+\frac{1}{x_2 x_3(1-x_3)}\frac{1}{y_2 y_3(1-y_1)},$$

(4.13b)

$$T_2 = -\frac{1}{x_1 x_3(1-x_1)}\frac{1}{y_1 y_3(1-y_3)},$$

and e_j is the electric charge (in units of e) of particle j. The hard-scattering amplitude T_H for form factors is most easily computed in the Breit frame ($\vec{p}_3' = -\vec{p}_3$) using Feynman gauge. [Recall
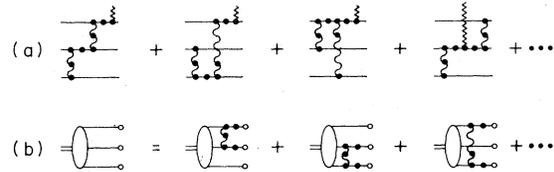

FIG. 13. (a) Diagrams contributing to T_H for baryonic form factors. (b) Bound-state equation for the baryon's three-quark wave function at large momenta.

that T_H is defined with its external lines on shell (for $m=0$) and is thus both gauge and Lorentz invariant.] Only the diagrams in Fig. 13(a) contribute.

The $\{e_j\}$ are determined by the flavor spin structure of the nucleon's distribution amplitude. The most general distribution amplitude for the proton is $(h=\frac{1}{2})$ (Ref. 28)

$$\phi_p = \left\{ \left[\frac{d_\uparrow(1)u_\uparrow(3) + u_\uparrow(1)d_\uparrow(3)}{\sqrt{6}} u_\downarrow(2) - (\tfrac{2}{3})^{1/2} u_\uparrow(1)d_\uparrow(2)u_\downarrow(3) \right] \phi^S(x_i, Q) \right.$$

$$\left. + \left[\frac{d_\uparrow(1)u_\uparrow(3) - u_\uparrow(1)d_\uparrow(3)}{\sqrt{2}} u_\downarrow(2) \right] \phi^A(x_i, Q) \right\} + (1 \leftrightarrow 2) + (2 \leftrightarrow 3). \tag{4.14}$$

Amplitude ϕ^S must be symmetric under interchange $x_1 \leftrightarrow x_3$, and ϕ^A antisymmetric, by Fermi statistics, since the color wave function $\epsilon_{abc}/\sqrt{n_c}$ is totally antisymmetric. The neutron's amplitude is $\phi_n = -\phi_p(u \leftrightarrow d)$ in the limit of exact isospin symmetry. From (4.11), ϕ^A becomes negligible as $Q^2 \to \infty$, and ϕ^S becomes totally symmetric under particle exchange. Consequently, the flavor-spin structure of (4.12) tends asymptotically to that assumed in the SU(6)-symmetric quark model.[29]

Convoluting (4.13) with (4.14), we obtain the prediction in QCD for $G_M(Q^2)$ (Ref. 1):

$$G_M(Q^2) = \frac{32\pi^2}{9} \frac{\alpha_s^2(Q^2)}{Q^4} \sum_{n,m} b_{nm} \left(\ln \frac{Q^2}{\Lambda^2} \right)^{-\gamma_n - \gamma_m} [1 + O(\alpha_s(Q^2), m^2/Q^2)]$$

$$\to \frac{32\pi^2}{9} C^2 \frac{\alpha_s^2(Q^2)}{Q^4} \left(\ln \frac{Q^2}{\Lambda^2} \right)^{-4/3\beta} (-e_{\text{-}\|}), \tag{4.15}$$

where $e_\|$ ($e_{\text{-}\|}$) is the mean total charge of quarks with helicity parallel (antiparallel) to the nucleon's helicity (in the fully symmetric flavor-helicity wave function). For protons and neutrons we have [Eq. (4.14)]

$$e_\|^p = 1, \quad e_{\text{-}\|} = 0, \quad e_\|^n = -e_{\text{-}\|}^n = -\tfrac{1}{3}.$$

TABLE I. Eigensolutions of the evolution Eq. (4.10) for $|h| = \frac{1}{2}$ ($\tilde{\phi}^{\prime\prime\prime}$) and $|h| = \frac{3}{2}$ ($\tilde{\phi}^{\prime\prime\prime}$) baryons. The procedure for systematically determining all $\tilde{\phi}_n$ is given in Appendix D.

	b_n	N	$a_{00}^{(n)}$	$a_{10}^{(n)}$	$a_{01}^{(n)}$	$a_{20}^{(n)}$	$a_{11}^{(n)}$	$a_{02}^{(n)}$
$\tilde{\phi}_n^{\prime\prime\prime}$	-1	120	1					
	$\tfrac{2}{3}$	1260		1	-1			
	1	420	2	-3	-3			
	$\tfrac{5}{3}$	756	2	-7	-7	8	4	8
	$\tfrac{7}{3}$	34020		1	-1	$-\tfrac{4}{3}$		$\tfrac{4}{3}$
	$\tfrac{5}{2}$	1944	2	-7	-7	$\tfrac{14}{3}$	14	$\tfrac{14}{3}$
$\tilde{\phi}_n^{\prime\prime\prime}$	0	120	1					
	$\tfrac{3}{2}$	420	1	-3				
	$\tfrac{3}{2}$	420	1		-3			
	$\tfrac{7}{3}$	5760	1	$-\tfrac{7}{2}$	$-\tfrac{7}{2}$	$\tfrac{7}{2}$	$\tfrac{7}{2}$	$\tfrac{7}{2}$
	$\tfrac{17}{6}$	3024	1	$-\tfrac{7}{2}$	$-\tfrac{7}{2}$	2	8	2
	$\tfrac{17}{6}$	34020	1		-1	$-\tfrac{4}{3}$		$\tfrac{4}{3}$

$$\gamma_n = \left(2b_n C_B + \tfrac{3}{2} C_F \right) / \beta \qquad \tilde{\phi}_n = \sqrt{N} \sum_{i,j} a_{ij}^{(n)} x_1^{\,i} x_3^{\,j}$$

The constants b_{nm}, C are generally unknown for baryons; however, by isospin symmetry, they are equal for protons and neutrons, and thus QCD predicts the ratios of form factors as $Q^2 \to \infty$.

Figure 14(a) illustrates the predictions for $Q^4 G_M^p(Q^2)$ assuming a wave function $\phi(x_i, Q_0)$ $\propto \delta(x_1 - \tfrac{1}{3}) \delta(x_2 - \tfrac{1}{3})$ at $Q_0^2 = 2$ GeV^2 (the absolute normalization is undetermined) and various values of the QCD scale parameter. Again we include an extra factor $(1 + m_\rho^2/Q^2)^{-2}$ in (4.15) to allow a smooth connection with data at low Q^2. Similar curves are obtained for any reasonably smooth distribution amplitude $\phi(x_i, Q_0)$. Only the ratio $G_M^p(Q^2)/G_M^n(Q^2)$ is particularly sensitive to the shape of the distribution amplitude. For illustration, this ratio is plotted versus η in Fig. 14(b) where $\phi(x_i, Q) = (x_1 x_2 x_3)^\eta$ is assumed for a given Q^2. For each choice of η, the ratio decreases to zero with increasing Q^2 as $(\ln Q^2/\Lambda^2)^{\gamma_0 - \gamma_3} = (\ln Q^2/\Lambda^2)^{-32/9\beta}$. The ratio $G_M^p/G_M^n = -1$ at Q_0^2 for the δ-function distribution amplitude used in Fig. 14(a). For comparison, note that in a theory with scalar or pseudoscalar gluons, diagrams in which the struck quark has antiparallel helicity vanish. Thus scalar QCD predicts a ratio $G_M^p/G_M^n \to e_\|^p/e_\|^n = -3$ independent of the distribution amplitude (assuming only symmetry under exchange $x_1 \leftrightarrow x_3$).

As for mesons [Eq. (4.7)], form factors for processes in which the baryon's helicity is changed ($\Delta h \neq 0$), or in which the initial or final baryon has $|h| > 1$, are suppressed by factors of m/Q, where m is an effective quark mass. Thus the helicity-flip nucleon form factor is predicted to fall roughly as $F_2 \sim mM/Q^6$, and the elastic ep and
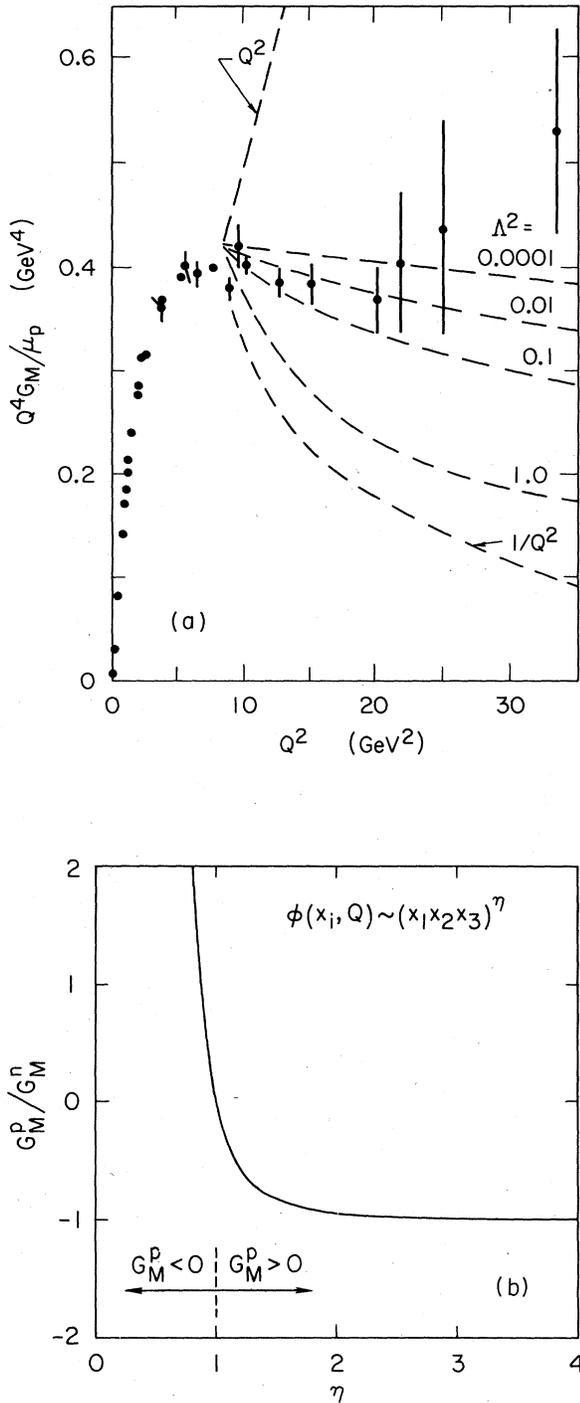
en cross sections become $(-t = Q^2 \to \infty)$

$$\frac{d\sigma}{dt} \to \frac{4\pi\alpha^2}{t^2}\left[\frac{s^2 + u^2}{2s^2}\right]G_M{}^2(-t) \, . \tag{4.16}$$

Cross sections for transitions such as $ep \to e\Delta$ $(|h_\Delta| = \frac{1}{2})$ are also given by Eq. (4.16) [with G_M as in (4.15) but with $C^2 \to C_p C_\Delta$]. Cross sections with $|h_\Delta| = \frac{3}{2}$ are suppressed (by m^2/t). The reaction $e^+ e^- \to \Delta^+ \Delta^-$ is dominated by baryons with $|h_\Delta| = \frac{1}{2}$; the cross section for production of $|h_\Delta| = \frac{3}{2}$ pairs or deltas with $|h_\Delta| = \frac{3}{2}$ and $\frac{1}{2}$ is suppressed. Again most of these predictions test the spin of the gluon. For example, transitions $ep \to e\Delta$ $(|h_\Delta| = \frac{3}{2})$ are not suppressed in scalar QCD.

Finally, notice that the x integrations in (4.8) diverge linearly as x_1 or $x_3 \to 1$ if the distribution amplitude ϕ is replaced by a constant. Since compositeness only ensures that $\phi(x_i, \tilde{Q}) \lesssim (1 - x_i)^\epsilon$ as $x_i \to 1$ with some $\epsilon > 0$ [Eq. (2.21)], end-point singularities are possible here. However, beyond the compositeness condition, there is strong evidence, both theoretical and experimental, suggesting that in fact $\epsilon > 1$ in which case the singularity is destroyed. The wave function's behavior near $x_i \sim 1$ can be analyzed perturbatively, since large momentum $[\sim(k_\perp^2 + m^2)/(1 - x_i)]$ flows through the wave function in that region. We show in the next section that $\psi(x_i, k_\perp) \sim (1 - x_i)$ as $x_i \to 1$ up to factors of $\ln(1 - x_i)$. By the Drell-Yan-West[7] connection, this behavior also determines the $x \sim 1$ dependence of the inelastic structure function νW_2, giving $\nu W_2 \sim (1 - x)^{2\epsilon + 1} = (1 - x)^3$. This agrees with the structure function data, once corrections due to gluonic bremsstrahlung have been included. From Eq. (4.11), the corresponding exponent $\epsilon = \epsilon(\tilde{Q})$ in the distribution amplitude $\phi(x, \tilde{Q})$ is increased (beyond $\epsilon = 1$) as $\tilde{Q} \to \infty$, tending ultimately to $\epsilon = 2$. This evolution is due to the higher-order corrections summed by the evolution equation for the baryon distribution amplitude. Thus the x integrations in the baryon form factor are well behaved as long as $\tilde{Q}$ $[=(1 - x_i)Q$ as $x_i \to 1]$ increases with Q—i.e., for all x_1 external to the infinitesimal region $1 - x_i \lesssim m/Q$. The contribution to the baryon form factor for end-point region $1 - x_i \lesssim m/Q$ (first discussed by Drell and Yan, and West) is strongly suppressed, as we show in the next section. Note that the correction δT_H $\sim O(\alpha_s{}^2(Q) \ln(Q/m)T_H)$ suggested in Ref. 6 does *not* occur when higher-order corrections, leading to evolution of ϕ, are properly included, since this term comes from the region $1 \gg 1 - x_i \gg m/Q$.

C. End-point singularities

An alternative mechanism for hadronic form factors was proposed some time ago by Drell and

FIG. 14. (a) Prediction for $Q^4 G_M^p(Q^2)$ for various QCD scale parameters Λ^2 (in GeV^2). The data are from Ref. 30. The initial wave function is taken as $\phi(x, \lambda) \propto \delta(x_1 - \frac{1}{3})\delta(x_2 - \frac{1}{3})$ at $\lambda^2 = 2$ GeV^2. The factor $(1 + m_p^2/Q^2)^{-2}$ is included in the prediction as a representative of mass effects, and the overall normalization is unknown. (b) The ratio of proton to neutron magnetic form factors for various distribution amplitudes.
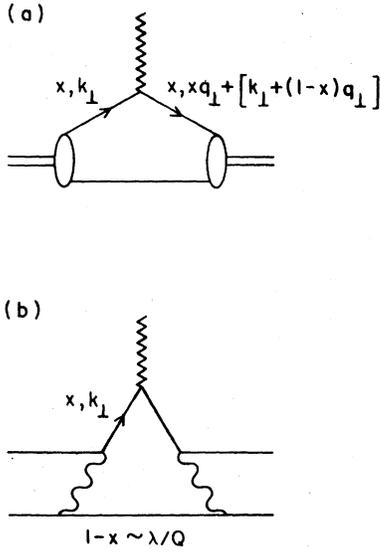
(a)

(b)

$1-x \sim \lambda/Q$

FIG. 15. (a) The pion form factor in lowest order. (b) Lowest order term in F_π requiring analysis of end-point region $1 - x \lesssim \lambda/Q$.

Yan, West,[7] and others. Writing the meson form factor as [Fig. 15(a)]

$$F(Q^2) = \int_0^1 dx \int \frac{d^2 k_\perp}{16\pi^3} \psi(x, k_\perp) \psi^*(x, k_\perp + (1-x) q_\perp),$$

(4.17)

they observed that large transverse momentum flows through neither wave function when x is restricted to the end-point region $1 - x \lesssim \lambda/Q$ where $\lambda^2 \sim \langle k_\perp^2 + m^2 \rangle$ is some typical hadronic scale. In this region, both wave functions are peaked at $k_\perp^2 \lesssim \lambda^2$ [i.e., $\psi \sim B/(k_\perp^2 + \lambda^2)$], and the integration over $k_\perp$ is convergent with only $k_\perp^2 \sim \lambda^2 \ll Q^2$ contributing. Thus the contribution to $F(Q^2)$ from the end-point region is governed only by the x behavior of $\psi(x, \lambda)$ as $x \rightarrow 1$:

$$\Delta F(Q^2) \sim \int_{1-\lambda/Q}^1 dx |\psi(x, \lambda)|^2$$

$$\rightarrow (\lambda/Q)^{1+2\delta},$$

(4.18)

where $\psi(x, \lambda) \sim (1 - x)^\delta$. The Drell-Yan-West connection relates the exponent δ to the behavior of inclusive structure functions before radiative corrections due to gluonic bremsstrahlung are included—i.e., $\nu W_2^{(0)} \rightarrow (1 - x)^{2\delta}$ as $x \rightarrow 1$.

Since the distribution amplitudes $\phi(x_i, \tilde{Q})$ in Eq. (4.1) vanish as $x_i \rightarrow 1$, the Born graphs for T_H [Eq. (4.3)] give negligible contributions from the end-point regions. The contributions which do correspond to the Drell-Yan-West analyses first appear in our analysis in the one-loop corrections to T_H. Consider the diagram in Fig. 15(b). Here
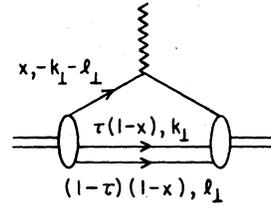

FIG. 16. The nucleon form factor.

the one-gluon interaction kernel plays the role of the wave function in (4.18). This kernel vanishes linearly as $x \rightarrow 1$ which implies $\delta = 1$; i.e., $K_{1g} \sim (1 - x) \alpha_s/(k_\perp^2 + m^2)$. Thus the end-point region in this diagram is suppressed by a full power of $\alpha_s(\lambda Q)(\lambda/Q)$ and is negligible relative to (4.4). It is readily demonstrated that higher-order corrections are similarly suppressed.[31] Terms in K_{1g} which flip quark helicities also vanish linearly near $x \sim 1$ [$K_{1g} \sim m^2(1 - x)/(k_\perp^2 + m^2)^2$], and therefore processes violating the helicity selection rules (4.7) are suppressed in the end-point region, as elsewhere.

Notice that based on this analysis, the Drell-Yan-West correction actually implies a pion structure function which vanishes as $\nu W_2^{(0)} \sim (1 - x)^2$ near $x = 1$, rather than $\nu W_2^{(0)} \sim (1 - x)$ as is usually assumed.[32] Such behavior is certainly consistent with the data when one allows for high-twist terms.[33]

For nucleons the end-point region contributes (Fig. 16)

$$\Delta F(Q^2) \sim \int_{1-\lambda/Q}^1 dx \int_0^1 (1 - x) d\tau |\psi(x, \tau, k_\perp^{(i)} \sim \lambda)|^2$$

$$\sim (\lambda/Q)^{2+2\delta}$$

(4.19)

if the wave function vanishes as $\psi \sim (1 - x)^\delta$ for $x \sim 1$ and $k_\perp^{(i)} \sim \lambda$ [then $\nu W_2^{(0)} \sim (1 - x)^{1+2\delta}$ as $x \rightarrow 1$]. Perturbation theory again implies $\delta = 1$ when, as in Fig. 17, the wave function is replaced by two-gluon interaction kernels—$K_{2g} \sim (1 - x) \alpha_s^2 m^2/$

(a)

(b)

$x \rightarrow 1$

$$\sim \int_0^1 [dy] \phi\left(y_i, \frac{\lambda^2}{1-x}\right) \left\{ \begin{array}{c} y_1 \\ y_2 \\ y_3 \end{array} + \cdots \right\}$$
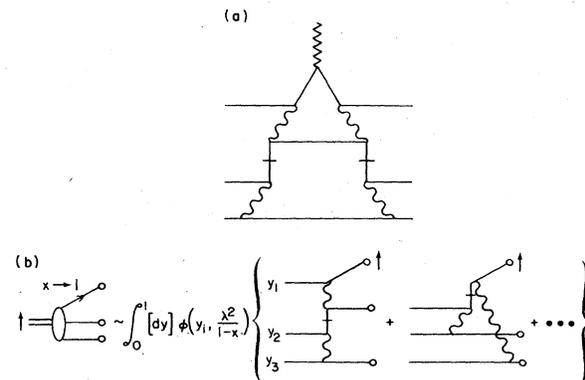
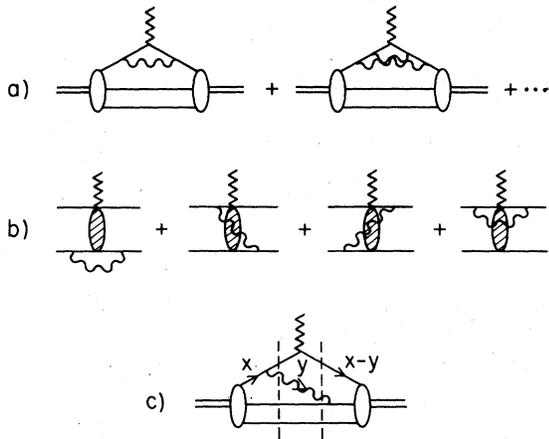FIG. 17. End-point contributions to $G_M(Q^2)$.

FIG. 18. (a) Terms contributing to the Sudakov suppression of the end-point region. (b) Terms in which the Sudakov (double) logarithms cancel when all are combined. (c) A term which cannot cancel the double logarithms in (a).

$[(k_\perp^2 + m^2)^2 (l_\perp^2 + m^2)]$. This is consistent with data for νW_2 and results in a correction to the hard-scattering amplitude of order $\delta T_H \sim (\alpha_s^4 (\lambda Q)/Q^4)$ $\sim \alpha_s^2 (\lambda Q) T_H$.[34] Although δT_H is itself negligible for large Q, further radiative corrections to this term are not obviously small since the presence of wee partons in the end-point region precludes use of the renormalization group. Potentially the most important are corrections to the photon-quark vertex [Fig. 18(a)]. Since the struck quark is off shell by only $\Delta^2 \sim \lambda^2/(1-x) \sim \lambda Q \ll Q^2$, these corrections result in factors of $\ln(Q/\lambda)$ in each order of perturbation theory (Appendix E). However, such terms combine to give a Sudakov form factor for the quark which falls as a power of (λ/Q).[35] This elastic quark form factor tends to further suppress δT_H, and consequently the end-point region makes no significant contribution to the hadronic form factor. Interactions between the wee spectator quarks are insensitive to Q and thus do not modify this conclusion.

It is significant that such Sudakov suppression arises only in the end-point region. Elsewhere (i.e., all $x_i, y_i \gg \lambda/Q$) Sudakov logarithms, which do occur in individual diagrams, ultimately cancel because hadrons are color singlets [see Fig. 18(b)]. Such cancellations cannot occur in the end-point region since a gluon joining the struck quark to a spectator quark [Fig. 18(c)] must transfer finite longitudinal momentum to the spectators ($y \gg \lambda/Q$) if it is to result in a Sudakov form factor (see Appendix E). This in turn destroys the end-point singularity of this contribution by forcing large transverse momentum through one wave function or the other. Thus there is no cancella-
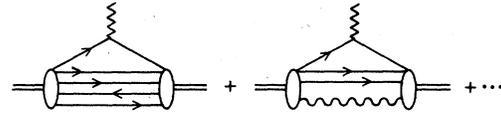
tion of the photon-vertex corrections in the end-point region.

End-point contributions involving higher Fock states (Fig. 19) are suppressed by integer powers of λ/Q due to phase space

$$\int_{1-\lambda/Q} dx_1 \int_0^1 dx_2 \cdots dx_n \delta\left(1 - \sum_i x_i\right) \sim (\lambda/Q)^{n-1}.$$

(Note ψ_n is finite as $x_i \to 0$ since singlet wave functions cannot couple to infinite-wavelength quanta.) Furthermore, the only two gluon kernels which vanish linearly as $x \to 1$ are those illustrated in Fig. 17(b) (in Feynman gauge). All others vanish quadratically and thus contribute (negligible) terms of order λ/Q^5 to $F(Q)$. In particular, a detailed analysis shows that helicity flip and $h = \frac{3}{2}$ terms are also suppressed in $F(Q)$, indicating that the selection rules (4.7) are valid for end-point contributions as well.

Finally, note that only end-point contributions to the form factor are directly related to the behavior of inclusive structure functions ($\nu W_2^{(0)}, \ldots$) near $x \sim 1$. Insofar as the end-point region is unimportant for hadronic form factors, the inclusive-exclusive connection as usually stated is incorrect.

V. FIXED-ANGLE HADRONIC SCATTERING

The techniques developed in Secs. II and III can be applied in a study of hadronic cross sections $d\sigma/dt(AB \to CD)$ at fixed (t/s), or center-of-mass angle $\theta_{c.m.}$, as $s \to \infty$. Here, as for baryon form factors, potentially significant contributions come not only from hard subprocesses, involving transfer of large $k_\perp$ between hadronic constituents, but from the end-point region as well (where $k_\perp^2 \sim \lambda^2$). The analysis is further complicated by pinch singularities (in the x integrations) of the sort first described by Landshoff.[11] However, as we will show, it is unlikely that either end-point or pinch singularities (i.e., "soft" subprocesses) are rele-
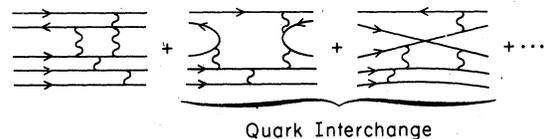

FIG. 19. Nonvalence Fock states in $G_M(Q^2)$.

Quark Interchange

FIG. 20. Diagrams contributing to T_H for $\pi p \to \pi p$.

vant for fixed-angle scattering, at least at current energies.

A. Hard subprocesses

For a process $AB \to CD$ the fixed-angle scattering amplitude due to hard subprocesses is

$$\mathfrak{M}(AB \to CD) = \int_0^1 \prod_{i=a,b,c,d} [dx_i] \phi_C^*(x_c, \tilde{p}\bot) \phi_D^*(x_d, \tilde{p}\bot)$$
$$\times T_H(x_i, s, \theta_{c.m.})$$
$$\times \phi_A(x_a, \tilde{p}\bot) \phi_B(x_b, \tilde{p}\bot) \quad (5.1)$$

as $s \to \infty$ $(p\bot^2 = tu/s)$, where the momentum transfer between hadronic constituents occurs via the hard-scattering amplitude T_H. In leading order, T_H is the sum of all connected tree diagrams in which each hadron is replaced by collinear valence quarks (Fig. 20). This amplitude falls as $\alpha_s(\alpha_s/s)^{n/2-2}$ as $s \to \infty$ with $\theta_{c.m.}$ fixed, where n is the total number of constituents in the initial and final states together (in agreement with dimensional counting[3]). The quark distribution amplitudes $\phi_A, \dots$ tend to their asymptotic forms, Eqs. (2.22) and (4.11), for sufficiently large $p\bot^2$, and the cross section becomes

$$\frac{d\sigma}{dt}(AB \to CD) \to \left(\frac{\alpha_s(p\bot^2)}{s}\right)^{n-2} \left(\ln\frac{p\bot^2}{\Lambda^2}\right)^{-2\Sigma_i \gamma_i} f(\theta_{c.m.})$$
$$\text{as } s \to \infty, \quad (5.2)$$

where for mesons $\gamma_i = 0$, $-4/3\beta$ for $|h| = 0$, 1 while for baryons $\gamma_i = -2/3\beta$, $-2/\beta$ for $|h| = \frac{1}{2}$, $\frac{3}{2}$. Given a process, function $f(\theta_{c.m.})$ is uniquely specified up to an overall normalization constant, which in principle can be determined from form-factor data. At lower $p\bot^2$, $f(\theta_{c.m.})$ varies slowly (logarithmically) with $p\bot^2$, as in Eq. (5.1).

The helicity structure of the amplitude is also completely determined. In particular, total hadronic helicity is conserved—i.e., $h_A + h_B = h_C + h_D$ (Ref. 36). This leads to strong correlations between final-state helicities which would be absent in scalar gluon theories, for example.

An important feature of this analysis is the enormous number of tree diagrams contributing to T_H. Given a particular routing for the quark lines, there are more than 60 000 ways to connect them with five gluons in baryon-baryon scattering. When all quark-flavor routings are included, there can be literally millions of Born diagrams in T_H. Consequently, amplitude (5.1) contains a very large dimensionless factor related to the number of diagrams—even if the various contributions, all roughly equal in magnitude, are completely random in sign, one still expects a factor $\sqrt{N} \sim 10^3$. With about 2000 diagrams per quark routing ($\sqrt{N} \sim 10^2$), one expects a similar though somewhat

smaller factor for meson-baryon amplitudes. Although it is impractical to evaluate T_H exactly for processes such as these, the amplitude (5.1) may well be calculable using Monte Carlo methods.[37] Such a procedure will be described in detail elsewhere.

One interesting class of elastic amplitudes involves external photons in place of one or more of the hadrons—e.g., $\gamma p \to \pi p$, $\gamma p \to \gamma p$, $\gamma \gamma \to \pi \pi$. For each of these the photon can be viewed as having two components: (a) the bare photon which contributes $\Delta n = 1$ to the exponent in (5.2), and (b) the photon as a $q\bar{q}$ composite state (i.e., vector dominance) which contributes $\Delta n = 2$ in (5.2).[36] While the first Fock state must certainly dominate for $s \to \infty$, it is unclear which will be more important at moderate energies since they differ by only a single power of $1/s$. Detailed calculations (currently in progress) will determine the relative importance of these two terms.

B. Soft subprocesses

Processes involving baryons receive contributions from the end-point region of the sort familiar from the form-factor analysis (Sec. IV C). Consider, for example, the amplitude in Fig. 21(a) which contributes to πp. When $1 - x \lesssim \lambda/q\bot$, only small $k\bot^2$ $[\sim O(\lambda^2)]$ flows through either wave function. The amplitude is then a product of two factors: one is precisely the end-point contribution to the form factor [Eq. (4.19)]; the other is the amplitude for $\pi q \to \pi q$, which falls as $1/s$. Here, just as for the form factor, the net contribution from this region is suppressed by $\alpha_s^2(\lambda q\bot)$. Furthermore, a Sudakov form factor develops when radiative corrections are included in the πq amplitude [Fig. 21(b)]. This tends to further suppress end-point contributions which therefore become negligible relative to (5.1) as $s \to \infty$.

Far more significant is Landhsoff's pinch singularity. Consider, for example, the diagrams in Fig. 22(a) which contribute to $\pi \pi$ elastic scattering.[38] Momentum conservation requires $(u = -r\bot^2$,

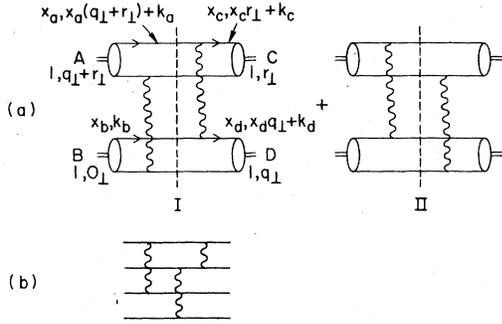FIG. 21. (a) The end-point region for $\pi p \to \pi p$. (b) Diagrams responsible for the Sudakov suppression of this region.

FIG. 22. (a) Amplitudes containing pinch singularities in $\pi\pi \to \pi\pi$. (b) Hard-scattering subprocess obtained from (a) when k_c is large.

$$t = -q_\perp^2, \quad r_\perp \cdot q_\perp = 0)$$

$$x_a + x_b = x_c + x_d,$$

$$k_a + k_b - k_c - k_d = (x_c - x_a)r_\perp + (x_d - x_a)q_\perp.$$

At least one of $k_a^2, \ldots, k_d^2$ is of order $s = r_\perp^2 + q_\perp^2$ for most values of $x_a, \ldots, x_d$. This results in a hard subprocess such as that depicted in Fig. 22(b) (where k_c^2 is large). However, in the region

$$|x_c - x_a| \lesssim \lambda/r_\perp, \quad |x_d - x_a| \lesssim \lambda/q_\perp \qquad (5.3)$$

all wave-function momenta can be small [$O(\lambda^2)$],

and will be since the wave functions peak at low $k_\perp^2$. Consequently, the energy denominators for the intermediate states indicated in Fig. 22(a) become singular in this region:

$$D_I = (x_c - x_a)r_\perp^2 + (x_d - x_a)q_\perp^2$$
$$+ 2(k_d - k_a) \cdot q_\perp + 2(k_c - k_a) \cdot r_\perp$$
$$- \frac{k_a^2}{x_a} - \frac{k_c^2}{1 - x_c} - \frac{k_b^2}{x_b} - \frac{k_d^2}{1 - x_d} + i\epsilon$$
$$\to (x_c - x_a)r_\perp^2 + (x_d - x_a)q_\perp^2 + 2(k_d - k_a) \cdot q_\perp$$
$$+ 2(k_c - k_a) \cdot r_\perp + O(\lambda^2) + i\epsilon,$$

$$D_{II} \to -D_I^* + O(\lambda^2).$$

These denominators combine to give a δ function when the two time orderings are added

$$\frac{1}{D_I} + \frac{1}{D_{II}} \simeq -2\pi i \delta(\Delta_c |r_\perp| + \Delta_d |q_\perp|),$$

where

$$\Delta_c \equiv (x_c - x_a)|r_\perp| + 2(k_c - k_a) \cdot \hat{r}_\perp$$

and

$$\Delta_d \equiv (x_d - x_a)|q_\perp| + 2(k_d - k_a) \cdot \hat{q}_\perp.$$

Thus the leading contribution from this region is

$$\mathfrak{M}_{rr} \propto \int_0^1 dx_a \int_{-\lambda}^\lambda \frac{d\Delta_c \, d\Delta_d}{|r_\perp| |q_\perp|} \psi_C^*(x_c) \psi_D^*(x_d) \psi_A(x_a) \psi_B(x_b) \mathfrak{M}_{qq}^2 \frac{4\pi}{i} \delta(\Delta_c |r_\perp| + \Delta_d |q_\perp|)$$

$$= -\frac{8\pi i \lambda}{(stu)^{1/2}} \int_0^1 dx_a \psi_C^*(x_a) \psi_D^*(x_a) \psi_A(x_a) \psi_B(x_a) \mathfrak{M}_{qq}^2(x_a, q_\perp, r_\perp), \qquad (5.4)$$

where $\mathfrak{M}_{qq}$ is the quark-quark elastic scattering amplitude [$\times(-1)$ for $q\bar{q}$ scattering]:

$$\mathfrak{M}_{qq} = 8\pi\alpha_s \times \begin{cases} s/t & \text{for equal quark helicities,} \\ u/t & \text{for opposite helicities,} \end{cases}$$

$$(5.5)$$

and where integrations over $k_a^2, \ldots \sim \lambda^2$ are implicit. In lowest order, the π-π cross section due to the pinch singularity is then

$$\left[\frac{d\sigma}{dt}(\pi\pi \to \pi\pi) \right]_{ps} \propto \frac{\alpha_s^4}{t^5} \frac{(s^2 + u^2)^2}{us^3}, \qquad (5.6)$$

which ultimately should dominate the hard subprocesses [Eq. (5.2) with $n = 8$] by a full power of $1/s$ as $s \to \infty$ at fixed $\theta_{c.m.}$. Note, however, that the hard subprocesses should be more important until very large s, given their anomalously large normalization.

In fact, perturbation theory strongly suggests that the pinch singularity is negligible at large angles for all s. The radiative corrections to

$\mathfrak{M}_{qq}$ result in Sudakov form factors which fall faster than any power of t as $|t| \to \infty$.[39] Corrections from gluons joining the two quark amplitudes cannot cancel the Sudakov (double) logarithms appearing in the separate amplitudes. For example, one might expect cancellation between the diagrams in Fig. 23 since pion B is a color singlet. However, if the singularity in D_{II} is to be preserved, momentum must flow through wave function ψ_B in the second diagram. Together the two terms give
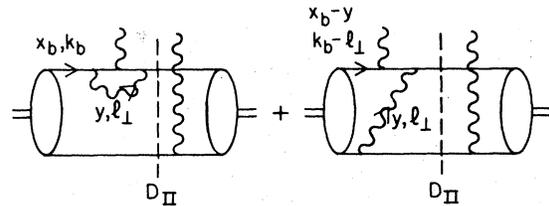

FIG. 23. Terms leading to the Sudakov suppression of the pinch singularity.

(see Appendix F)

$$-C \int_{\lambda^2/|\bar{t}|}^{1} \frac{dy}{y} \int_{y\lambda^2}^{y^2|\bar{t}|} \frac{dl_\perp^2}{l_\perp^2} \frac{\alpha_s(l_\perp^2)}{\pi} [\psi_B(x_b, k_b)$$

$$- \psi_B(x_b - y, k_b - l_\perp)],$$

where C is a color factor, $\bar{t} = x_a^2 t$ is the momentum transferred in $\mathfrak{M}_{qq}$, and the external quarks are off shell by $k^2 \sim O(\lambda^2)$. We can neglect y and $l_\perp$ in the second wave function only when $l_\perp^2 \lesssim \lambda^2$ and $y^2 \lesssim \lambda^2/|\bar{t}|$. So while there is a partial cancellation[12] (i.e., of the infrared region) between the two diagrams, there still remains

$$-C \int_{(\lambda^2/|\bar{t}|)^{1/2}}^{1} \frac{dy}{y} \int_{\lambda^2}^{y^2|\bar{t}|} \frac{dl_\perp^2}{l_\perp^2} \frac{\alpha_s(l_\perp^2)}{\pi} \psi_B(x_b, k_\perp)$$

$$\sim \frac{-2C}{\beta} \ln\left|\frac{\bar{t}}{\lambda^2}\right| \ln\ln\left(\frac{|\bar{t}|}{\lambda^2}\right)^{1/2} \psi(x_b, k_b).$$

Such double logarithms exponentiate to give an overall factor $|\bar{t}|^{-2(C_F/\beta)\ln\ln|\bar{t}/\lambda^2|^{1/2}}$ in $\mathfrak{M}_{qq}$ when higher-order corrections are included together with radiative corrections in the s and u channels. Thus the effective exponent of $(1/t)$ appearing in the Landshoff cross section (5.6) is increased by $8(C_F/\beta)\ln\ln|\bar{t}/\lambda^2|^{1/2}$, and the cross section is negligible as $|t| \sim s \to \infty$.

Notice that the leading contribution for meson-meson scattering from the pinch singularity is purely imaginary. Thus there remains at most a logarithmic singularity near the pinch region (5.3) in (5.1) for meson-meson hard-scattering amplitudes (which are purely real) such as in Fig. 22(b). (An analogous result holds for meson-baryon and baryon-baryon scattering.) In perturbation theory, this singularity is again destroyed by Sudakov form factors. For realistic processes such as $pp \to pp$, terms in T_H containing such a residue of the pinch singularity constitute a small fraction of the number of tree diagrams in T_H.[40]

Landshoff pinch singularities occur in both meson-baryon and baryon-baryon elastic scattering giving cross sections

$$\frac{d\sigma}{dt_{\text{ps}}}(MB) \sim \frac{\alpha_s^6(\bar{t})}{\bar{t}^{7+4\delta(\bar{t})}} f_{MB}(u/s),$$

$$\frac{d\sigma}{dt_{\text{ps}}}(BB) \sim \frac{\alpha_s^6(\bar{t})}{\bar{t}^{8+6\delta(\bar{t})}} f_{BB}(u/s),$$

(5.7)

where $\delta(\bar{t}) \equiv 2(C_F/\beta)\ln\ln|\bar{t}/\lambda^2|^{1/2}$ in leading order, and $\bar{t} \sim t/4$, $t/9$ for MB and BB scattering, respectively. Note that these cross sections are s independent at fixed $|t| \ll s$, unlike the majority of hard subprocesses which fall as $1/s^2$ or faster. Consequently, the pinch terms might dominate $d\sigma/dt$ for very large s when $|t| \ll s$ is held fixed. Conversely, the relative normalizations may be such that the s-independent *hard* subprocesses
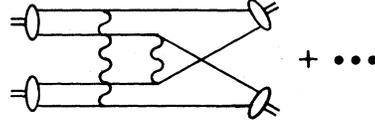
FIG. 24. The pinch singularity for a process with flavor exchange.

prevail even in this region, in which case $d\sigma/dt$ falls as $1/t^8$ for $MB \to MB$, and $1/t^{10}$ for $BB \to BB$ (up to logarithms). In any case, perturbation theory suggests that the pinch contributions are ultimately overwhelmed by the others as $|t|$ is increased, since $\delta(\bar{t})$ grows with $|t|$.

It is interesting to compare elastic scattering amplitudes with those involving charge or flavor exchange (e.g., $\pi^- p \to \pi^0 n$, $\pi p \to K\Sigma, \ldots$) for $|t| \ll s$. These latter processes require quark interchange (Fig. 24), and therefore pinch contributions to $d\sigma/dt$ at fixed t fall with increasing energy—$1/t$ is replaced by $1/s$ in at least one of the qq amplitudes, which implies $d\sigma/dt \sim 1/s^2$. Also interesting are processes in which spin or helicity is exchanged (e.g., $\pi p \to \rho p$). These have s-independent pinch contributions, but they are suppressed by an additional factor m^2/t in the cross section. Hard subprocesses are much harder to distinguish from pinch contributions for processes such as these, and they may very well dominate $d\sigma/dt$ even in the region $|t| \ll s$.

Finally, note that pinch singularities in photon-induced reactions (i.e., $\gamma p \to \pi p, \ldots$) occur only for the composite Fock states in the photon (i.e., vector dominance; see Sec. VA). As the hard subprocesses for these Fock states are nonleading for large s, it is unlikely that pinch singularities are important for such processes.

C. Comparison with data

Hard subprocesses account naturally for the two outstanding features exhibited by the data for fixed-angle scattering. First the measured energy dependences of baryon-baryon[41] amd meson-baryon[42] cross sections are consistent with Eq. (5.2) over a large range of $\theta_{\text{c.m.}}$, provided only that the effective QCD scale Λ^2 in (5.2) is assumed small ($\Lambda^2 \lesssim 0.1$)—see Figs. 25–27. Second, the measured pp and πp amplitudes are substantially larger than the naive estimates, as is expected because of the large number of diagrams in T_H. For example, defining the amplitudes at $\theta_{\text{c.m.}} = 90°$ in terms of electromagnetic form factors,

$$\mathfrak{M}_{pp} = K_{pp}(4\pi\alpha_s)G_M^2(t),$$

$$\mathfrak{M}_{\pi p} = K_{\pi p}(4\pi\alpha_s)F_\pi(t)G_M(t),$$

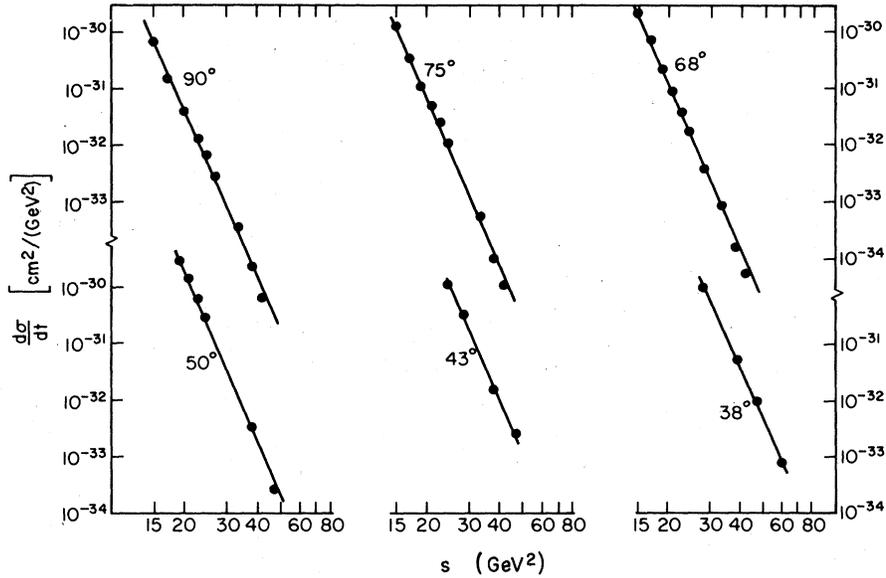we find $K_{pp} \sim 5000$ and $K_{\pi p} \sim 200$ are required to fit

FIG. 25. Cross sections for $pp \to pp$ at wide angles (Ref. 41). The straight lines correspond to a falloff of $1/s^{10}$.

the data. However, the analysis leading to Eqs. (5.1) and (5.2) does not explain the small oscillations observed about the dimensional-counting prediction in both πp and pp elastic scattering. Also, it is not yet clear whether the large, rapidly varying spin correlations observed in large-angle polarized pp scattering are consistent with Eq. (5.1).

The cross section[43] for $\gamma p \to \gamma p$ appears to fall as $\sim 1/s^6$ at fixed angles [Fig. 28(a)] as would be expected from Eq. (5.2) if the photon is treated as an elementary particle [i.e., $\Delta n = 1$ due to

each γ in (5.2)]. Data[44] for $\gamma p \to \pi^+ n$ is also consistent with this picture giving a cross section $d\sigma/dt \sim 1/s^7$ [Fig. 28(b)]. Other meson-photoproduction cross sections ($\gamma p \to \pi^0 p, K\Lambda, \pi\Delta$) show $1/s^n$ falloff with n ranging from 7 to 8, suggesting that in some of these the hadronic component of the photon may be important (it gives $1/s^8$ rather than
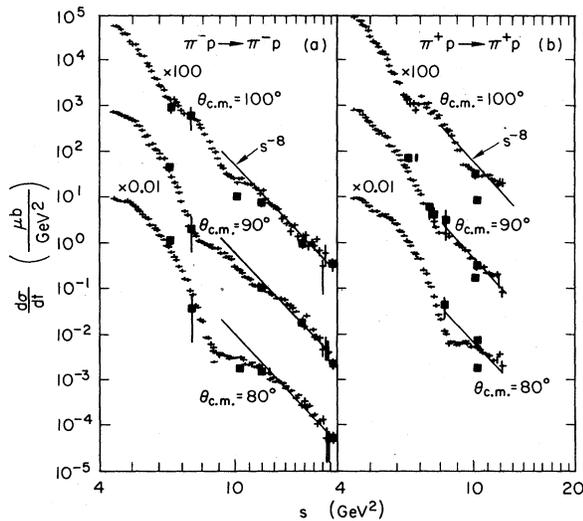
FIG. 26. Cross sections for $\pi^{\pm}p \to \pi^{\pm}p$ at wide angles (Ref. 42).
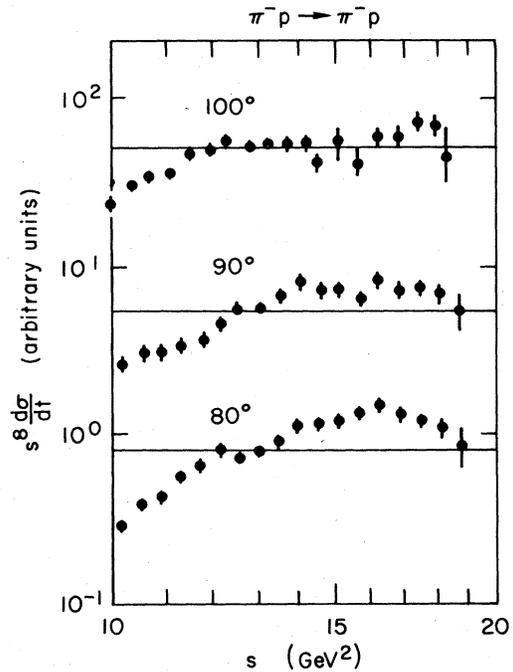
FIG. 27. Cross sections for $\pi^- p \to \pi^- p$ scaled by s^8 (Ref. 42).
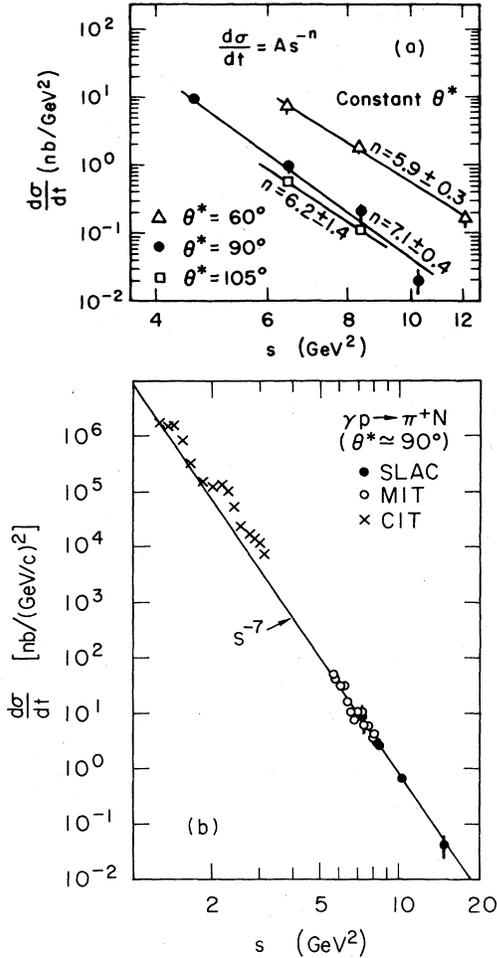
FIG. 28. Cross sections for (a) $\gamma p \to \gamma p$ at wide angles (Ref. 43). (b) $\gamma p \to \pi^+ n$ at wide angles (Ref. 44).

$1/s^7$), at least for $s < 10$ GeV^2.

The data for $pp \to pp$ may also show evidence for the Landshoff process in the region $s \gg |t|$. Experimental results[45] for 5 GeV$^2 \lesssim |t| \lesssim 15$ GeV^2 at energies $s \sim 400$, 800, and 3000 GeV^2 are well fit by ($\Lambda_{QCD} = 0.1$ GeV)

$$\frac{d\sigma}{dt} = \frac{1}{16\pi s^2}\left[[4\pi\alpha_s(\bar t)]^3 \left(\frac{M_p}{t}\right)^4 \frac{s}{M_p} K_L \right.$$

$$\left. + 4\pi\alpha_s(t)G_M{}^2(t)K_{HS} \right]^2 , \qquad (5.8)$$

where $K_L \simeq 0.05$ is the strength of the pinch contribution [Eq. (5.7) with $\delta(\bar t)$ set to zero since $\bar t \sim 1$ GeV^2 is so small], and $K_{HS} \simeq 500$ gives the leading contribution in this region from hard subprocesses [Eq. (5.2)]—see Fig. 29. As expected from diagram counting, K_L is much smaller than K_{HS}, but the additional factor s/M_p enhances the
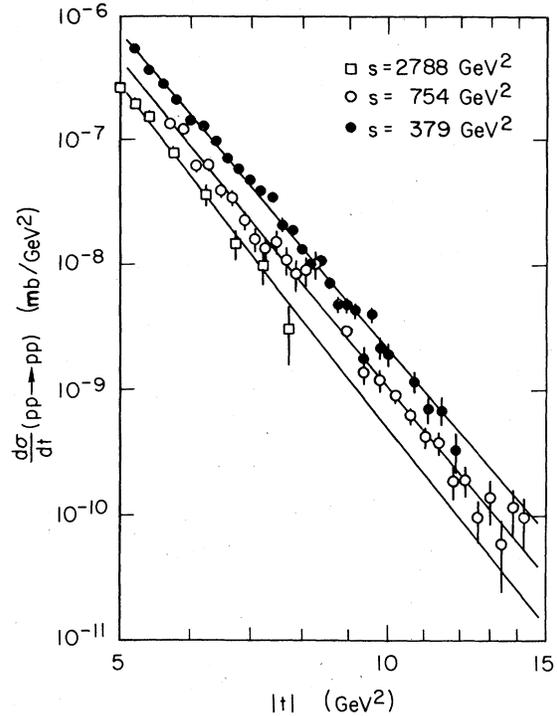
FIG. 29. Fits using Eq. (5.8) for pp elastic scattering with $|t| \ll s$. The best fits obtained using Eq. (5.9) are indistinguishable from these. The data are from Ref. 45.

pinch contribution so that it predominates in the $s \sim 3000$ GeV^2 data. Unfortunately for this interpretation, the data is equally well fit by

$$\frac{d\sigma}{dt} = \frac{1}{16\pi s^2}\left[4\pi\alpha_s(t)G_M{}^2(t)\left(K_{HS} + \frac{s}{t}\tilde K_{HS}\right) \right]^2 , \qquad (5.9)$$

where now both $K_{HS} \simeq 510$ and $\tilde K_{HS} = 8$ represent hard subprocesses. Higher-energy data may distinguish between (5.8) and (5.9)—the first predicts $d\sigma/dt \to (1/t)^{8+66} \times$ logarithms, while the second gives $d\sigma/dt \to (1/t)^{10} \times$ logarithms. However, even then the Sudakov suppression of the pinch [i. e., $\delta(\bar t)$] may obscure the differences. It is clearly important to compute K_{HS} and $\tilde K_{HS}$ in QCD [Eq. (5.2)].

Notice finally that, even assuming (5.8), the pinch contribution at wide angles ($\theta_{c.m.}$) is insignificant relative to hard subprocesses until energies $s \sim 10^5$ GeV^2. [The contribution expected from hard subprocesses is extrapolated from lower-energy data using (5.2).] This is true even though we have neglected Sudakov suppression of the pinch, by setting $\delta(\bar t) = 0$. Thus, as expected, pinch singularities are unimportant in the analysis of wide-angle scattering, at least at current energies and probably for all energies.

VI. SUMMARY AND CONCLUSIONS

Thus far, the most extensive efforts in testing perturbative QCD have been concentrated in the area of inclusive reactions. In the case of deep-inelastic lepton scattering, lepton-pair production, and e^+e^- annihilation cross sections, the basic scale-invariance of QCD is revealed through logarithmic modifications of QED or weak-interaction amplitudes which must be verified over a large range of kinematics. Direct checks of the coupling of QCD at the Born level are possible in inclusive reactions such as e^+e^- annihilation into three or more jets, and the production of hadrons, jets, or photons at very large transverse momenta in hadron-hadron collisions.

As we have discussed in this paper, large-momentum-transfer exclusive reactions provide an extensive, experimentally accessible, and perhaps definitive testing ground for perturbative QCD. In particular, the power-law behavior of these reactions directly tests the scale invariance of the basic quark and gluon interactions at short distances, as well as the SU(3)-color symmetry of the hadronic valence wave functions. The normalizations of the exclusive amplitudes (both relative and absolute) test the basic flavor and spin symmetry structure of the theory as well as the asymptotic boundary condition for meson valence-state wave functions obtained from the meson leptonic decay rates. The angular variation, helicity structure, and absolute sign of exclusive amplitudes test the spin and bare couplings of quarks and gluons. In addition, the predicted logarithmic modifications of exclusive amplitudes reflect the asymptotic-freedom variation of the running coupling constant and the singularities in the operator-product expansion of hadronic wave functions at short distances. The non-Abelian nature of QCD enters in a dramatic way in the normalization of hadronic scattering amplitudes. In the case of ratios such as $G_M^p(Q^2)/G_M^n(Q^2)$ and $M(e^+e^- \to K_L K_S)/M(e^+e^- \to K^+K^-)$, nonleading anomalous dimensions of the hadronic wave functions can be observed directly. In other cases we can obtain a direct measure of $\alpha_s(Q^2)$; e.g.,

$$\alpha_s(Q^2) = \frac{1}{4\pi} \frac{F_\pi(Q^2)}{Q^2 |F_{\pi'}(Q^2)|^2} [1 + O(\alpha_s(Q^2))].$$

It is now possible to extend the rigorous predictions of perturbative QCD to the entire domain of large-momentum-transfer exclusive reactions. The analysis presented here provides a systematic method for calculating elastic and inelastic form factors and the hard-scattering contributions which dominate fixed-angle hadronic scattering amplitudes as a perturbation expansion in the QCD run-

ning coupling constant α_s. An essential part of this derivation is the determination of the short-distance structure of hadronic wave functions. In particular, the process-independent distribution amplitudes $\phi(x_i, Q)$ (which specify the longitudinal-momentum distributions for valence quarks collinear up to the scale Q) have a logarithmic dependence in Q which is completely determined by the QCD evolution equations derived here, or equivalently, by the operator-product expansion of the hadronic Bethe-Salpeter wave function near the light cone. The large-transverse-momentum tail of the hadronic wave functions $\psi(x_i, k_{\perp i})$ is thus calculable in perturbative QCD; we emphasize that (modulo calculable logarithms) $\psi(x_i, k_{\perp i})$ falls only as $1/k_{\perp i}^2$ at large quark transverse momenta—not exponentially as is often assumed in phenomenological applications.

The central issue in this QCD analysis is the demonstration in perturbation theory that the large-momentum-transfer exclusive reactions of hadrons are indeed dominated by the interactions of the valence quarks at short distances. The absence of true infrared divergences in color-singlet matrix elements, together with the fact that the evolution of the distribution amplitudes at large Q^2 prevents anomalous contributions from the end-point $x_i \sim 1$ integration regions, are the critical elements in the proof of short-distance dominance for elastic and inelastic form factors at large momentum transfer. In the case of large-transverse-momentum hadron-hadron exclusive scattering at fixed $\theta_{c.m.}$, Sudakov form factors—which fall faster than any power—asymptotically suppress pinch contributions to the amplitude which are not short-distance dominated. However, even without this Sudakov suppression, the pinch contributions are numerically overwhelmed at experimentally accessible energies by the large number of hard-scattering subprocesses which contribute to meson-baryon and baryon-baryon scattering at large c.m. angles.

Thus, as shown in Secs. II–V, each hadronic scattering amplitude can be computed at large momentum transfer Q from a hard-scattering amplitude $T_H(x_i, Q, \theta_{c.m.})$—calculated by replacing each hadron by collinear on-shell valence quarks—convoluted with the distribution amplitudes $\phi(x_i, \tilde{Q})$ for finding the constituents with light-cone momentum fractions x_i at transverse separations $\sim O(1/\tilde{Q}^2)$, with $\tilde{Q} = (\min x_i)Q$. By definition, all loops containing collinear divergences are summed in the distribution amplitudes rather than in T_H. The gauge-invariant distribution amplitude $\phi(x_i, Q)$ plays the same role in exclusive amplitudes as the quark and gluon probability distribution functions $q(x, Q)$ and $g(x, Q)$ play in inclusive reactions.[46] In

each case, the large-Q^2 behavior of these functions can be analyzed from the operator-product expansion or, equivalently, evolution equations

$$\partial F(x, Q^2)/\partial \ln Q^2 = \int V(x, y, \alpha_s(Q)) F(y, Q^2) dy$$

with distinct kernels $V(x, y, \alpha_s(Q^2))$ for each quantity. After renormalization, T_H and V can then be developed in a perturbative expansion in $\alpha_s(Q^2)$. All the results are covariant and gauge invariant, although the analysis is most easily carried out in the light-cone gauge using light-cone perturbation theory (see Appendix A). The infrared singularity which occurs in the gauge-dependent anomalous dimension for colored fields in this gauge always cancels in physical matrix elements. A completely covariant analysis for $F_\pi(Q^2)$ and the connections with the Bethe-Salpeter wave function are given in Appendix C. The procedures required to extend the analyses to higher order in $\alpha_s(Q^2)$ are given in Sec. III. Alternatively, one could obtain the higher-order connections by calculating the perturbative amplitude for the scattering of collinear, massless on-shell quarks to a given order, and then identifying the contributions not already included in the leading-order results given here, in analogy to the methods used for inclusive processes.

The most important dynamical features of the hadronic amplitudes at large momentum transfer—their power-law falloff in Q^2, their angular dependence, and their helicity dependence—are all determined by the Born contributions to $T_H(x_i, Q, \theta_{\text{c.m.}})$. We are thus led to a large number of detailed, experimentally testable, predictions of QCD which critically reflect its elementary scaling and spin properties at short distances. In particular, there are two sets of universal predictions of QCD which follow from the properties of $T_H(x, Q^2, \theta_{\text{c.m.}})$ to leading order in $1/Q$ and to *all orders* in $\alpha_s(Q^2)$.

(A) The dimensional-counting rules for the power-law behavior of exclusive processes: $\mathfrak{M} \sim Q^{4-n}$, where n is the minimum number of external elementary fields (leptons, quarks, transversely polarized gluons or photons) participating in T_H.

(B) The QCD helicity selection rules: $\Delta h = 0$ (hadron helicity conservation).

In the case of electromagnetic or weak form factors, hadron helicity conservation leads to an even more restrictive rule: $|h_I| \leq \frac{1}{2}$ (minimal helicity for each interacting hadron). These helicity rules are special features of a vector-gluon gauge theory.

Thus form factors for processes in which the hadron's helicity is changed, or in which the initial or final hadron has helicity ≥ 1, are suppres-

sed by powers of m/Q where m is an effective quark mass. Form factors for particles with opposite helicity dominate for q^2 timelike. The QCD selection rules imply power-law suppression of $F_2^N(Q^2)/F_1^N(Q^2)$, $\gamma^* p \to \Delta(h = \frac{3}{2})$, and $e^+ e^- \to \pi \rho, \rho_L \rho_T, \rho_T \rho_T, \Delta(h = \frac{3}{2}) + \Delta(h = -\frac{3}{2})$, etc.

The techniques developed here can be readily extended to other hadronic systems, including large-momentum-transfer reactions involving nuclei, pure gluonic states, heavy-quark bound states, etc. Applications to the elastic and inelastic weak and electromagnetic form factors of baryons will be given in Ref. 2. We have also used similar methods to analyze the end-point $x \to 1$ behavior of meson and baryon structure and fragmentation functions in perturbative QCD, taking into account the correct kinematic limits on structure-function evolution.[47] As we have emphasized in Sec. IV, the Drell-Yan-West connection does not work in detail in QCD: For example, the perturbative diagrams which control the $x \to 1$ behavior of baryon structure functions [giving the nominal power $F_2(x) \sim (1 - x)^3$] lead to contributions to baryon form factors which are suppressed by at least two powers of $\alpha_s(Q^2)$. The leading contributions to form factors in QCD come from the short-distance region $k_\perp < O(Q)$, and not from $(1 - x) \sim (m/Q)$, $k_\perp$ small—as assumed in the Drell-Yan-West analysis.

We can also apply the methods of this paper to the calculation of "high-twist" subprocesses in inclusive reactions, such as the C/Q^2 terms in the meson longitudinal structure functions,[33,48] power-law-suppressed terms in the baryon structure function, and subprocesses involving more than the minimal number of interacting fields in high-transverse-momentum reactions.[49]

The testing of QCD in exclusive reactions is just beginning, but already there are a number of important phenomenological successes. The power laws predicted by QCD for the pion, nucleon (and deuteron) form factors, and for large-angle $pp \to pp$, $np \to np$, $\pi^\pm p \to \pi^\pm p$, $\gamma p \to \gamma p$, and $\gamma p \to \pi^+ n$ scattering are consistent with the data. These scaling results give the best test so far for the essential scale invariance of $qq \to qq$ scattering and the q and g propagators. We emphasize that the specific integral powers predicted by perturbative QCD reflect both the scale invariance of the basic interactions and the fact that the minimal color-singlet wave functions of hadrons contain either three quarks or quark plus antiquark (or two or three gluons). The dynamics and symmetries of QCD are thus directly tested. The fact that logarithmic modifications are not yet apparent in the data—particularly in $s^{10} d\sigma/dt(pp \to pp)$, which should roughly scale at fixed angle as $\alpha_s^{10}(s)$

gives evidence that $\alpha_s(Q^2)$ is slowly varying—i.e., that the QCD scale constant Λ is relatively small: $\Lambda_{eff} \lesssim 100$ to 300 MeV. (The larger value is only possible if mass corrections are important.)

A more qualitative success of QCD is the fact that the pion form factor, computed with the asymptotic wave function normalized to the pion decay constant, is within a factor of ~2 of the observed spacelike data. The definitive check of the predictions for $F_\pi(Q^2)$ will require an evaluation of the order $\alpha_s(Q^2)$ correction, as well as further constraints on the pion distribution amplitude $\phi(x, Q)$. As we shall show in a subsequent paper,[50] measurements of the scaling properties and angular dependence of the two-photon processes $d\sigma/dt(\gamma\gamma \to M\bar{M})$, with $M = \pi^{\pm,0}, \rho_{L,T}^{\pm,0}$ and their ratio to the corresponding $e^+e^- \to M^+M^-$ cross sections can provide extraordinary checks on QCD and important constraints on the form of the distribution amplitudes at nonasymptotic momenta. These two-photon processes are the simplest nontrivial hadronic scattering amplitudes computable in perturbative QCD. Pinch contributions are power-law suppressed in this case. We also emphasize the importance of experimentally checking the ratio of π^+ to K^+ to ρ_L^+ form factors which are predicted to asymptotically approach the ratios $f_\pi^2 : f_K^2 : 2f_\rho^2 \sim 1 : 1.5 : 2.5$. The fact that the pion form factor has the same sign as its value at $Q^2 = 0$ (i.e., no zeros) is a nontrivial check of QCD; for scalar gluons, the meson form factor would change sign as Q^2 increases. Another qualitative success of QCD is its apparent explanation of the surprisingly large normalization of the $pp \to pp$ and $\pi p \to \pi p$ scattering amplitudes and the magnitude of large-momentum-transfer nuclear form factors. It remains an open question whether the large spin polarization observed in large-angle $pp \to pp$ scattering at Argonne can be explained in terms of perturbative QCD mechanisms.

Finally, we emphasize that the quark distribution amplitudes

$$\phi(x_i, Q) \sim \int^Q d^2k_\perp \psi(x_i, k_{\perp i})$$

which control exclusive reactions at large momentum transfer, and the quark probability distributions

$$q(x_i, Q) \sim \int^Q d^2k_\perp |\psi(x_i, k_{\perp i})|^2$$

(summed over all Fock states), which control inclusive reactions at large momentum transfer, are each determined by the hadronic Fock-state wave functions $\psi(x_i, k_{\perp i})$. In principle, the $\psi(x_i, k_{\perp i})$ describe all hadronic matrix elements. A central goal of hadronic physics will be to utilize these

wave functions to unify short- and long-distance physics, and make contact with hadronic spectroscopy, low-momentum-transfer reactions, and the whole range of nonperturbative physics.

APPENDIX A: LIGHT-CONE PERTURBATION THEORY

One of the most convenient and physical formalisms for studying processes with large transverse momenta is light-cone quantization, or its equivalent, time-ordered perturbation theory in the infinite-momentum frame.[8] Defining $p^\pm \equiv p^0 \pm p^3$, we can parametrize a particle's momentum as

$$p^\mu = (p^+, p^-, \vec{p}_\perp) = \left(p^+, \frac{p_\perp^2 + m^2}{p^+}, \vec{p}_\perp\right),$$

where $p^2 = p^+ p^- - p_\perp^2 = m^2$. [Note that in general $p \cdot k = \frac{1}{2}(p^+ k^- + p^- k^+) - p_\perp \cdot k_\perp$.] These variables naturally distinguish between a particle's longitudinal and transverse degrees of freedom and when used in an appropriate frame lead to much simplification. This is particularly true in any analysis of collinear singularities as these appear as divergences only in integrations over transverse momenta, $k_\perp^2$.

For each time-ordered graph, the rules of light-cone perturbation theory are the following.

(R1) Assign a momentum k_μ to each line such that (a) $k^+, k_\perp$ are conserved at each vertex, and (b) $k^2 = m^2$; i.e., $k^- = (k_\perp^2 + m^2)/k^+$ and k_μ is on mass shell.

(R2) Include a factor $\theta(k^+)$ for each line—all quanta are forward moving $(k^3 > 0)$ in the infinite-momentum frame.

(R3) For each gluon (or other vector-boson) line include a factor $d_{\mu\nu}^{(k)}/k^+$ where $d_{\mu\nu}$ is the (gauge-dependent) polarization sum. In Feynman gauge $d_{\mu\nu}$ equals $-g_{\mu\nu}$. In light-cone gauge $\eta \cdot A = A^+ = 0$,

$$d_{\mu\nu}^{(k)} = \sum_{\lambda=1,2} \epsilon_\mu(k, \lambda)\epsilon_\nu(k, \lambda)$$

$$= -g_{\mu\nu} + \frac{\eta_\mu k_\nu + \eta_\nu k_\mu}{\eta \cdot k},$$

where $k \cdot \epsilon = \eta \cdot \epsilon = 0$.[51] The singularity at $\eta \cdot k = 0$
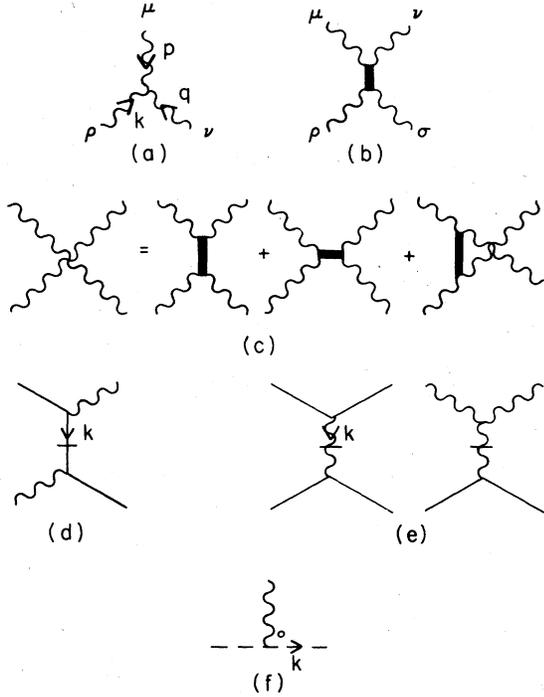
FIG. 30. Vertices appearing in QCD light-cone perturbation theory.

is regulated by replacing $1/\eta \cdot k \to \eta \cdot k/((\eta \cdot k)^2 + \epsilon^2)$. Dependence on ϵ cancels in the total amplitude for a process.

(R4) The gluon-fermion vertices are

$$e_0 \frac{\bar{u}(k)}{(k^+)^{1/2}} \gamma^\mu \frac{u(l)}{(l^+)^{1/2}} , \quad e_0 \frac{\bar{u}(k)}{(k^+)^{1/2}} \gamma^\mu \frac{v(l)}{(l^+)^{1/2}} ,$$

$$-e^0 \frac{\bar{v}(k)}{(k^+)^{1/2}} \gamma^\mu \frac{u(l)}{(l^+)^{1/2}} , \quad -e_0 \frac{\bar{v}(k)}{(k^+)^{1/2}} \gamma^\mu \frac{v(l)}{(l^+)^{1/2}} .$$

The factors $1/(k^+)^{1/2}$, $1/(l^+)^{1/2}$ are omitted for external fermions in a scattering amplitude.

(R5) The trigluon vertex is [Fig. 30(a)]

$$-e_0[(p - q)^\rho g^{\mu\nu} + (q - k)^\mu g^{\rho\nu} + (k - p)^\nu g^{\mu\rho}]$$

and the four-gluon vertex is [Fig. 30(b)]

$$e_0^2 (g^{\mu\rho} g^{\nu\sigma} - g^{\mu\sigma} g^{\nu\rho}) .$$

Generally there are three independent ways of inserting the four-gluon vertex [Fig. 30(c)]; all must be included.

(R6) For each intermediate state there is a factor

$$\frac{1}{\displaystyle\sum_{\text{inc}} k^- - \sum_{\text{interm}} k^- + i\epsilon} ,$$

where the sums in the "energy denominator" are over the light-cone "energies," k^-, of the incident (inc) and intermediate (interm) particles.

(R7) In Feynman gauge, ghost loops occur. For each ghost line [with momentum as in (R1)] include a factor $-\theta(k^+)/k^+$. The gluon-ghost vertex is $e_0 k^\nu$ for Fig. 30(f). There are no ghosts in light-cone gauge.

(R8) The fermion propagator has an instantaneous part $[\gamma^+/2k^+;$ Fig. 30(d)], as do the gluon propagator $[\eta^\mu \eta^\nu/k^{+2}$ in light-cone gauge; Fig. 30(e)] and the ghost propagator (in Feynman gauge). In each case, the instantaneous propagator can be absorbed into the regular propagator by replacing k, the momentum associated with the line, by

$$\bar{k} = \left(k^+, \sum_{\text{inc}} k^- - \sum_{\text{interm}}' k^-, k \right)$$

in the numerator for those diagrams in which the fermion, gluon, or ghost propagates only over a single time interval (Fig. 31). Here $\sum_{\text{inc}}$ denotes summation over all initial particles in the diagram, while $\sum_{\text{interm}}'$ denotes summation over all particles in the intermediate state other than the particle of interest. Thus, in light-cone gauge, $\bar{k}$ replaces k in the polarization sum $d_{\mu\nu}^{(k)}$, as well as in the trigluon coupling, for gluons appearing in a single intermediate state [Fig. 31(a)]. Similarly, $\sum_{\text{spins}} u(k)\bar{u}(k)$ is replaced by $\bar{k} + m$, and $\sum_{\text{spins}} v(k) \times \bar{v}(k)$ by $\bar{k} - m$, as in Fig. 31(b).

(R9) Integrate $\int_0^\infty dk^+ \int d^2k_\perp/16\pi^3$ over each independent k and sum over internal spins and polarizations.

(R10) Color factors are computed as for covariant diagrams (see Ref. 52, for example).

In addition to these rules, there are several tricks which are useful in certain applications.

(T1) In amplitudes with an external line off shell (having momentum q^μ, $q^2 \neq m^2$), the energy denominators for intermediate states following the ver-
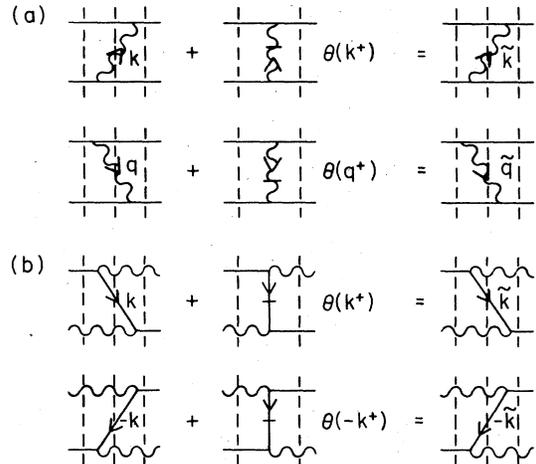

FIG. 31. Procedure for removing instantaneous propagators by redefining the noninstantaneous propagators.
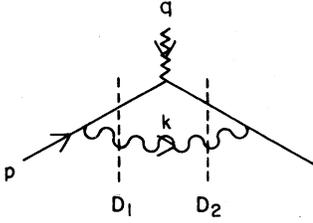
FIG. 32. Sample vertex in light-cone perturbation theory.

tex with the virtual external line are modified by the replacement $\sum_{\text{inc}} k^- \to \sum_{\text{inc}} k^- + q^-$ where the light-cone energy $q^- = (q^2 + q_\perp^2)/q^+$ is specified by momentum conservation (and *not* by on-shell kinematics as is usual). Thus the form factor in Fig. 32 has energy denominators

$$D_1 = p^- - \frac{(p_\perp - k_\perp)^2 + m^2}{p^+ - k^+} - \frac{k_\perp^2}{k^+} + i\epsilon \,,$$

$$D_2 = p^- + \frac{q^2 + q_\perp^2}{q^+} - \frac{(p_\perp + q_\perp - k_\perp)^2 + m^2}{p^+ + q^+ - k^+} - \frac{k_\perp^2}{k^+} + i\epsilon \,.$$

This rule is equivalent to treating the (external) virtual particle as an on-shell particle but with mass q^2 rather than m^2 (=0 in Fig. 32). Amplitudes having several external lines off shell are analyzed in a similar fashion.

(T2) The contribution from each time-ordered graph is separately invariant under boosts along the 3 direction—i.e., $p^+ \to K p^+$, $p^- \to K^{-1} p^-$, $p_\perp \to p_\perp$ for each momentum (internal and external) in the diagram. Each time-ordered amplitude is also invariant under transverse boosts: $p^+ \to p^+$, $p^- \to p^- + 2 p_\perp \cdot Q_\perp + p^+ Q_\perp^2$, $p_\perp \to p_\perp + p^+ Q_\perp$ for each momentum. This is true in both Feynman and light-cone gauges.

A particularly useful spinor basis is constructed from the eigenstates of the projection operators:

$$\Lambda_+ \equiv \frac{\gamma^- \gamma^+}{4} = \frac{\gamma^0 \gamma^+}{2} = \frac{\gamma^- \gamma^0}{2} \,,$$

$$\Lambda_- \equiv \frac{\gamma^+ \gamma^-}{4} = \frac{\gamma^0 \gamma^-}{2} = \frac{\gamma^+ \gamma^0}{2} \,, \tag{A1}$$

where $(\Lambda_\pm)^2 = \Lambda_\pm$, $\Lambda_\pm \Lambda_\mp = 0$, $\Lambda_\pm^\dagger = \Lambda_\pm$, $\beta \Lambda_\pm = \Lambda_\mp \beta$, $\alpha_\perp \Lambda_\pm = \Lambda_\mp \alpha_\perp$, and $\beta \equiv \gamma_0$, $\vec{\alpha}_\perp \equiv \gamma^0 \vec{\gamma}_\perp$. The eigenstates of Λ_+ are

$$\Lambda_+ \chi = \chi \Rightarrow \chi(\uparrow) = \frac{1}{\sqrt{2}} \begin{pmatrix} 1 \\ 0 \\ 1 \\ 0 \end{pmatrix}, \quad \chi(\downarrow) = \frac{1}{\sqrt{2}} \begin{pmatrix} 0 \\ 1 \\ 0 \\ -1 \end{pmatrix}, \quad (A2)$$

and the associated spinor bases for particles and

TABLE II. Dirac matrix elements for the helicity spinors of Appendix A.

Matrix element $\bar{u}_{\lambda'} \cdots u_\lambda$	Helicity $(\lambda \to \lambda')$ $\uparrow \to \uparrow$ $\downarrow \to \downarrow$	$\uparrow \to \downarrow$ $\downarrow \to \uparrow$
$\dfrac{\bar{u}(p)}{(p^+)^{1/2}} \gamma^+ \dfrac{u(q)}{(q^+)^{1/2}}$	2	0
$\dfrac{\bar{u}(p)}{(p^+)^{1/2}} \gamma^- \dfrac{u(q)}{(q^+)^{1/2}}$	$\dfrac{2}{p^+ q^+}(p_\perp \cdot q_\perp \pm i p_\perp \times q_\perp + m^2)$	$\mp \dfrac{2m}{p^+ q^+}[(p^1 \pm i p^2) - (q^1 \pm i q^2)]$
$\dfrac{\bar{u}(p)}{(p^+)^{1/2}} \gamma_\perp^i \dfrac{u(q)}{(q^+)^{1/2}}$	$\dfrac{p_\perp^i \mp i\epsilon^{ij} p_\perp^j}{p^+} + \dfrac{q_\perp^i \pm i\epsilon^{ij} q_\perp^j}{q^+}$	$\mp m\left(\dfrac{p^+ - q^+}{p^+ q^+}\right)(\delta^{i1} \pm i\delta^{i2})$
$\dfrac{\bar{u}(p)}{(p^+)^{1/2}} \dfrac{u(q)}{(q^+)^{1/2}}$	$m\left(\dfrac{p^+ + q^+}{p^+ q^+}\right)$	$\mp\left(\dfrac{p^1 \pm i p^2}{p^+} - \dfrac{q^1 \pm i q^2}{q^+}\right)$
$\dfrac{\bar{u}(p)}{(p^+)^{1/2}} \gamma^- \gamma^+ \gamma^- \dfrac{u(q)}{(q^+)^{1/2}}$	$\dfrac{8}{p^+ q^+}(p_\perp \cdot q_\perp \pm i p_\perp \times q_\perp + m^2)$	$\mp \dfrac{8m}{p^+ q^+}[(p^1 \pm i p^2) - (q^1 \pm i q^2)]$
$\dfrac{\bar{u}(p)}{(p^+)^{1/2}} \gamma^- \gamma^+ \gamma_\perp^i \dfrac{u(q)}{(q^+)^{1/2}}$	$4\left(\dfrac{p_\perp^i \mp i\epsilon^{ij} p_\perp^j}{p^+}\right)$	$\pm \dfrac{4m}{p^+}(\delta^{i1} \pm i\delta^{i2})$
$\dfrac{\bar{u}(p)}{(p^+)^{1/2}} \gamma_\perp^i \gamma^+ \gamma^- \dfrac{u(q)}{(q^+)^{1/2}}$	$4\left(\dfrac{q_\perp^i \pm i\epsilon^{ij} q_\perp^j}{q^+}\right)$	$\mp \dfrac{4m}{q^+}(\delta^{i1} \pm i\delta^{i2})$
$\dfrac{\bar{u}(p)}{(p^+)^{1/2}} \gamma_\perp^i \gamma^+ \gamma_\perp^j \dfrac{u(q)}{(q^+)^{1/2}}$	$2(\delta^{ij} \pm i\epsilon^{ij})$	0

$$\bar{v}_\mu(p) \gamma^\alpha v_\nu(q) = \bar{u}_\nu(q) \gamma^\alpha u_\mu(p) \qquad\qquad \bar{v}_\mu(p) v_\nu(q) = -\bar{u}_\nu(q) u_\mu(p)$$

$$\bar{v}_\mu(p) \gamma^\alpha \gamma^\beta \gamma^\delta v_\nu(q) = \bar{u}_\nu(q) \gamma^\delta \gamma^\beta \gamma^\alpha u_\mu(p)$$

TABLE III. Dirac matrix elements for the helicity spinors of Appendix A.

Matrix element $\bar{v}_{\lambda'}\cdots u_\lambda$	Helicity ($\lambda\to\lambda'$)	
	$\uparrow\to\uparrow$ $\downarrow\to\downarrow$	$\uparrow\to\downarrow$ $\downarrow\to\uparrow$
$\dfrac{\bar{v}(p)}{(p^+)^{1/2}}\gamma^+\dfrac{u(q)}{(q^+)^{1/2}}$	0	2
$\dfrac{\bar{v}(p)}{(p^+)^{1/2}}\gamma^-\dfrac{u(q)}{(q^+)^{1/2}}$	$\mp\dfrac{2m}{p^+q^+}[(p^1\pm ip^2)+(q^1\pm iq^2)]$	$\dfrac{2}{p^+q^+}(p_\perp\cdot q_\perp \pm ip_\perp\times q_\perp - m^2)$
$\dfrac{\bar{v}(p)}{(p^+)^{1/2}}\gamma^i_\perp\dfrac{u(q)}{(q^+)^{1/2}}$	$\mp m\left(\dfrac{p^++q^+}{p^+q^+}\right)(\delta^{i1}\pm i\delta^{i2})$	$\dfrac{p^i_\perp\mp i\epsilon^{ij}p^j_\perp}{p^+}+\dfrac{q^i_\perp\pm i\epsilon^{ij}q^j_\perp}{q^+}$
$\dfrac{\bar{v}(p)}{(p^+)^{1/2}}\dfrac{u(q)}{(q^+)^{1/2}}$	$\mp\left(\dfrac{p^1\pm ip^2}{p^+}-\dfrac{q^1\pm iq^2}{q^+}\right)$	$m\left(\dfrac{p^+-q^+}{p^+q^+}\right)$
$\dfrac{\bar{v}(p)}{(p^+)^{1/2}}\gamma^-\gamma^+\gamma^-\dfrac{u(q)}{(q^+)^{1/2}}$	$\mp\dfrac{8m}{p^+q^+}[(p^1\pm ip^2)+(q^1\pm iq^2)]$	$\dfrac{8}{p^+q^+}(p_\perp\cdot q_\perp \pm ip_\perp\times q_\perp - m^2)$
$\dfrac{\bar{v}(p)}{(p^+)^{1/2}}\gamma^-\gamma^+\gamma^i_\perp\dfrac{u(q)}{(q^+)^{1/2}}$	$\mp\dfrac{4m}{p^+}(\delta^{i1}\pm i\delta^{i2})$	$4\left(\dfrac{p^i_\perp\mp i\epsilon^{ij}p^j_\perp}{p^+}\right)$
$\dfrac{\bar{v}(p)}{(p^+)^{1/2}}\gamma^i_\perp\gamma^+\gamma^-\dfrac{u(q)}{(q^+)^{1/2}}$	$\mp\dfrac{4m}{q^+}(\delta^{i1}\pm i\delta^{i2})$	$4\left(\dfrac{q^i_\perp\pm i\epsilon^{ij}q^j_\perp}{q^+}\right)$
$\dfrac{\bar{v}(p)}{(p^+)^{1/2}}\gamma^i_\perp\gamma^+\gamma^j_\perp\dfrac{u(q)}{(q^+)^{1/2}}$	0	$2(\delta^{ij}\pm i\epsilon^{ij})$

antiparticles are

$$\left.\begin{matrix}u_\uparrow(p)\\ u_\downarrow(p)\end{matrix}\right\} = \frac{1}{(p^+)^{1/2}}(p^+ + \beta m + \vec{\alpha}_\perp\cdot\vec{p}_\perp)\times\left\{\begin{matrix}\chi(\uparrow)\\ \chi(\downarrow)\end{matrix}\right.,$$

$$\left.\begin{matrix}v_\uparrow(p)\\ v_\downarrow(p)\end{matrix}\right\} = \frac{1}{(p^+)^{1/2}}(p^+ - \beta m + \vec{\alpha}_\perp\cdot\vec{p}_\perp)\times\left\{\begin{matrix}\chi(\downarrow)\\ \chi(\uparrow)\end{matrix}\right. . \qquad (A3)$$

Taking $p^+\to\infty$, we find that these are helicity eigenstates when viewed from the infinite-momentum frame. Notice also that the phases assigned the antiparticle spinors are conventional for spin-$\frac{1}{2}$ eigenstates. Thus a state $u_\uparrow\bar{v}_\downarrow - u_\downarrow\bar{v}_\uparrow$ has spin zero (in the infinite-momentum frame), for example.

Matrix elements involving these states are tabulated in Tables II and III.

In light-cone perturbation theory, a two-body bound state with total momentum $p^\mu = (p^+, (M^2 + p_\perp^2)/p^+, p_\perp)$ is described by a wave function

$$\Psi(x_i, k_\perp; p) = \frac{u_\lambda^{(1)}(x_1 p^+, k_\perp + x_1 p_\perp)}{\sqrt{x_1}}\frac{u_{\lambda'}^{(2)}(x_2 p^+, -k_\perp + x_2 p_\perp)}{\sqrt{x_2}}\psi_{\lambda\lambda'}(x_i, k_\perp), \qquad (A4)$$

where $x_i p^+$ is the longitudinal momentum carried by the ith constituent ($x_1 + x_2 = 1$), and $\pm k_\perp$ is the constituents' transverse momentum relative to the bound states ($u^{(2)}$ is replaced by v for a bound state of a particle and an antiparticle). By Lorentz invariance [see (T2) above], $\psi(x_i, k_\perp)$ is independent of p^+ and $p_\perp$, and thus we can set $p^\mu = (1, M^2, 0_\perp)$ without loss of generality. This wave function is the positive-energy projection of the familiar Bethe-Salpeter wave function evaluated with the constituents at equal "time" $\tau = (z + t)$,

$$\int\frac{dk^-}{2\pi}\Psi_{BS}(k;p) = \frac{u^{(1)}(x_1, k_\perp)}{\sqrt{x_1}}\frac{u^{(2)}(x_2, -k_\perp)}{\sqrt{x_2}}\psi(x_i, k_\perp)$$

+ negative-energy components,

and satisfies an exact bound-state equation [Fig. 33(a)]:

$$\left(M^2 - \frac{k_\perp^2 + m_1^2}{x_1} - \frac{k_\perp^2 + m_2^2}{x_2}\right)\psi(x_i, k_\perp) = \int_0^1 [dy]\int_0^\infty \frac{d^2 l_\perp}{16\pi^3}\tilde{K}(x_i, k_\perp; y_i, l_\perp; M^2)\psi(y_i, l_\perp), \qquad (A5)$$

where $[dy]\equiv dy_1 dy_2\delta(1 - y_1 - y_2)$. The interaction kernel $\tilde{K}$ is defined as

$$\tilde{K}_{\mu\nu,\rho\sigma} = \frac{\bar{u}^{(1)}(x_1, k_\perp)}{\sqrt{x_1}} \frac{\bar{u}^{(2)}(x_2, -k_\perp)}{\sqrt{x_2}} \bar{K}(x_i, k_\perp; y_i, l_\perp; M^2) \frac{u^{(1)}(y_1, l_\perp)}{\sqrt{y_1}} \frac{u^{(2)}(y_2, -l_\perp)}{\sqrt{y_2}} ,$$ (A6)

where in perturbation theory $\bar{K}$ is the sum of all truncated, two-particle irreducible[54] amplitudes as illustrated in Fig. 33(b). A scattering amplitude involving the bound state is given by

$$T = \int_0^1 [dx] \int_0^\infty \frac{d^2 k_\perp}{16\pi^3} \mathfrak{M} \Psi(x_i, k_\perp; p) = \int_0^1 [dx] \int_0^\infty \frac{d^2 k_\perp}{16\pi^3} \mathfrak{M} \frac{u^{(1)}}{\sqrt{x_1}} \frac{u^{(2)}}{\sqrt{x_2}} \psi(x_i, k_\perp) ,$$ (A7)

where $\mathfrak{M}$ is the amplitude with the bound state replaced its constituents. Amplitude $\mathfrak{M}$ must be two-particle irreducible with respect to the constituent lines if double counting is to be avoided (Fig. 34). [Note that Eq. (A7) is consistent with rule (R4) which assigns the spinor factor $u/\sqrt{x}$ (or $v/\sqrt{x}$) to the interaction vertex of each internal fermion.] Equation (A7) has conventional (relativistic) normalization if the wave function is normalized so that

$$1 = \int [dx] \frac{d^2 k_\perp}{16\pi^3} |\psi(x_i, k_\perp)|^2 - \int [dx] \frac{d^2 k_\perp}{16\pi^3} \int [dy] \frac{d^2 l_\perp}{16\pi^3} \psi^*(x_i, k_\perp) \frac{\partial}{\partial M^2} \bar{K}(x_i, k_\perp; y_i, l_\perp; M^2) \psi(y_i, l_\perp) .$$ (A8)

Notice that the second term in (A8) contributes only when the interaction potential is energy dependent (which is not the case in most nonrelativistic analyses).

For illustration, consider positronium. The kernel for one-photon exchange is

$$\bar{K} \simeq \frac{-16 e^2 m^2}{(k_\perp - l_\perp)^2 + (x - y)^2 m^2}$$ (A9)

in the nonrelatistic region $k_\perp, l_\perp \sim O(\alpha m)$ and $x \equiv x_1 - x_2 \sim O(\alpha)$, $y \equiv y_1 - y_2 \sim O(\alpha)$. Using this kernel and writting $M^2 \simeq 4m^2 + 4m\epsilon$, Eq. (A5) is approximately

$$\left(\epsilon - \frac{k_\perp^2 + x^2 m^2}{m}\right) \psi(x_i, k_\perp) = (4x_1 x_2) \int_{-1}^1 m\, dy \int_0^\infty \frac{d^2 l_\perp}{(2\pi)^3} \frac{-e^2}{(k_\perp - l_\perp)^2 + (x - y)^2 m^2} \psi(y_i, l_\perp) .$$

This equation has ground-state energy $\epsilon \simeq -\alpha^2 m/4$, as expected, and nonrelativistic wave functions

$$\Psi = \left(\frac{m\beta^3}{\pi}\right)^{1/2} \frac{64\pi\beta x_1 x_2}{[k_\perp^2 + (x_1 - x_2)^2 m^2 + \beta^2]^2} \times \begin{cases} \dfrac{u_\uparrow \bar{v}_\downarrow - u_\downarrow \bar{v}_\uparrow}{(2x_1 x_2)^{1/2}}, & \text{parapositronium}, \\[2ex] \dfrac{u_\uparrow \bar{v}_\uparrow}{(x_1 x_2)^{1/2}}, & \text{orthopositronium}, \\[2ex] \cdots, \end{cases}$$

where $\beta = \alpha m/2$.

For use in Secs. II and III, the free propagator in (A5) (i. e., S_0 in $S_0^{-1}\psi = \bar{K}\psi$) is replaced by the fully corrected propagator. Then $\bar{K}$ includes only those two-particle irreducible amplitudes in which the q-$\bar{q}$ lines are connected, to avoid double counting. Analyses for Fock states containing three or

more particles are similar to that presented here for $q\bar{q}$ states. For example, the qqq Fock state in the nucleon is described by a wave function

$$\Psi(x_i, k_{\perp i}; p) = \prod_{i=1}^3 \frac{u_{\lambda_i}^{(i)}(x_i p^+, k_{\perp i} + x_i p_\perp)}{\sqrt{x_i}} \psi_{\lambda_1 \lambda_2 \lambda_3}(x_i, k_{\perp i}) ,$$

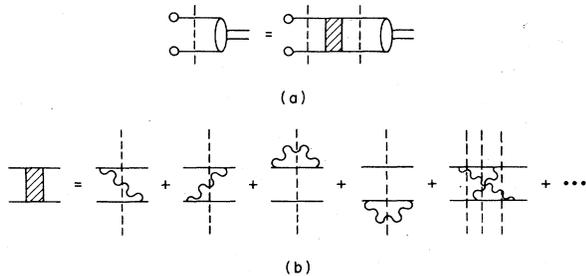where again ψ is independent of p^+ and $p_\perp$.

(a)

(b)

FIG. 33. The two-body bound-state equation in light-cone perturbation theory.

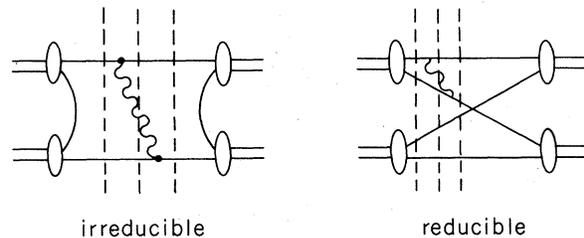irreducible   reducible

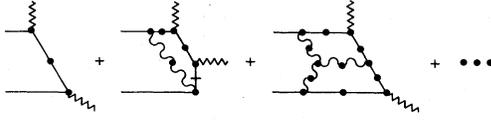FIG. 34. Two-particle irreducible and reducible diagrams.

FIG. 35. UV-finite skeleton expansion of the two-particle irreducible amplitude for $\gamma^* + q\bar{q} \rightarrow \gamma$.

APPENDIX B: COLLINEAR SINGULARITIES AND TWO-PARTICLE IRREDUCIBILITY IN LIGHT-CONE GAUGE

In this appendix, we demonstrate why higher-order corrections to the two-particle irreducible amplitude $T(\gamma^* + q\bar{q} \rightarrow \gamma)$ are free of collinear singularities. It is convenient to express this amplitude as a sum of UV-finite skeleton graphs composed of fully renormalized propagators and vertices (Fig. 35). These diagrams are free of infrared divergences because the initial $q\bar{q}$ state is a color singlet. Being UV finite, the skeleton diagrams involve loop momenta of order $q_\perp$ or less. In fact, we shall argue that only momenta $l_\perp^2 \sim O(q_\perp^2)$ contribute. Consequently, each virtual gluon in Fig. 35 is off shell by order Q^2 and leads to a factor $\alpha_s(Q^2)$. Again it is the vertex and propagator corrections which combine to give these factors of $\alpha_s(Q^2)$, as well as an overall factor $d_F^{-1}(Q^2)$ related to the renormalization of the initial $q, \bar{q}$ fields (see Sec. III). Thus an n-loop graph in Fig. 35 contributes

$$\frac{d_F^{-1}(Q^2)}{Q^2}\left[\alpha_s^n(Q^2)f_n(x_i) + \alpha_s^{n+1}(Q^2)f_{n+1}(x_i) + \cdots\right].$$

To illustrate why only $l_\perp^2 \sim q_\perp^2$ contribute in an irreducible n-loop amplitude $T^{(n)}$, we assume this to be true in all irreducible skeleton diagrams having $(n-1)$ or fewer loops. Generally, $T^{(n)}$ can be expressed in terms of an amplitude $T^{(n-1)}$ having $(n-1)$ loops, as in Fig. 36. There are then two possibilities:

(a) $T^{(n-1)}$ is itself irreducible. Then by hypothesis all of its internal momenta are $O(q_\perp)$, and the corrected amplitude has the form

$$T^{(n)} \sim \int \frac{dl_\perp^2}{l_\perp^2}\alpha_s(l_\perp^2)\bar{u}(-l_\perp)\gamma_\mu u(0)d^{\mu\nu}T_\nu^{(n-1)}(l_\perp, q_\perp)$$

$$\sim \int \frac{dl_\perp^2}{l_\perp^2}\alpha_s(l_\perp^2)\frac{l_\perp \cdot q_\perp + l_\perp^2}{(l_\perp^2 + q_\perp^2)^2}\alpha_s(Q^2)^{n-1}, \qquad (B1)$$

where, as in Eq. (2.6), $T_\nu^{(n-1)}(l_\perp, q_\perp)$ is independent of $l_\perp^2 \ll q_\perp^2$ and falls as $1/l_\perp^4$ or faster when $l_\perp^2 \gg q_\perp^2$ becomes infinite.

(b) $T^{(n-1)}$ is two-particle reducible. The reducible loops lead to collinear logarithms in $T^{(n-1)}$ [i.e., $\int_{m^2}^{Q_\perp^2} dk_\perp^2/k_\perp^2 \sim \ln(Q^2/m^2)$] which tend to cancel explicit factors of $\alpha_s(Q^2)$. However, upon
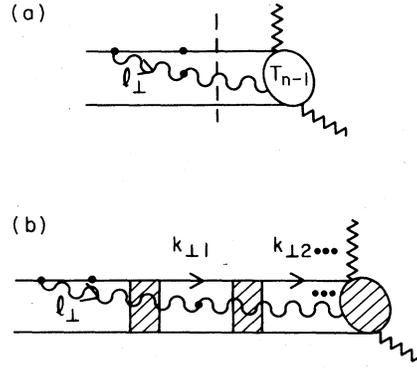

(a)

(b)

FIG. 36. Generic structure of diagrams contributing to T_H.

adding a gluon, $T^{(n)}$, which must be irreducible, has the general structure [Fig. 36(b)]

$$T^{(n)} \sim \int \frac{dl_\perp^2}{l_\perp^2}\alpha_s(l_\perp^2)\frac{q_\perp \cdot l_\perp + l_\perp^2}{(l_\perp^2 + q_\perp^2)^2}$$

$$\times \prod_i\left[\int^{Q^2}\frac{dk_{\perp i}^2}{k_{\perp i}^2 + l_\perp^2}\alpha_s(k_{\perp i}^2)\right]\alpha_s(Q^2)^m.$$

$$(B2)$$

The transverse momentum $l_\perp$ of the added gluon enters as a lower cutoff in the logarithmically divergent loops $(k_{\perp i})$ of $T^{(n-1)}$, because of the topology of $T^{(n)}$. Clearly, only $l_\perp \sim O(q_\perp)$ contribute and therefore only $k_{\perp i} \gtrsim O(l_\perp) \sim O(q_\perp)$ are important—the collinear logarithms in $T^{(n-1)}$ are destroyed by the extra gluon loop. In both Eqs. (B1) and (B2), all loop momenta obviously are of order $q_\perp$, and so by induction this is true in all two-particle-irreducible amplitudes for $\gamma^* + q\bar{q} \rightarrow \gamma$. Notice that the integrations over longitudinal momenta cannot affect this conclusion since each internal line, having transverse momentum $l_\perp^2 \sim q_\perp^2$, is far off shell; there are no singularities in the x integrations for these diagrams.

As emphasized repeatedly here, the essential characteristic of these diagrams is that $q_\perp$ is the only momentum scale, aside from the UV scale parameter in $\alpha_s(Q^2)$. Infrared and collinear cutoffs, quark and hadron masses, etc., can all be taken equal to zero—i.e., they appear in the form λ/Q, m/Q, $\ldots$, and are nonleading for Q^2 large. Indeed the absence of infrared and collinear singularities implies that the contribution from the infrared and collinear regions of phase space is negligible. For, rather than integrals such as $\int_{m^2}^{Q_\perp^2} dk_\perp^2/k_\perp^2 \sim \ln(Q^2/m^2)$ ($\rightarrow\infty$ as $m^2 \rightarrow 0$) in which $k_\perp^2 \sim m^2$ are significant, one finds integrals like $\int^{Q^2} dk_\perp^2/k_\perp q_\perp$ in which the region $k_\perp^2 \lesssim m^2$ is suppressed by m/Q. Since $q_\perp$ is then the only scale, the amplitudes are determined by the short-dis-
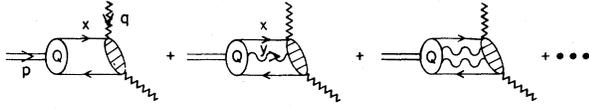
FIG. 37. Covariant-gauge expansion of $F_{\pi\gamma}$ in terms of $q\bar{q}g^n$ distribution amplitudes, and hard-scattering amplitudes for $\gamma^* + q\bar{q}g^n \to \gamma$.

tance structure of the theory, and perturbative QCD is applicable.

APPENDIX C: COVARIANT ANALYSIS OF $F_{\pi\gamma}$

In this appendix, we reproduce the results of Sec. II using covariant perturbation theory and Feynman gauge. This leads to a gauge-invariant formulation of the general analysis. We only sketch the derivation here; most of the underlying principles are thoroughly discussed in Secs. II and III. Also, only the Abelian theory is analyzed [assuming $\alpha_s(Q) \ll 1$]. The results are trivially generalized for non-Abelian theories.

Using the same frame as in Sec. II [i.e., $p^\mu = (1, 0, 0_\perp)$ and $q^\mu = (0, q_\perp^2, q_\perp)$], the exact $\pi\gamma$ transition form factor can be written (Fig. 37)

$$F_{\pi\gamma}(Q^2) = \int_0^1 dx \, \mathrm{Tr}\left[T(x, q) \frac{\gamma_5 \not{p}}{\sqrt{2}} \right] \Phi(x, Q) \qquad \text{(C1a)}$$

$$+ (- e_s) \int_0^1 dx \, dy \, \mathrm{Tr}\left[T_\alpha(x, y, q) \frac{\gamma_5 \not{p}}{\sqrt{2}} \right]$$

$$\times \Phi^\alpha(x, y, Q) \qquad \text{(C1b)}$$

$$+ (- e_s)^2 \int_0^1 dx \, dy_1 dy_2 \, \mathrm{Tr}\left[T_{\alpha\beta}(x, y_i, q) \frac{\gamma_5 \not{p}}{\sqrt{2}} \right]$$

$$\times \Phi^{\alpha\beta}(x, y_i, Q) \qquad \text{(C1c)}$$

$$+ \cdots .$$

Here the pion is replaced by collinear, on-shell constituents in the hard-scattering amplitudes $T, T_\alpha, \ldots$ for

$$\gamma^* + \begin{cases} q\bar{q} \\ q\bar{q}g \\ \cdots \end{cases} \to \gamma .$$

The constituent quark, gluons, and antiquark carry fractions x, y_i, and $1 - x - \sum_i y_i$, respectively, of the hadron's longitudinal momentum ($p^+ = 1$). The amplitude for finding the $q\bar{q}g^n$ Fock state in the pion, collinear up to scale Q, is

$$\Phi^{\alpha_1 \cdots \alpha_n}(x, y_i, Q) \equiv \int \frac{d^2 k_\perp}{16\pi^3} \prod_i \frac{d^2 r_{\perp i}}{16\pi^3} \int \frac{dk^-}{2\pi} \prod_i \frac{dr_i^-}{2\pi} \psi^{\alpha_1 \cdots \alpha_n}(k, r_i) \theta\left(Q - |k_\perp| - \sum_i |r_{\perp i}| \right), \qquad \text{(C2)}$$

where $\psi^{\alpha_1 \cdots \alpha_n}(k, r_i)$ is the Bethe-Salpeter wave function, k and r_i are the quark and gluon four momenta, and $\alpha_1, \ldots, \alpha_n$ are the gluon polarization indices. Only that part of the general wave function having spinor structure $\gamma_5 \not{p}$ is retained:

$$\Psi_{BS}^{\alpha_1 \cdots} \to \frac{\gamma_5 \not{p}}{\sqrt{2}} \psi^{\alpha_1 \cdots} ,$$

$$\psi^{\alpha_1 \cdots} = \mathrm{Tr}\left[\frac{\gamma^+ \gamma_5}{2\sqrt{2}} \Psi_{BS}^{\alpha_1 \cdots} \right] . \qquad \text{(C3)}$$

All other components result in additional factors of m/Q, and can be dropped.

The hard-scattering amplitudes are collinear irreducible in the sense of Sec. III. The contribution from the collinear region—i.e., from $k^+ k^- \sim k_\perp^2 \ll Q^2$—of each loop is largely removed by subtractions as illustrated in Fig. 38. These subtractions are necessary to avoid double counting of lower-order terms; soft, collinear interactions, with $k_\perp^2 \ll Q^2$, are all absorbed into the distribution amplitudes (C2). Consequently, only $k_\perp^2 \gtrsim Q^2$ contribute in the hard-scattering amplitudes, other regions being suppressed by factors of m/Q. The amplitudes $T, T_\alpha, \ldots$ then have valid perturbative expansions in $\alpha_s(Q^2)$. For example, the terms
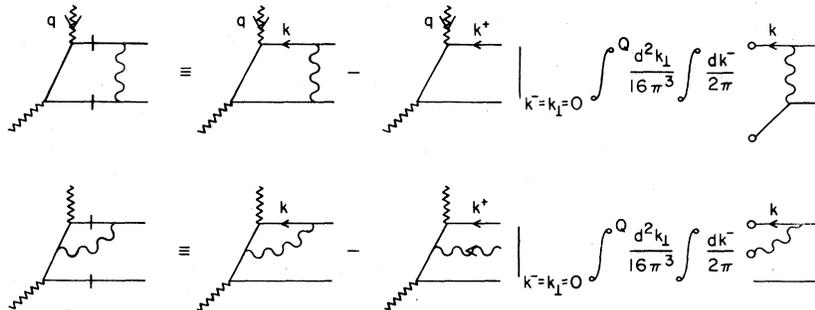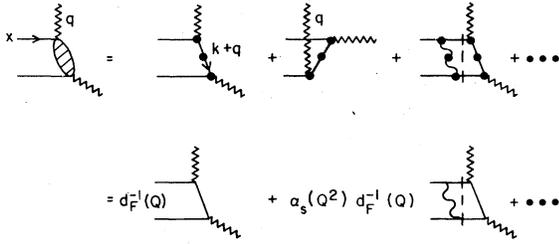

FIG. 38. Collinear irreducible contributions to T_H.

FIG. 39. Leading-order terms in T_H for $q\bar{q}$ Fock state.

FIG. 40. Multiquark nonvalence states are suppressed in $F_{\pi\gamma}$.

contributing to $T(x, q)$ can be organized as a series of UV-finite skeleton graphs (Fig. 39) with renormalized vertices and propagators. Since the skeletons are UV-finite and have only $k_\perp^2 \gtrsim Q^2$, all loop momenta are scaled by Q—the only scale greater than or equal to Q. Thus vacuum polarization corrections to an internal gluon line can be absorbed into a running coupling constant $\alpha_s(Q^2)$. Furthermore, the photon vertex and fermion-propagator corrections are then related by the Ward identity, giving factors $d_F^{-1}(Q)$ and $d_F(Q)$, respectively, in leading order where

$$d_F(Q) = e^{\gamma_F \xi}[1 + O(\alpha_s(Q^2))], \qquad (C4)$$

$$\xi \equiv \int^{Q^2} \frac{dk^2}{k^2} \frac{\alpha_s(k^2)}{4\pi}, \qquad (C5)$$

and $\gamma_F = 1$. Thus only the first term in Fig. 39 contributes to (C1a) to lowest order in $\alpha_s(Q^2)$ (assumed $\ll 1$); an n-loop skeleton is suppressed by at least $\alpha_s(Q^2)^n$. Amplitudes for the remaining Fock states $(q\bar{q}g, \ldots)$ are analyzed in the same fashion. In each case only the renormalized tree graph contributes to leading order in $\alpha_s(Q^2)$.

In principle, one must also include states having additional $q\bar{q}$ pairs (Fig. 40). However, these are suppressed relative to (C1) by powers of m^2/Q^2 coming from the additional hard propagators, and can be ignored. That this is not the case for multigluon states will become clear.

Consider now the term (C1a). Setting $k^\mu = (x, 0, 0_\perp)$, we find (in leading order)

$$\Gamma_\mu^{(0)} = -ie^2 \epsilon_{\mu\nu\rho\sigma} p^\nu e^\rho q^\sigma F_{\pi'}^{(0)}(Q^2)$$

$$= -\frac{e^2(e_u^2 - e_d^2)}{2} \int_0^1 dx\, \Phi(x, Q)d_F^{-1}(Q)$$

$$\times \left\{ \frac{\text{Tr}[\not{e}(\not{q} + \not{k})\gamma_\mu \gamma_5 \not{p}]}{-(1-x)q_\perp^2} \right.$$

$$\left. + [x \rightarrow (1 - x)] \right\}. \qquad (C6)$$

Thus $F_{\pi'}^{(0)}$ is

$$F_{\pi'}^{(0)}(Q^2) = \int_0^1 dx\, \Phi(x, Q)d_F^{-1}(Q)T_H(x, Q) \qquad (C7)$$

with the hard-scattering amplitude

$$T_H(x, Q) = \frac{2(e_u^2 - e_d^2)}{x(1 - x)Q^2}. \qquad (C8)$$

The $q\bar{q}g$ contribution, Eq. (C1b), has two denominators of order Q^2 after rationalizing the quark propagators (Fig. 41). This term is negligible unless one of these is canceled by the numerator. Consequently, only the longitudinal gluon polarization contributes—i.e., $\Phi^\alpha T_\alpha \rightarrow \frac{1}{2}\Phi^+ T^-$ since $q^- = q_\perp^2 \gg q^+, q_\perp$ in T_α. Thus, to leading order, (C1b) can be rewritten

$$\Gamma_\mu^{(1)} = -\frac{e^2(e_u^2 - e_d^2)}{2} \int_0^1 dx\, \frac{dy}{y}(-e_s)\Phi^+(x, y, Q)d_F^{-1}(Q)$$

$$\times \left\{ \text{Tr}\left(\not{e} \frac{1}{\not{q} + \not{k} + \not{y}} \not{y} \frac{1}{\not{q} + \not{k}} \gamma_\mu \gamma_5 \not{p} \right) \right.$$

$$\left. + [x \rightarrow (1 - x)] \right\}, \qquad (C9)$$

where $y^\mu \equiv (y, 0, 0_\perp)$ is the gluon's momentum in T_α and where $y^-/2 = \not{y}/y$ has been used in the numerator. Adding and subtracting $\not{q} + \not{k}$ to $\not{y}$ in the numerator, we can relate this $q\bar{q}g$ amplitude to the $q\bar{q}$ amplitude in Eq. (C6) via a collinear Ward identity:

$$y^\alpha T_\alpha(x, y, q) = T(x, q) - T(x + y, q). \qquad (C10)$$

Thus Eq. (C9) implies

$$F_{\pi'}^{(1)}(Q^2) = -e_s \int_0^1 dx\, \frac{dy}{y} \Phi^+(x, y, Q)d_F^{-1}(Q)$$

$$\times [T_H(x, Q) - T_H(x + y, Q)].$$

This equation can be written more compactly as

$$F_{\pi'}^{(1)}(Q^2) = e_s \int_0^1 ds\, \frac{d}{ds} \int_0^1 dx\, \frac{dy}{y} \Phi^+(x, y, Q)d_F^{-1}(Q)$$

$$\times T_H(x + sy, Q)$$

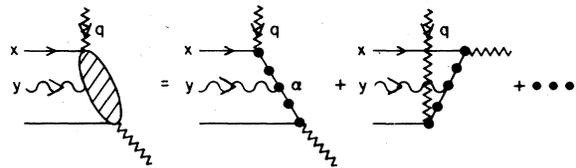$$= \int_0^1 dx\, \phi_1(x, Q)d_F^{-1}(Q)T_H(x, Q), \qquad (C11)$$

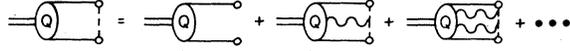FIG. 41. Leading terms in T_H for $q\bar{q}g$ states.

FIG. 42. Definition of the effective $q\bar{q}$ distribution amplitude.

where now

$$\phi_1(x, Q) \equiv e_s \int_0^1 ds \frac{d}{ds} \int_0^1 \frac{dy}{y} \Phi^+(x - sy, y, Q)$$

(C12)

is an effective $q\bar{q}$ distribution amplitude describing the $q\bar{q}g$ state.

Again for the $q\bar{q}gg$ state (C1c) only longitudinally polarized gluons contribute since two factors of Q^2 are required to cancel the additional large denominators. Bose statistics require $\Phi^{\alpha\beta}(x, y_1, y_2, Q) = \Phi^{\beta\alpha}(x, y_2, y_1, Q)$, and so we can apply the collinear Ward identity (C10) twice to reduce $\Phi^{\alpha\beta}T_{\alpha\beta} \simeq \frac{1}{4}\Phi^{++}T^{--}$ to

$$\frac{\Phi^{++}}{y_1 y_2} \frac{r_1^\alpha r_2^\beta + r_2^\alpha r_1^\beta}{2} T_{\alpha\beta} = \frac{\Phi^{++}}{2y_1 y_2}[T(x, Q) - T(x + y_1, Q)$$

$$- T(x + y_2, Q)$$

$$+ T(x + y_1 + y_2, Q)].$$

Thus term (C1c) can be rewritten

$$F_{\pi\gamma}^{(2)}(Q^2) \simeq \int_0^1 dx \, \phi_2(x, Q) d_F^{-1}(Q) T_H(x, Q)$$

in leading order, where once more

$$\phi_2(x, Q) \equiv \frac{e_s^2}{2!} \int_0^1 ds_1 ds_2 \frac{d}{ds_1} \frac{d}{ds_2}$$

$$\times \int_0^1 \frac{dy_1}{y_1} \frac{dy_2}{y_2} \Phi^{++}(x - y_1 s_1 - y_2 s_2, y_i, Q)$$

is an effective two-particle distribution amplitude.

Terms involving three or more gluons are analyzed in the same manner. The final result for the $\pi\gamma$ form factor is then

$$F_{\pi\gamma}(Q^2) = \int_0^1 dx \, \phi(x, Q) T_H(x, Q)$$

$$\times [1 + O(\alpha_s(Q^2), m^2/Q^2)]$$

(C13)

with the complete distribution amplitude defined as (Fig. 42)

$$\phi(x, Q) \equiv d_F^{-1}(Q) \sum_{n=0}^\infty \phi_n(x, Q)$$

$$= d_F^{-1}(Q)\phi_\infty(x, Q),$$

(C14)

where for the $q\bar{q}g^n$ state

$$\phi_n(x, Q) = \frac{e_s^n}{n!} \int_0^1 ds_1 \cdots ds_n \frac{d}{ds_1} \cdots \frac{d}{ds_n} \int_0^1 \frac{dy_1}{y_1} \cdots \frac{dy_n}{y_n} \Phi^{+\cdots+}\left(x - \sum_i y_i s_i, y_i, Q\right).$$

(C15)

All effects due to longitudinally polarized gluons have been absorbed into $\phi(x, Q)$—an effective $q\bar{q}$ distribution amplitude.

The variation of $\phi(x, Q)$ as $Q \to \infty$ is determined from Eqs. (C2), (C14), and (C15) by the behavior of the Bethe-Salpeter wave functions $\psi^{+\cdots+}(k, r_i)$ for large $k_\perp$ and/or $r_{\perp i}$ [$\sim O(Q)$]. We can analyze this behavior as we did $F_{\pi\gamma}(Q^2)$ itself. For example, in leading order $\psi(k)$ for $k_\perp$ large is given in terms of the distribution amplitudes $\Phi^{\alpha_1 \cdots \alpha_n}$ by the diagrams in Figs. 43(a) and 43(b). As above, higher-order (collinear-irreducible) interactions are suppressed, here by $\alpha_s(k_\perp^2)$ or more, and can be ignored [Fig. 43(b)]. The analogous series for $\psi^+(k, r)$ is illustrated in Fig. 43(c); all terms shown are leading order in $\alpha_s(Q^2)$.

We now combine these series, as indicated in Eqs. (C14) and (C15), and integrate over k^- and $\lambda^2 \leq k_\perp^2 \leq Q^2$ to obtain an expression for $\phi_\infty(x, Q^2) - \phi_\infty(x, \lambda^2)$, as in Fig. 44. Once more, the collinear Ward identity can be used to combine sets of diagrams (e.g., Fig. 45), since only wave functions with longitudinally polarized gluons contribute. In this way the series pictured in Fig. 44 can be reduced to an integral equation for $\phi_\infty(x, Q)$ (Fig. 46):

$$\phi_\infty(x, Q) = \phi_\infty(x, \lambda) + \int \frac{dk^-}{2\pi/i} \int_{\lambda^2}^{Q^2} dk_\perp^2 \frac{\alpha_s(k_\perp^2)}{4\pi} \int_0^1 dy \, \phi_\infty(y, k_\perp) \frac{-\frac{1}{4}\mathrm{Tr}(\gamma^+\gamma_5 \slashed{k}\gamma_\mu \gamma_5 \slashed{p}\gamma^\mu \slashed{k} - \slashed{p})}{(xk^- - k_\perp^2 + i\epsilon)[(x-1)k^- - k_\perp^2 + i\epsilon][(x-y)k^- - k_\perp^2 + i\epsilon]}$$

$$+ \int \frac{dk^-}{2\pi/i} \int_{\lambda^2}^{Q^2} dk_\perp^2 \frac{\alpha_s(k_\perp^2)}{4\pi} \int_0^1 ds \frac{d}{ds} \int_0^1 \frac{dy}{y} \phi_\infty(x + (1-s)y) \frac{\frac{1}{4}\mathrm{Tr}(\gamma^+\gamma_5 \slashed{\bar{k}}\gamma^+\gamma_5 \slashed{p})}{[(x-sy)k^- - k_\perp^2 + i\epsilon][-yk^- - k_\perp^2 + i\epsilon]}$$

$$+ \int \frac{dk^-}{2\pi/i} \int_{\lambda^2}^{Q^2} dk_\perp^2 \frac{\alpha_s(k_\perp^2)}{4\pi} \int_0^1 ds \frac{d}{ds} \int_0^1 \frac{dy}{y} \phi_\infty(x - sy) \frac{\frac{1}{4}\mathrm{Tr}[\gamma^+\gamma_5 \gamma_5 \slashed{p}\gamma^+(-\slashed{\bar{k}})]}{\{[1 - x - (1-s)y]k^- - k_\perp^2 + i\epsilon\}(-yk^- - k_\perp^2 + i\epsilon)},$$

(C16)

where (C3) is used to project out the relevant component of the wave function, and where $k = (x, k^-, k_\perp)$, $\bar{k} = (x - sy, k^-, k_\perp)$, and $\tilde{k} = (1 - x - (1 - s)y, k^-, k_\perp)$. We integrate over k^- by closing the integration contour at infinity in the complex k^- plane—above (below) the real axis for $x > y$ ($x < y$) in the first term, and al-
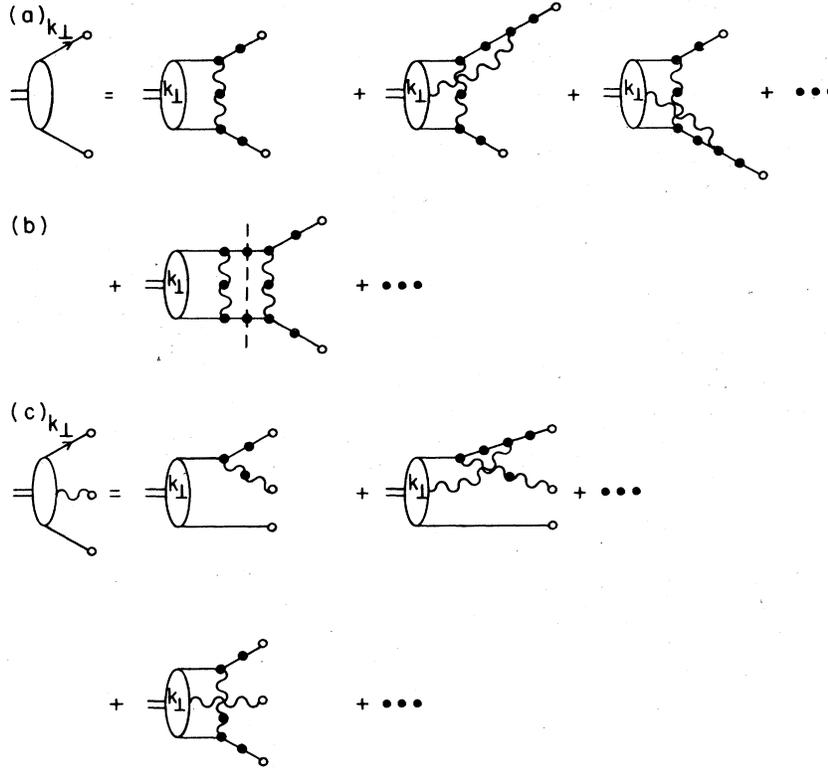
FIG. 43. (a) The $q\bar{q}$ wave function at large $k_\perp$ in terms of distribution amplitudes. (b) Nonleading contribution to $\psi(x_i, k_\perp)$ which is collinear irreducible. (c) The $q\bar{q}g$ wave function at large $k_\perp$.

ways below the axis for the remaining terms. Using Cauchy's theorem, the integral equation becomes

$$\phi_\infty(x, Q) = \phi_\infty(x, \lambda) + 2 \int_{\lambda^2}^{Q^2} \frac{dk_\perp^2}{k_\perp^2} \frac{\alpha_s(k_\perp^2)}{4\pi} \int_0^1 dy \left[\theta(x-y) \frac{1-x}{1-y} + \theta(y-x) \frac{x}{y} \right] \phi_\infty(y, k_\perp)$$

$$+ 2 \int_{\lambda^2}^{Q^2} \frac{dk_\perp^2}{k_\perp^2} \frac{\alpha_s(k_\perp^2)}{4\pi} \int_0^1 dy \left[\frac{\theta(y-x)}{y-x} \frac{x}{y} \phi_\infty(y, k_\perp) - \frac{\theta(x-y)}{x-y} \frac{y}{x} \phi_\infty(x, k_\perp) \right]$$

$$+ 2 \int_{\lambda^2}^{Q^2} \frac{dk_\perp^2}{k_\perp^2} \frac{\alpha_s(k_\perp^2)}{4\pi} \int_0^1 dy \left[\frac{\theta(x-y)}{x-y} \frac{1-x}{1-y} \phi_\infty(y, k_\perp) - \frac{\theta(y-x)}{y-x} \frac{1-y}{1-x} \phi_\infty(x, k_\perp) \right] .$$

Here the substitution $y \to (y-x)(1-2s)$ was made in the second and third terms. Differentiating with respect to ξ [Eq. (C5)], we obtain an evolution equation for $\phi(x, Q) = d_F^{-1}(Q)\phi_\infty(x, Q) \equiv x(1-x)\tilde\phi(x, Q)$:

$$x(1-x)\left[\frac{\partial}{\partial \xi} \tilde\phi(x, Q) + \gamma_F \tilde\phi(x, Q) \right] = \int_0^1 dy\, V(x, y)\tilde\phi(y, Q), \tag{C17}$$

where $\gamma_F = 1$ in Feynman gauge and, in the same gauge,

$$V(x, y) = 2\left[x(1-y)\theta(y-x)\left(1 + \frac{\Delta}{y-x}\right) + \begin{pmatrix} x \to (1-x) \\ y \to (1-y) \end{pmatrix} \right]$$

with $\Delta\tilde\phi = \tilde\phi(y, Q) - \tilde\phi(x, Q)$.

Equations (C8), (C13), and (C17) completely determine the large-Q^2 behavior of $F_{\pi'}(Q^2)$. Aside from color factors, these results are identical to those found in Sec. II [Eqs. (2.11), (2.12), (2.17b), and (2.18)]. Furthermore, definition (C14) of the distribution amplitude $\phi(x, Q)$ is the same in both gauges, since in light-cone gauge ($\eta \cdot A = A^+ = 0$)$\phi_n(x, Q) = 0$ for $n \neq 0$. Although γ_F and $V(x, y)$ are separately gauge dependent, this dependence explicitly cancels in Eq. (C17). Thus the formulation presented here allows a gauge-invariant analysis of $F_{\pi'}(Q^2)$. The analysis of higher-order [in $\alpha_s(Q^2)$] corrections to T_H and V follows much the same pattern. These methods are also easily generalized for the study of other elastic processes.
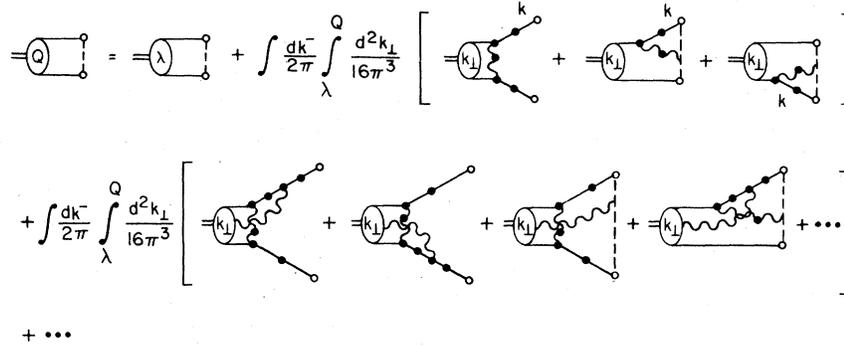
FIG. 44. The effective $q\bar{q}$ distribution amplitude (as defined in Fig. 42) in terms of $q\bar{q}g^n$ distribution amplitudes.

The structure of the complete distribution amplitude ϕ is best understood by Fourier transforming to coordinate space. First, from definition (C2), the $q\bar{q}g^n$ distribution amplitude can be written

$$\Phi^{\alpha_1\cdots\alpha_n}(x, y_i, Q) = (-1)^n \int \frac{dz^-}{2\pi}\frac{dz_1^-}{2\pi}\cdots\frac{dz_n^-}{2\pi}\exp\{(i/2)[(1-x)z^- + y_1 z_1^- + \cdots + y_n z_n^-]\}$$

$$\times i\langle 0|\, T\bar{\psi}(z)\tilde{A}^{\alpha_1}(z_1)\cdots\tilde{A}^{\alpha_n}(z_n)\psi(0)\,|\pi\rangle,\tag{C18}$$

where $z^+ = z_\perp = z_i^+ = z_{\perp i} \equiv 0$ $(\Rightarrow z^2 = z_i^2 = 0)$, and where the fields $\tilde{\psi}$, $\tilde{A}^\alpha$ are *not* local operators but rather are smeared in the transverse direction over a region of radius $z_\perp \sim 1/Q$. This smearing is a consequence of the finite range of the $k_\perp$, $r_{\perp i}$ integrations in (C2), and follows immediately from the uncertainty principle.[55] Substituting (C18) into (C15) we find

$$\phi_n(x, Q) = \int\frac{dz^-}{2\pi}e^{(i/2)(1-x)z^-}i\left\langle 0\left|T\bar{\psi}(z)\left(\frac{1}{n!}\prod_{i=1}^{n}(-ie_s)\int_0^1 ds_i\, z\cdot A((1-s_i)z)\right)\psi(0)\right|\pi\right\rangle,$$

where each derivative in (C15) brings down a factor $iz^- y_i/2$ from the exponential ultimately giving $z^-\tilde{A}^+/2$ $= z\cdot\tilde{A}$. Thus the full distribution amplitude is $(1-s\to s)$

$$\phi(x, Q) = d_F^{-1}(Q)\int\frac{dz^-}{2\pi}e^{(i/2)(1-x)z^-}i\left\langle 0\left|T\bar{\psi}(z)\exp\left(-ie_s\int_0^1 ds\, z\cdot\tilde{A}(zs)\right)\psi(0)\right|\pi\right\rangle,\tag{C19}$$

where again all fields are smeared in the transverse direction, and the line integral in the exponential is along the light cone (i.e., $z^2 = 0$).

The operator appearing in (C19) is closely related to the gauge-invariant operator (now with local fields)

$$T\bar{\psi}(z)\exp\left(-ie_s\int_0^1 ds\, z\cdot A(zs)\right)\psi(0).\tag{C20}$$

The two operators have the same collinear divergences (i.e., as $m\to 0$), which must then be gauge invariant in each case. Since $e_0 A^\mu = (e_0/\sqrt{Z_3})\sqrt{Z_3}A^\mu$ is renormalized, the ultraviolet divergences of the operator is (C19) are the same as for $T\bar{\psi}\psi$. By including a factor $d_F^{-1}(Q)$ in (C19), we guarantee that the Q^2 variation of $\phi(x, Q)$ is determined solely by the collinear singularities in leading order—i.e., the anomalous dimension of ϕ is zero and ϕ is UV finite. Thus the evolution equation for ϕ is gauge invariant, since the collinear singularities are invariant (up to negligible corrections of order m^2/Q^2).

The ultraviolet structure of (C20) is quite different. Since the fields are not smeared, additional divergences come from the s integration (including linear UV divergences). Note that $\phi(x, Q)$ is *not* simply the Fourier transform of a matrix element of the gauge-invariant operator (C20), as was assumed in Ref. 10, for example. Among other differences, these two wave functions have different anomalous dimensions[56]— $\gamma = 6 + O(\alpha_s(Q^2))$ for (C20) (in any gauge). The derivation given in Ref. 10 mistreats the fermion propagator in the UV region (i.e., where gluon momenta are $\gg Q$).

Finally, note that scaling violations in inelastic structure functions and fragmentation functions can be analyzed in close analogy to the discussion given here. In particular, the nonsinglet structure function is closely related to (C19), as it is given by

$$\phi_{NS}(x, Q) = d_F^{-1}(Q)\int\frac{dz^-}{2\pi}e^{(i/2)(1-x)z^-}i\left\langle p\left|T\bar{\psi}(z)\exp\left(-ie_s\int ds\, z\cdot\tilde{A}(zs)\right)\psi(0)\right|p\right\rangle.\tag{C21}$$
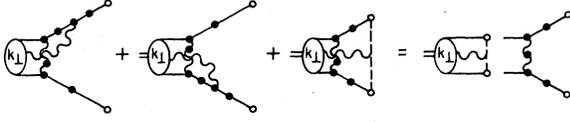
FIG. 45. Use of collinear Ward identities to combine terms appearing in Fig. 44.

The only different is that here the matrix element is for forward scattering, unlike the nonforward matrix element in (C19). Thus the same anomalous dimensions control the asymptotic behavior of (C19) and (C21).

APPENDIX D: ANALYTIC SOLUTIONS OF EVOLUTION EQUATIONS

The meson evolution equation (2.18) is a first-order differential equation similar in form to a one-dimensional diffusion (or Schrödinger) equation, but in which ξ plays the role of time t (or it). It is sometimes convenient to expand the general solution of this equation in terms of its eigenfunctions $\phi_n(x_i, Q)$, where

$$\frac{\partial}{\partial \xi} \phi_n(x_i, Q) = -\gamma_n \phi_n(x_i, Q)$$

$$\Rightarrow \phi_n(x_i, Q) = x_1 x_2 \tilde{\phi}_n(x_i) e^{-\gamma_n \xi}$$

$$= x_1 x_2 \tilde{\phi}_n(x_i) \left(\ln \frac{Q^2}{\Lambda^2} \right)^{-\gamma_n} \qquad (D1)$$

and [Eqs. (2.17) and (2.18)]

$$x_1 x_2 \left(\frac{C_F}{\beta} - \gamma_n \right) \tilde{\phi}_n(x_i) = \frac{C_F}{\beta} \int_0^1 [dy] V(x_i, y_i) \tilde{\phi}_n(y_i) . \qquad (D2)$$

The eigenvalues γ_n are real since $V(x_i, y_i)$ is both real and symmetric $[V(x_i, y_i) = V(y_i, x_i)]$. Furthermore, the $\{\tilde{\phi}_n\}_{n=0}^{\infty}$ are then orthogonal with respect to weight $w(x_i) = x_1 x_2$,

$$\int_0^1 [dx] w(x_i) \phi_n^*(x_i) \phi_m(x_i) = K_n \delta_{nm}, \qquad (D3)$$

and complete on the set of functions $f(x)$ for which

$$\int_0^1 [dx] \frac{|f(x_i)|^2}{w(x_i)} < \infty . \qquad (D4)$$

Thus boundary condition (2.21) ensures that the distribution amplitude has a convergent expansion for all Q^2:

$$\phi(x_i, Q) = w(x_i) \sum_n a_n \left(\ln \frac{Q^2}{\Lambda^2} \right)^{-\gamma_n} \tilde{\phi}_n(x_i), \qquad (D5a)$$

where by (D3)

$$a_n \left(\ln \frac{Q^2}{\Lambda^2} \right)^{-\gamma_n} = \frac{1}{K_n} \int_0^1 [dx] \tilde{\phi}_n^*(x_i) \phi(x_i, Q) . \qquad (D5b)$$

To find its eigenfunctions we first rewrite the potential [Eq. (2.17b)] in terms of $x \equiv x_1 - x_2$ and $y \equiv y_1 - y_2$:

$$V(x, y) = \left\{ (1 + x)(1 - y) \theta(y - x) \left[\frac{\delta_{h_1 \bar{h}_2}}{2} + \frac{\Delta}{y - x} \right] \right.$$

$$\left. + \left[\begin{matrix} x \to -x \\ y \to -y \end{matrix} \right] \right\} .$$

This potential can readily be diagonalized through use of the basis functions $\{x^n\}_{n=0}^{\infty}$ for which

$$V|x^n\rangle \equiv \int_{-1}^1 \frac{dy}{2} V(x, y) y^n$$

$$= \frac{1 + x}{2} \int_x^1 dy (1 - y) \left(\frac{\delta_{h_1 \bar{h}_2}}{2} y^n + \frac{y^n - x^n}{y - x} \right) + (-1)^n \{x \to -x\}$$

$$= \frac{1 - x^2}{4} \left[\sum_{j=0}^{n-1} \left(\frac{\delta_{h_1 \bar{h}_2}}{(n+1)(n+2)} + \frac{2(j+1)}{(n-j)(n+1)} \right) x^j + \left(\frac{\delta_{h_1 \bar{h}_2}}{(n+1)(n+2)} - 2 \sum_{k=2}^{n+1} \frac{1}{k} \right) x^n \right] + (-1)^n \{x \to -x\}$$

$$\equiv w(x) \sum_{j=0}^n |x^j\rangle U_{jn},$$

where

$$U_{jn} = \begin{cases} \dfrac{1 + (-1)^{n-j}}{2} \left[\dfrac{2\delta_{h_1 \bar{h}_2}}{(n+1)(n+2)} + \dfrac{4(j+1)}{(n-j)(n+1)} \right], & j < n, \\[4mm] \dfrac{2\delta_{h_1 \bar{h}_2}}{(n+1)(n+2)} - 4 \sum_{k=2}^{n+1} \dfrac{1}{k}, & j = n, \\[4mm] 0, & j > n, \end{cases}$$

is a matrix representation of the linear (integral) operator $w^{-1}V$ on the basis $\{x^n\}$. As $U_{jn} = 0$ for $j > n$, its eigenvalues are just the diagonal matrix elements U_{nn}. Furthermore, the corresponding eigensolution
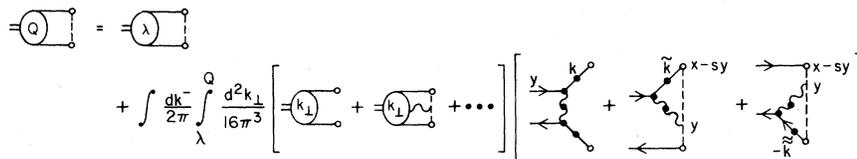
FIG. 46. Integral equation for the effective $q\bar{q}$ distribution amplitude.

$\tilde{\phi}_n(x_i)$ must then be a polynomial in x of degree n. Since only the Gegenbauer polynomials $C_n^{3/2}(x)$ are orthogonal on $-1 < x < 1$ with weight $w(x) = (1 - x^2)/4$, the eigensolutions of the meson evolution equation are

$$\phi_n(x_i, Q) = x_1 x_2 C_n^{3/2}(x_1 - x_2)\left(\ln\frac{Q^2}{\Lambda^2}\right)^{-\gamma_n}$$

with

$$\gamma_n = \frac{C_F}{\beta}\left(1 + 4\sum_2^{n+1}\frac{1}{j} - \frac{2\delta_{h_1\bar{h}_2}}{(n+1)(n+2)}\right).$$

The same Gegenbauer polynomials appear in other theories—scalar-gluon theories, QED, etc.—though with different anomalous dimensions. This follows because the eigenfunctions of the evolution equation in each theory are polynomials orthogonal with respect to the same weight, $w(x_i) = x_1 x_2$. This weight function is defined so that $V(x_i, y_i) = V(y_i, x_i)$.

For baryons, the eigenfunctions $\tilde{\phi}_n(x_i)$ and the anomalous dimension γ_n appearing in Eq. (4.11) are defined by

$$x_1 x_2 x_3\left(\frac{3}{2}\frac{C_F}{\beta} - \gamma_n\right)\tilde{\phi}_n(x_i) = \frac{C_B}{\beta}\int_0^1 [dy]V(x_i, y_i)\tilde{\phi}_n(y_i),$$

where the potential $V(x_i, y_i) = V(y_i, x_i)$ is defined in Eq. (4.10b). The γ_n are again real, and the $\{\tilde{\phi}_n(x_i)\}$ form a complete, orthogonal polynomial basis with weight $w(x_i) = x_1 x_2 x_3$.[57] To determine these, we expand V on a polynomial basis $\{x_1^m x_3^n\}_{m,n=0}^{\infty}$:

$$\frac{1}{2}\frac{V|x_1^m x_3^n\rangle}{w(x_i)} = x_1^m x_3^n\left(\frac{\delta_{h_2\bar{h}}}{(m+1)(m+2)} - 3\sum_{j=2}^{m+1}\frac{1}{j} + \frac{\delta_{h_2\bar{h}}}{(n+1)(n+2)} - 3\sum_{j=2}^{n+1}\frac{1}{j}\right)$$

$$+ \left[\sum_{i=1}^m\frac{m-i+1+\delta_{h_2\bar{h}}}{i(m+2)}x_1^{m-i}\sum_{j=0}^i\binom{i}{j}(-1)^j n_3^{n+j} + \begin{bmatrix}1 \to 3 \\ m \to n\end{bmatrix}\right]$$

$$- \left[\sum_{i=1}^n x_1^{m+i}x_3^{n-i}\sum_{j=0}^i\binom{n}{j}\binom{n-j}{n-i}(-1)^j\sum_{k=2}^{m+j+1}\frac{1}{k} + \begin{bmatrix}1 \to 3 \\ m \to n\end{bmatrix}\right]$$

$$= \frac{1}{2}\sum_{i,j}|x_1^i x_3^j\rangle U_{ij,mn}.$$

Here particles 1 and 3 have helicity parallel to the hadron's helicity h, and $\delta_{h_2\bar{h}}$ equals 1(0) when the helicity of particle 2 is antiparallel (parallel) to h—i. e., $\delta_{h_2\bar{h}} = 1$ for $|h| = \frac{1}{2}$ baryons, while $\delta_{h_2\bar{h}} = 0$ for $|h| = \frac{3}{2}$. Since $U_{ij,mn} = 0$ when $i + j > m + n$, the eigenfunctions are polynomials of degree $M = m + n = 0, 1, 2, \ldots$ with $M + 1$ eigenfunctions for each M. Furthermore, the corresponding $(M + 1)$ eigenvalues are obtained by diagonalizing the $(M + 1) \times (M + 1)$ matrix $U_{ij,mn}$ with $i + j = m + n = M$. The leading eigenfunctions are given in Table I.

APPENDIX E: SUDAKOV FORM FACTORS

In this appendix we review the features characterizing the double logarithms appearing in the free-fermion vertex function (i. e., Sudakov form factor). Using Feynman gauge in an Abelian theory, the lowest-order correction to the vertex is (Fig. 47)

$$\Gamma^+ = -\frac{e^2}{16\pi^3}\gamma^+\int_0^1\frac{dx}{x(1-x)}\int_0^\infty d^2k_\perp\frac{\bar{u}(1, q_\perp)\gamma_\mu u(1-x, q_\perp - k_\perp)\bar{u}(1-x, -k_\perp)\gamma^\mu(1, 0_\perp)}{\left(-\Delta^2 - \frac{k_\perp^2}{1-x} - \frac{k_\perp^2}{x}\right)\left(-\Delta^2 + q_\perp^2 - \frac{(q_\perp - k_\perp)^2}{1-x} - \frac{k_\perp^2}{x}\right)}$$

$$\simeq -\frac{\alpha}{2\pi}\gamma^+\int_0^1 dx\, x(1-x)\int_0^\infty d^2k_\perp\frac{q_\perp^2}{[k_\perp^2 + x(1-x)\Delta^2][(xq_\perp - k_\perp)^2 + \Delta^2 x(1-x)]},$$
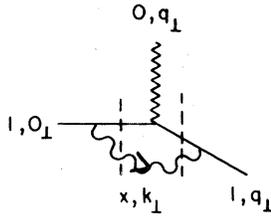
FIG. 47. The Sudakov form factor in lowest order.

where the external fermions are off shell by $-\Delta^2$. The dominant regions of integration are

(a) $\Delta^2 x \ll k_\perp^2 \ll x^2 q_\perp^2$, $x \gg \Delta^2/q_\perp^2$

(b) $\Delta^2 x \ll (k_\perp - x q_\perp)^2 \ll x^2 q_\perp^2$, $x \gg \Delta^2/q_\perp^2$

where the gluon is collinear with the initial fermion in region (a) and with the final fermion in region (b). These nonoverlapping regions contribute equally, and therefore the total contribution (in leading order) is twice that from region (a):

$$\Gamma_\mu \simeq -\frac{\alpha}{\pi} \gamma_\mu \int_{\Delta^2/q_\perp^2}^1 \frac{dx}{x} \int_{x\Delta^2}^{x^2 q_\perp^2} \frac{dk_\perp^2}{k_\perp^2}$$

$$\simeq -\frac{\alpha}{2\pi} \gamma_\mu \left(\ln \frac{q_\perp^2}{\Delta^2} \right)^2 . \tag{E1}$$

Notice that logarithms are generated by both the x and $k_\perp^2$ integrations. The leading logarithms in each order of perturbation theory are readily summed to give the Sudakov form factor

$$\Gamma_\mu \sim \gamma_\mu e^{-\alpha/2\pi(\ln q_\perp^2/\Delta^2)^2} = \gamma_\mu \left(\frac{\Delta^2}{q_\perp^2}\right)^{\alpha/2\pi(\ln q_\perp^2/\Delta^2)} \tag{E2}$$

which falls faster than any power as $q_\perp^2 \to \infty$. In Abelian theories at least, nonleading logarithms are similarly suppressed.

In QCD, α is replaced by the running coupling constant $\alpha_s(k_\perp^2)$. This softens the high-energy behavior of the loop integral and results in a Sudakov form factor that falls as $(\Delta^2/q_\perp^2)^{c \ln \ln q_\perp^2/\Delta^2}$, assuming we can simply sum the leading logarithm in each order of perturbation theory.

---

[1]Reports and applications of this work have been given in S. J. Brodsky and G. P. Lepage, in *Quantum Chromodynamics*, proceedings of the La Jolla Institute Summer Workshop, 1978, edited by W. Frazer and F. Henyey (AIP, New York, 1979); G. P. Lepage and S. J. Brodsky, Phys. Lett. 87B, 359 (1979); Phys. Rev. Lett. 43, 545 (1979); 43, 1625(E) (1979); in Proceedings of the 1979 Summer Institute on Particle Physics, SLAC, Stanford, California (to be published).

[2]A systematic treatment of weak and electromagnetic baryon form factors will be given in S. J. Brodsky, G. P. Lepage, and S. A. A. Zaidi, Report No. SLAC-PUB-2588 (unpublished).

[3]S. J. Brodsky and G. R. Farrar, Phys. Rev. Lett. 31, 1153 (1973); Phys. Rev. D 11, 1309 (1975); V. A. Matveev, R. M. Muradyan, and A. V. Tavkheldize, Lett. Nuovo Cimento 7, 719 (1973). A discussion of mass corrections and the application to nuclei is given in S. J. Brodsky and B. T. Chertok, Phys. Rev. D. 14, 3003 (1976); Phys. Rev. Lett. 37, 269 (1976).

[4]Note that the amplitude T_H includes a factor $1/\sqrt{x_i}$ for each external fermion and a power of $\alpha_s(Q^2)$ for each exchanged gluon.

[5]An operator-product analysis of hadronic wave functions at short distances is given in S. J. Brodsky, Y. Frishman, G. P. Lepage, and C. Sachrajda, Phys. Lett. 91B, 239 (1980). See also Efremov and Radyushkin, Ref. 10. The baryon wave-function anomalous dimensions derived in Ref. 1 and Table I have been confirmed by M. Peskin, Phys. Lett. 88B, 128 (1979).

[6]A. Duncan and A. H. Mueller, Phys. Lett. 90B, 159 (1980); Phys. Rev. D 21, 1636 (1980).

[7]S. D. Drell and T. M. Yan, Phys. Rev. Lett. 24, 181 (1970); G. West, ibid. 24, 1206 (1970). The potential significance of this region has recently been emphasized in Ref. 6.

[8]See especially J. B. Kogut and D. E. Soper, Phys. Rev.

D 1, 2901 (1970), and J. B. Bjorken, J. B. Kogut, and D. E. Soper, ibid. 3, 1382 (1971). For earlier references and development see S. Weinberg, Phys. Rev. 150, 1313 (1966); L. Susskind and G. Frye, ibid. 165, 1535 (1968); S. D. Drell, D. Levy, and T. M. Yan, ibid. 187, 2159 (1969); Phys. Rev. D 1, 1617 (1970); 1, 1035 (1970). Renormalization is discussed in S. J. Brodsky, R. Roskies, and R. Suaya, Phys. Rev. D 8, 4574 (1973).

[9]The $\pi^0 \to \gamma^*\gamma^*$ amplitude with $q_1^2, q_2^2 \to \infty$ is given in H. Suura, T. F. Walsh, and B. L. Young, Lett. Nuovo Cimento 4, 505 (1972). See also, M. K. Chase, Nucl. Phys. B167, 125 (1980).

[10]A. V. Efremov and A. V. Radyushkin, Dubna Reports Nos. JINR-E2-11535, 11983, and 12384 (unpublished); Phys. Lett. 94B. 245 (1980).

[11]P. V. Landshoff, Phys. Rev. D 10, 1024 (1974). See also, P. Cvitanovic, ibid. 10, 338 (1974); S. J. Brodsky and G. R. Farrar, Ref. 3; A. Donnachie and P. V. Landshoff, Z. Phys. C 2, 55 (1979); 2, 372(E) (1979).

[12]This result has also been obtained independently by P. V. Landshoff and D. J. Pritchard, Cambridge Report No. DAMTP 80/04 (unpublished).

[13]The result (4.4) for the pion form factor has also been derived using renormalization-group methods by Duncan and Mueller, Ref. 6.

[14]The $Q^2 \to \infty$ asymptotic result (4.5) was first obtained by G. R. Farrar and D. R. Jackson, Phys. Rev. Lett. 43, 246 (1979); D. R. Jackson, Ph.D. Thesis, Cal Tech, 1977 (unpublished). See also, V. L. Chernyah and A. R. Zhitniskii, Pis'ma Zh. Eksp. Teor. Fiz. 25, 544 (1977) [JETP Lett. 25, 510 (1977)]; G. Parisi, Phys. Lett. 84B, 225 (1979). Earlier analyses of form factors in renormalizable field theories include A. M. Polyakov, in *Proceedings of the International Symposium on Lepton and Photon Interactions at High Energies, Stanford, California, 1975*, edited by W. T. Kirk

(SLAC, Stanford, 1976); T. Appelquist and E. Poggio, Phys. Rev. D **10**, 3280 (1970); P. Menotti, *ibid.* **14**, 3560 (1976); **11**, 2828 (1975); M. L. Goldberger, A. H. Guth, and D. E. Soper, *ibid.* **14**, 1117 (1976).

[15]By choosing the "+" component of Γ^μ, we avoid diagrams containing instantaneous fermion propagators since $\gamma^+\gamma^+ = 0$. Of course, identical results are obtained for any other nonzero component of Γ^μ, but then there are usually additional diagrams to be considered.

[16]The spinor combination $[u_i\bar{u}_i + u_i\bar{u}_i - (u \to d)]$ does not contribute to the pion wave function (2.3) if the π^0 is assumed an eigenstate of parity and charge conjugation (0^{-+}). Note that the phase convention adopted in Appendix A for antiparticle spinors is such that $u_i\bar{v}_i - u_i\bar{v}_i$ is normally associated with spin-zero bosons, and $u_i\bar{v}_i + u_i\bar{v}_i$ with spin-one bosons.

[17]Such behavior is expected in any renormalizable field theory. It leads to (ultraviolet) logarithmic divergences in each order of perturbation theory for the wave function at the origin—i.e., for the operator $\bar{\psi}_\alpha(0)\psi_\beta(0)$. In theories having a nonzero ultraviolet fixed point, the logarithmic factors can exponentiate to modify the power of $1/k_\perp^2$. This is not the case for QCD.

[18]This boundary condition assures the self-adjointness of the light-cone "kinetic energy" operator $\sum_i (k_\perp^2 + m^2)^{(i)}/x_i$ [Eq. (A5)]. It is analogous to requiring $\sqrt{r}\psi_{\text{NR}}(\vec{r}) \to 0$ as $r \to 0$ for nonrelativistic wave functions describing the hydrogen atom. Physically, Eq. (2.1) implies that a composite system has a vanishing amplitude for existing with one constituent carrying all of the longitudinal momentum, leaving the others behind.

[19]We note that in such a theory, $F_{\pi\gamma}(Q^2)$ would be essentially constant as $Q^2 \to \infty$. This is evidently experimentally untenable since $\sigma(e^+e^- \to \pi^0\gamma)/\sigma(e^+e^- \to \mu^+\mu^-)$ would increase with Q^2.

[20]Figure 6 is the only time ordering contributing to the "+" component of this matrix element. Since $(\gamma^+)^2 = 0$, instantaneous fermion propagators cannot occur. Thus f_π is directly related only to the $q\bar{q}$ component of the pion (in this frame).

[21]Here we use the identity $\int_{-1}^{1} dx\, C_n^{3/2}(x) = 2$, $n = 0, 2, 4, \ldots$.

[22]Note that $\mathcal{P}_Q$ is *not* a diagonal operator in transverse momentum (but is diagonal in longitudinal momentum). It is, however, a true projection operator in that $\mathcal{P}_Q \mathcal{P}_Q = \mathcal{P}_Q$.

[23]In general,
$$d_F = d_F(Q^2/\mu^2, \alpha_s(\mu^2))$$
and
$$\tilde{\gamma}(\alpha_s(Q^2)) \equiv \left[\beta(\alpha_s)\frac{d}{d\alpha_s}\ln d_F(1, \alpha_s) - \gamma(\alpha_s)/2\right]_{\alpha_s = \alpha_s(Q^2)},$$
where $Q^2(\partial/\partial Q^2)\alpha_s(Q^2) = \beta(\alpha_s)$ and where γ is the conventionally defined anomalous dimension for $\bar{\psi}(x)\psi(0)$.

[24]C. Bebek *et al.*, Phys. Rev. D **13**, 25 (1976).

[25]The distribution amplitude is of course expected to be strongly skewed in the case of mesons containing a light and heavy quark.

[26]See also, A. I. Vainshtein and V. I. Zakharov, Phys. Lett. **72B**, 368 (1978); G. R. Farrar and D. R. Jackson, Phys. Rev. Lett. **35**, 1416 (1975).

[27]Aside from an overall sign, the form (4.13b) for T_H also agrees with the $x_i \equiv \frac{1}{3}$ result of I. G. Aznaurian *et al.*, Phys. Lett. **90B**, 151 (1980); **92B**, 371 (E) (1980).

[28]Notice that in the infinite-momentum frame (or on the light cone) helicity—but not total angular momentum— is well defined and conserved. Thus, contrary to naive expectations, the $J = \frac{1}{2}$ and $\frac{3}{2}$ baryon wave functions with $J_z = +\frac{1}{2}$ have the same general structure (4.14).

[29]This is a nontrivial dynamical prediction of QCD; it is *not* an assumption.

[30]M. D. Mestayer, SLAC Report No. 214, 1978 (unpublished) and references therein.

[31]These corrections can generate factors of $(\ln\ln(1-x))^n$ in nth order which can modify $\psi(x, \lambda)$ for $x \sim 1$ by powers of $\ln(1-x)$. Such factors are unimportant for this analysis. A detailed analysis of the $x \sim 1$ behavior of wave functions will be given elsewhere.

[32]See also, F. Ezawa, Nuovo Cimento **23A**, 271 (1974); G. R. Farrar and D. R. Jackson, Ref. 26.

[33]See E. L. Berger and S. J. Brodsky, Phys. Rev. Lett. **42**, 940 (1979); and G. R. Farrar and D. R. Jackson, Ref. 26.

[34]Duncan and Mueller assert in Ref. 6 that this correction in $O(\alpha_s T_H)$ rather than $O(\alpha_s^2 T_H)$. However, by restricting their analysis to two loops, they in effect ignore the evolution of $\phi(x_i, \tilde{Q})$ in the region $1 \gg 1-x \gg \lambda/Q$. As discussed in the previous section, this destroys any logarithmic contribution from that region because $\tilde{Q}$ is growing. Figure 17(a) has contributions only from $k_\perp, l_\perp > (1-x)Q$, from the definition of T_H, and as such is definitely $O(\alpha_s^2 T_H)$.

[35]While perturbation theory may not be rigorously applicable here, it is characteristic of vector gauge theories that elastic form factors of charged particles fall with increasing $q_\perp$. Being colored, the quark tends to radiate gluons when struck with large $q_\perp$, the amount of radiation growing with $q_\perp$. A falling elastic form factor represents the shadow of these inclusive channels. The quark form factor increases the effective δ in (4.19), in close analogy to the effects of gluon bremsstrahlung on $\nu W_2^{(0)}$. Note also that because the quark legs are far off shell, the Sudakov form factor falls as a fixed power of λ/Q when effects of the QCD running coupling constant are included. The importance of Sudakov form factors has also been discussed by A. Duncan and A. Mueller, Phys. Lett. **90B**, 159 (1980).

[36]We emphasize that hadronic helicity conservation is rigorous to all orders in $\alpha_s(Q^2)$. Corrections are of order m/Q where m is an effective quark mass. The helicity of external photons (or weak bosons) is not included in the definition of the hadronic helicity. Thus the helicity structure of vector-meson-dominated amplitudes (which are always power-law suppressed in hard-scattering processes) in general differs from the leading direct contributions.

[37]We wish to thank K. Wilson for discussions on this point.

[38]This analysis follows that of Brodsky and Farrar, Ref. 3.

[39]The possibility of Sudakov form-factor suppression of pinch singularities in wide-angle scattering has been discussed by J. C. Polkinghorne, Phys. Lett. **49B**, 277 (1974); Brodsky and Farrar, Ref. 3; and J. Cornwall and G. Tiktopoulos, Phys. Rev. D **13**, 3370 (1976); **15**, 2937 (1977). We also wish to thank Y. Frishman for helpful discussions on this problem.

[40]Note that, in general, there are pinch-singularity contributions which occur in nonleading power-law-suppressed amplitudes. It also should be noted that pinch singularities corresponding to multiple-scattering reactions also contribute to high-momentum-transfer inclusive processes. The analysis of pinch singularities for flavor-exchange diagrams (constitutent-interchange-model contributions) in nucleon-nucleon scattering is given by C. J. Burrows, Z. Phys. C 5, 245 (1980). The complete calculation of the angular dependence of hadron-hadron scattering processes will clearly require a detailed analysis of the Sudakov suppression of the pinch-singularity region. The point has been emphasized by A. Duncan and A. Mueller (Ref. 35). In the case of photon-induced reactions, such as $\gamma\gamma \rightarrow M\bar{M}$, the pinch singularities are power-law suppressed even at the Born level. The QCD predictions for two-photon and Compton processes will be given in a separate paper (Ref. 50).

[41]The data compilation is from P. V. Landshoff and J. C. Polkinghorne, Phys. Lett. 44B, 293 (1973).

[42]K. A. Jenkins et al., Phys. Rev. D 21, 2445 (1980); Phys. Rev. Lett. 40, 425 (1979).

[43]M. A. Shupe et al., Phys. Rev. D 19, 1921 (1979).

[44]R. Anderson et al., Phys. Rev. Lett. 30, 627 (1973).

[45]S. Connetti et al., Phys. Rev. Lett. 41, 924 (1978); H. Dekerret et al., Phys. Lett. 68B, 374 (1977).

[46]L. N. Lipatov, Yad. Fiz. 20, 181 (1974) [Sov. J. Nucl. Phys. 20, 94 (1974)]. G. Altarelli and G. Parisi, Nucl. Phys. B126, 298 (1977).

[47]S. J. Brodsky and G. P. Lepage, in Proceedings of the 1979 SLAC Summer Institute (to be published).

[48]E. Berger, S. J. Brodsky, and G. P. Lepage (in preparation).

[49]For phenomenological applications of high-twist subprocesses, see, e.g., R. Blankenbecler, S. J. Brodsky, and J. F. Gunion, Phys. Rev. D 18, 900 (1978); R. Blankenbecler and I. Schmidt, ibid. 16, 1318 (1977); L. Abbott, W. Atwood, and R. M. Barnett, Phys. Rev. D 22, 582 (1980).

[50]S. J. Brodsky and G. P. Lepage, Report No. SLAC-PUB-2587 (unpublished).

[51]The polarization sum is sometimes more conveniently written as

$$d_{\mu\nu}^{(k)} = \sum_{i=1,2} \left[-\eta_\mu \frac{\epsilon^{(i)} \cdot k}{\eta \cdot k} + \epsilon_\mu^{(i)}\right] \times \left[-\eta_\nu \frac{\epsilon^{(i)} \cdot k}{\eta \cdot k} + \epsilon_\nu^{(i)}\right],$$

where the $\epsilon^{(i)}$ are purely transverse vectors:

$$\epsilon^{(i)+} = \epsilon^{(i)-} = 0 \text{ and } \epsilon_\perp^{(i)*} \cdot \epsilon_\perp^{(j)} = \delta^{ij}.$$

Thus, for example,

$$\bar{u}\gamma^\mu u d_{\mu\nu} \bar{u}\gamma^\nu u = \bar{u}\left[\frac{\gamma^+}{k^+} k_\perp - \gamma_\perp\right] u \bar{u} \left[\frac{\gamma^+}{k^+} k_\perp - \gamma_\perp\right] u.$$

[52]P. Cvitanovic, Phys. Rev. D 14, 1536 (1976) and references therein.

[53]S. J. Brodsky, R. Roskies, and R. Suaya, Ref. 8.

[54]An amplitude is two-particle irreducible here if it does not contain an intermediate state composed solely of a $q\bar{q}$ pair.

[55]For example, in $\langle 0 | T\bar{\psi}(z)\tilde{\psi}(0) | \pi \rangle$, the smeared field is

$$\tilde{\psi}(0) = \int d^2 z_\perp \int^Q \frac{d^2 k_\perp}{(2\pi)^2} e^{-ik_\perp \cdot z_\perp} \psi(z_\perp),$$

where ψ is the local field.

[56]O. Alvarez and G. P. Lepage (unpublished).

[57]Note that because there are two independent x_i, orthogonality with respect to $w(x_i)$ is not sufficient to determine the $\tilde{\phi}_n(x_i)$.